Combining Multicomponent Seismic Attributes, New Rock Physics Models, and In Situ Data to Estimate Gas-Hydrate Concentrations in Deep-Water, Near-Seafloor Strata of the Gulf of Mexico

Phase 2 Report: Log-Based Evidence of Hydrate across Green Canyon Study Sites

Principal Investigators:
Bob A. Hardage
Paul E. Murray
Diana C. Sava

Report Date: November 2006

DOE Award DE-PS26-05NT42667

Submitting Organization:
Bureau of Economic Geology
The University of Texas at Austin
University Station, Box X
Austin, TX 78713-8924

Disclaimer

Abstract

Log data have been amassed and interpreted to confirm that gas hydrate is present in stratigraphic units that span the two sites in the Green Canyon area of the Gulf of Mexico that have been selected for our hydrate research. This report describes the data and the methodology that were used to interpret hydrate concentration from resistivity logs and presents cross-section views of the hydrate systems at each study site.

Contents

List of Figures

Abbreviations, Acronyms, and Definitions

BHSZ: base of the hydrate stability zone

BHDZ: base of the hydrate depletion zone

critical porosity: the porosity at which sediment grains convert from a suspended state to a condition where each grain touches at least one other grain

density inversion: a process in which dense, heavy sediment is deposited on top of fine-grained sediment and is thought to be one mechanism that produces polygonal faults and fractures.

GOM: Gulf of Mexico

HS-: Hashin-Shtrikman Lower Bound

HS+: Hashin-Shtrikman Upper Bound

LWD: logging-while-drilling

pdf: probability distribution function

polygonal faults (fractures): a unique polygonal grid of faults (fractures) that appear in fine-grained sediments as a result of syneresis.

syneresis: the spontaneous volumetric contraction of a gel without evaporation

Introduction

We show that either the Archie Equation or the Hashin-Shtrikman Lower Bound can be applied to resistivity logs to infer the concentration of dispersed hydrate in deep-water unconsolidated sediments. We apply each of these predictive functions to resistivity data acquired in wells across the two sites in the Green Canyon lease area that we selected for our research study. These analyses confirm that abundant hydrate exists at each site. Our log interpretations indicate that the hydrate-bearing interval is as thick as 725 m (2380 ft) at some locations inside our research sites. Across this hydrate interval, some units at each site have hydrate concentrations that exceed 60 percent of the available pore space.

Executive Summary

We present evidence that the classical Archie Equation that is used to interpret hydrocarbon concentration from resistivity logs in consolidated media may also be used to predict hydrate concentration in high-porosity, unconsolidated, deep-water sediments if appropriate constants are used to adjust the equation response to the resistivity of the medium that hosts deep-water hydrate. We present further evidence that the Hashin-Shtrikman Lower Bound is important for defining the response of any function that is used to estimate hydrate concentration from deep-water resistivity logs. Neither the Archie Equation nor the Hashin-Shtrikman Lower Bound should be used to interpret hydrate concentration when layers of pure hydrate are intercalated with sediment layers. An additional restriction is that the Hashin-Shtrikman Lower Bound should be used to estimate hydrate concentration only when hydrate is uniformly dispersed throughout the sediment and each sediment grain and each clathrate cluster is surrounded by brine. We apply the Hashin-Shtrikman Lower Bound and a calibrated formulation of the Archie Equation to resistivity logs acquired across our selected study areas in the Green Canyon lease area to build evidence that thick intervals of hydrate are present at each site and that some zones within these intervals have hydrate concentrations that exceed 60 percent of the pore space.

Published Examples of Logged Hydrate Intervals

We have selected four published examples of well log data acquired across hydrate-bearing intervals to illustrate the general petrophysical responses of log data when hydrate is present in a logged medium. Two of these logged hydrate systems are located in deep water, as are our Green Canyon study areas, and two systems are located onshore in arctic environments.

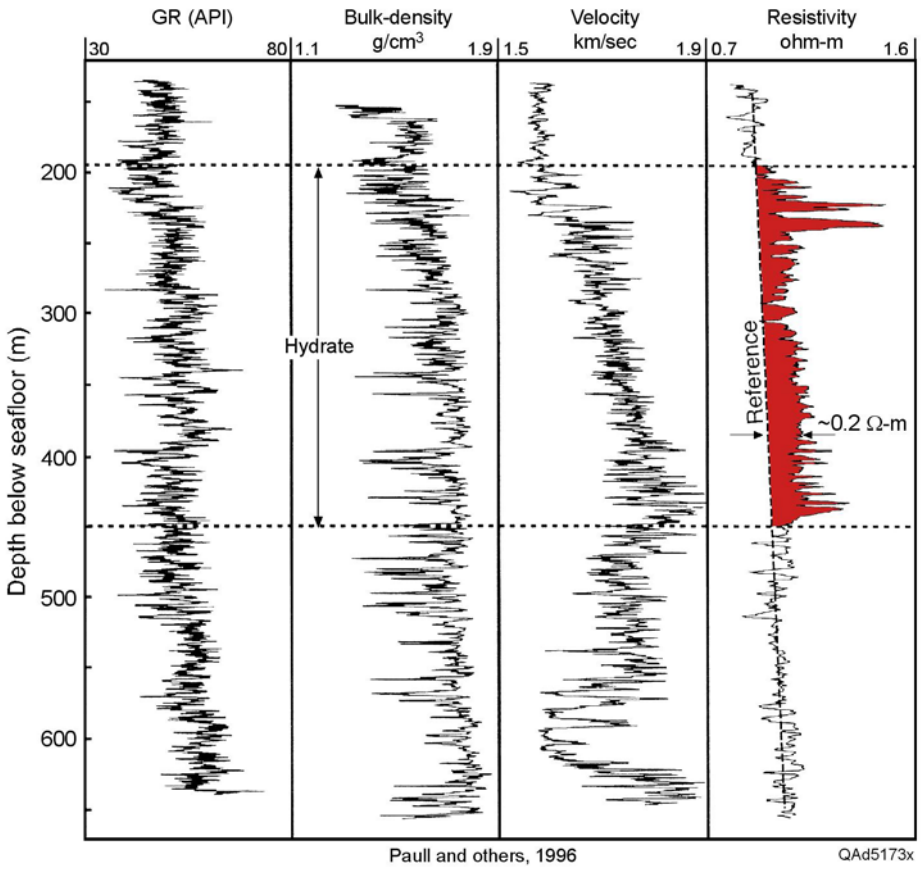

Figure 1. Well log data acquired in test hole 994D at Blake Ridge (Paull and others, 1996).

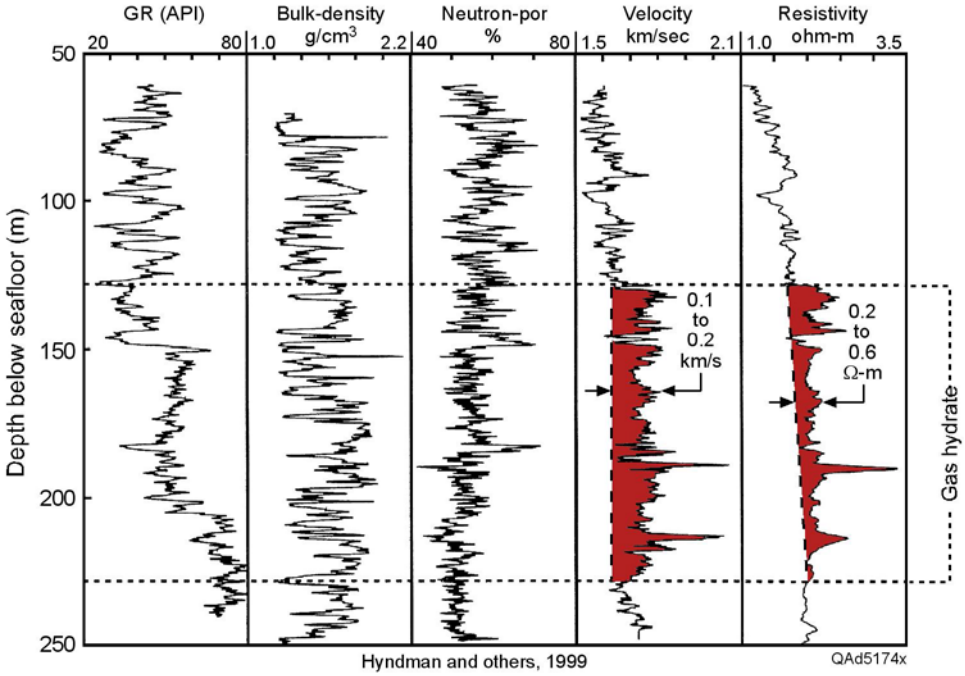

Figure 2. Log data acquired at Cascadia Margin (Hyndman and others, 1999)

Because the objective of the logging programs at each of these four sites was to study hydrate systems, complete log suites were acquired that included gamma-ray, resistivity, sonic, neutron porosity, and density data, and even an FMI log in at least one instance. Although we show several of the log curves from each of these published logging suites, we focus our attention on the gamma-ray and resistivity curves because gamma-ray and resistivity measurements are the only log data that are available across hydrate-bearing intervals at our Green Canyon study sites.

Offshore Examples

To date, most U.S.-based research related to deep-water hydrate systems has been done at Blake Ridge, offshore South Carolina, and at Cascadia Margin, offshore Oregon northward to offshore Canada. Logs across the interpreted hydrate interval at Blake Ridge are shown in Figure 1; logs describing the hydrate interval at Cascadia Margin are reproduced in Figure 2.

The log data displayed in Figure 1 are from one of three test holes that have been drilled at Blake Ridge and are excellent examples of the log responses across the hydrate interval at this site. Examination of the gamma-ray and resistivity curves illustrates the following principles that will be useful in our analysis of logs across our Green Canyon study sites:

1. The gamma-ray response indicates that the lithofacies across the hydrate zone is dominated by fine-grained sediments.
2. Resistivity increases by only 0.2 ohm-m across the hydrate-bearing interval.
3. An abrupt decrease in resistivity occurs at the base of the hydrate stability zone.

Collett and Ladd (2000) analyzed the resistivity data shown in Figure 1 and estimated hydrate concentration across the hydrate zone was approximately 10 percent. Lee (2000) analyzed the sonic log data and made similar estimates of hydrate concentration.

Equivalent principles are illustrated by resistivity and gamma-ray data acquired at Cascadia Margin (Fig. 2). Although the gamma-ray response indicates that there is a greater range of grain sizes at this Pacific coast site than at Blake Ridge, the amount of resistivity increase across the variable-grain-size hydrate interval is again a modest anomaly of only 0.2 to 0.6 ohm-m.

Onshore Examples

Onshore hydrate systems have been drilled and logged in several wells in the Prudhoe Bay area, North Slope, Alaska, and in the Mallik well in the Mackenzie Delta, Canada. Logs from one of the Prudhoe Bay wells (Northwest Eileen State 2) are displayed as Figure 3; logs from the Mallik well are plotted in Figure 4. The hydrate-bearing interval interpreted at each drilling location is identified on the log displays. Inspection of these logs shows the following petrophysical principles:

1. The gamma-ray log indicates a wide range of grain sizes across the hydrate-stability interval. Lithofacies vary from good-quality sands to high-quality shales.
2. The resistivity of a hydrate-bearing zone is 1 to 2 orders of magnitude greater than the resistivity measured across the deep-water hydrate zones that were logged at Blake Ridge and at Cascadia Margin (Figs. 1 and 2). The large difference between the resistivity of onshore and offshore hydrate systems is due mostly to the fact that the pore fluid at the onshore sites is fresh water, whereas the pore fluid at the offshore sites is a conductive brine.
3. The highest resistivity values occur in coarse-grain (sand) units.

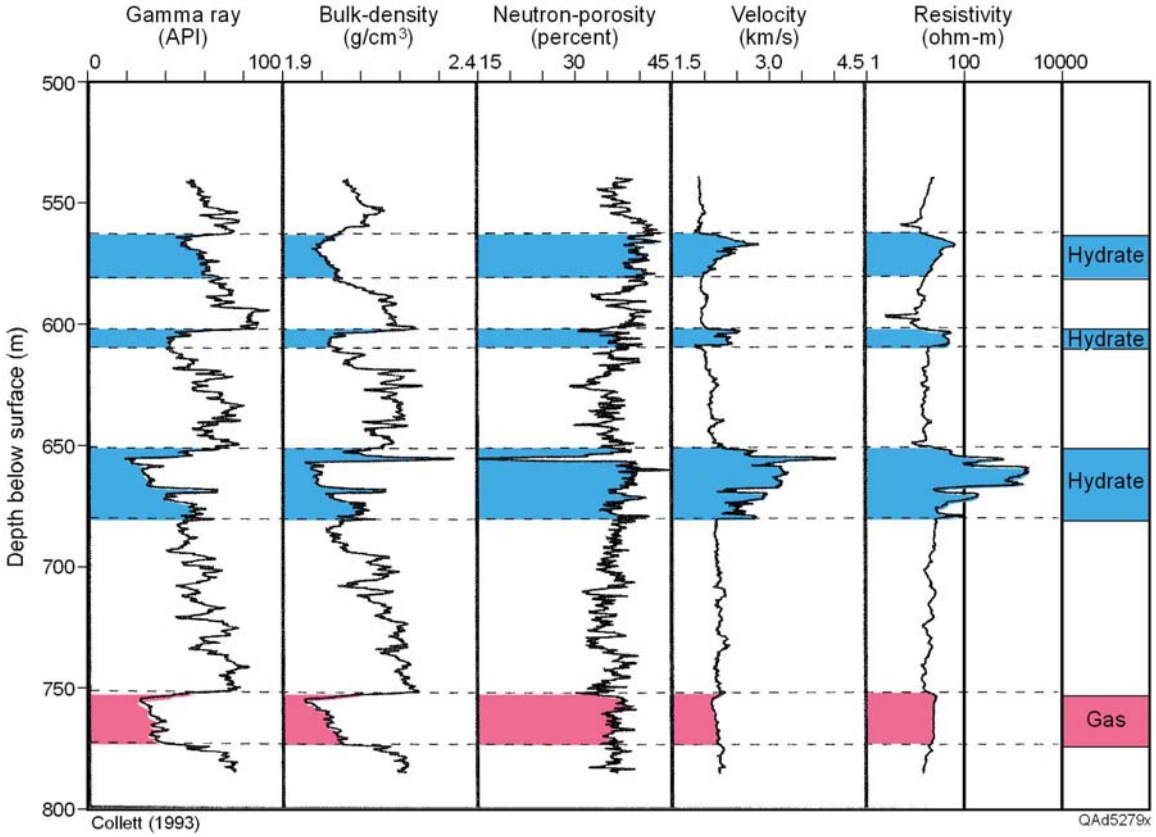

Figure 3. Log data acquired in the Northwest Eileen State 2 well, Prudhoe Bay, Alaska. (Collett, 1993).

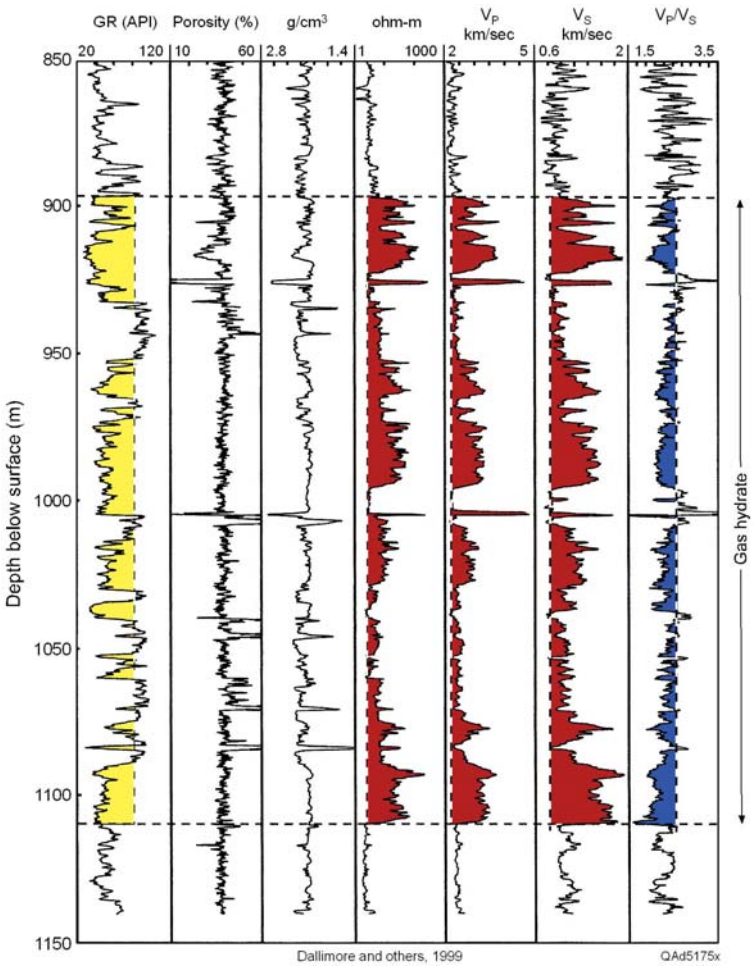

Figure 4. Log data acquired in the Mallik well, Mackenzie River Delta, Canada (Dallimore and others, 1999).

Unpublished Examples of Logged Hydrate Intervals

We have acquired unpublished log data from one GOM well that penetrated what several respected scientists and engineers think are significant hydrate intervals. This well is located in Alaminos Canyon Block AC818 approximately 400 km (250 mi) southwest of our study sites in Green Canyon. We have also seen log data from a second well drilled offshore Trinidad, approximately 1,000 km (600 mi) southeast of our selected study sites. This well penetrated an interval that the operator was convinced was a robust hydrate zone that caused severe drilling problems. We were not able to obtain permission to include these latter log examples in this report. Even though these wells are remote from the hydrate systems that we are studying, the logs acquired at these locations are valuable for our research because they come from GOM environments where sediment types, geothermal gradients, and thermogenic gas supplies are similar to those at Green Canyon.

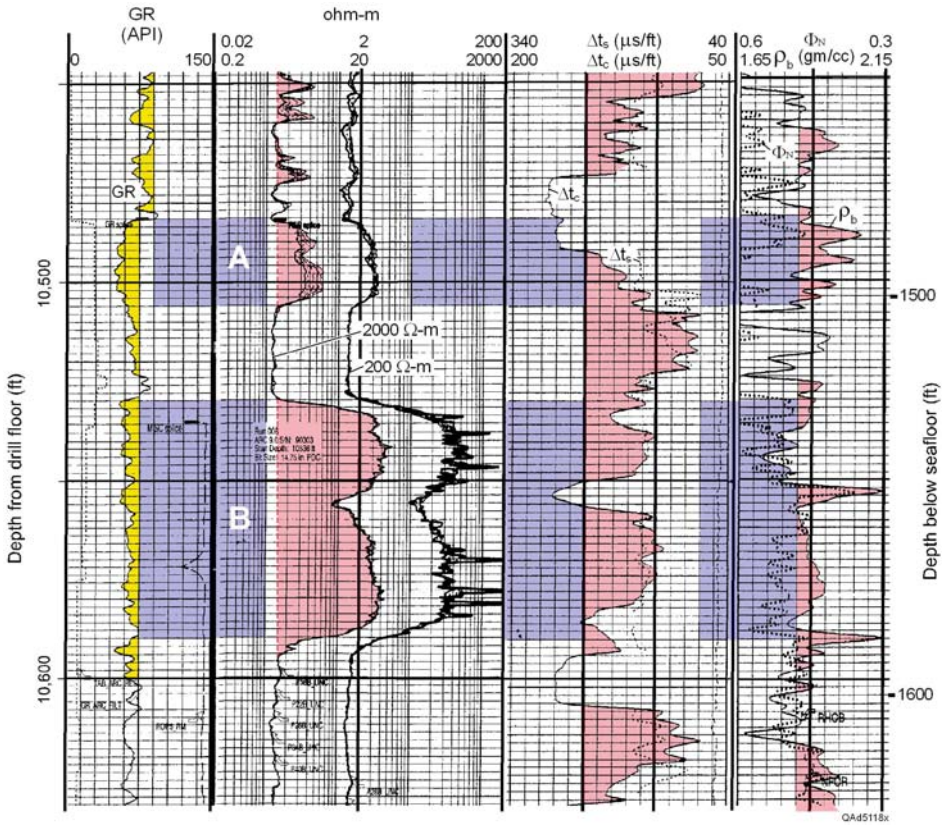

Figure 5. Log data acquired in Chevron's Tiger Shark well in Alaminos Canyon Block AC818, Gulf of Mexico. Water depth is 9,004 ft.

Alaminos Canyon

Log data from Chevron's Tiger Shark well in Alaminos Canyon Block AC818 are displayed as Figure 5. The colored shadings added to the logs are our interpretations of the hydrate system. Although this log suite includes several petrophysical measurements, we focus on only the resistivity and gamma-ray curves because these are the log types that have to be utilized in our study. Because of its high resistivity (~40 ohm-m), interval **B** is considered by Chevron and other members of the Joint Industry Project (JIP) to be a zone with a high concentration of hydrate. Lower resistivity intervals such as **A** (~4 ohm-m) are assumed to have lower concentrations of hydrate. Interpretation of the resistivity and gamma-ray data provides the following important guidelines for interpreting log data from Green Canyon hydrate systems:

1. The gamma-ray curve decreases toward the coarser-grain axis by only 15 API units across zone **B**, which is assumed to be an interval with a high concentration of hydrate.
2. The largest local deflection of the gamma-ray curve occurs across zone **A,** where there is a smaller resistivity response than at zone **B**.

We conclude that in the GOM, high concentrations of hydrate can occur in relatively fine grained sediment and that finer-grained sediment is sometimes a better nucleation site for hydrate than is coarser-grained sediment.

Resistivity Models of Sediment-Hydrate Systems

Log data across our Green Canyon hydrate study areas were acquired by petroleum companies who were interested in deep oil and gas targets, not in near-seafloor gas hydrate systems. Consequently, these companies acquired minimal lithofacies-sensitive log data consisting of only gamma-ray and resistivity measurements across shallow, near-seafloor intervals where hydrates occur. All other logs acquired across hydrate-bearing zones were measurements such as temperature and rate of penetration, which provided no useful lithofacies information. For this reason, any log-based evidence of subseafloor hydrates across Green Canyon lease blocks has to be inferred from resistivity logs.

We developed two Earth models to describe the resistivity properties of GOM hydrate systems. The first model, illustrated in Figure 6, assumes that hydrate is uniformly dispersed throughout the sediment. This model is appropriate for resistivity analyses of hydrate-sediment mixtures whether the hydrate is load-bearing or pore-filling. The only requirement is that each clathrate cluster and each mineral grain be surrounded by fluid except at their points of contact with neighboring hydrate clusters and mineral grains. This dispersed-hydrate model will be used as the principal Earth-resistivity model for our Green Canyon study sites.

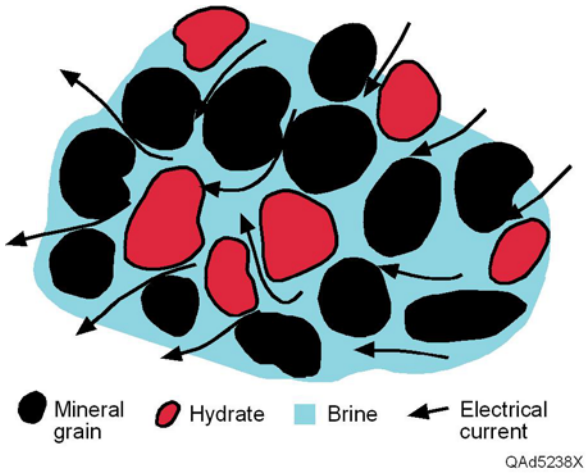

Figure 6. Resistivity model for a hydrate system in which hydrate is uniformly distributed throughout its host sediment. A fundamental assumption is that each mineral grain (black) and each clathrate cluster (red) is surrounded by conductive brine (blue), which creates a many pathways for electrical current flow (arrows).

Our second model, illustrated in Figure 7, assumes that the hydrate is layered. This model allows pure-hydrate layers to be either horizontal (Fig. 7a) or vertical (Fig. 7b). Although this layered-hydrate model will not be utilized in this

report, it is a resistivity model that may apply to some GOM hydrate systems and deserves consideration. We call attention to several zones in the logs shown later in which hydrate appears to be present as layers having high hydrate concentration (Fig. 23, Well E; Fig. 25a; Fig. 26a). This model is intriguing in that it illustrates that a layered-hydrate system can have a high resistivity, similar to that of resistors connected in series, if the pure-hydrate/sediment layering is perpendicular to the direction in which resistivity is measured (Fig. 7a), but a low resistivity, like that of resistors connected in parallel, if the layering is parallel to the direction of the resistivity measurement (Fig. 7b). In both situations, the layer geometries have the same amount of hydrate in a unit Earth volume. The arrow drawn beside each layered system shows the direction in which the sonde measures Earth resistivity. The terms “perpendicular layering” and “parallel layering” are defined relative to this indicated measurement direction of the sonde.

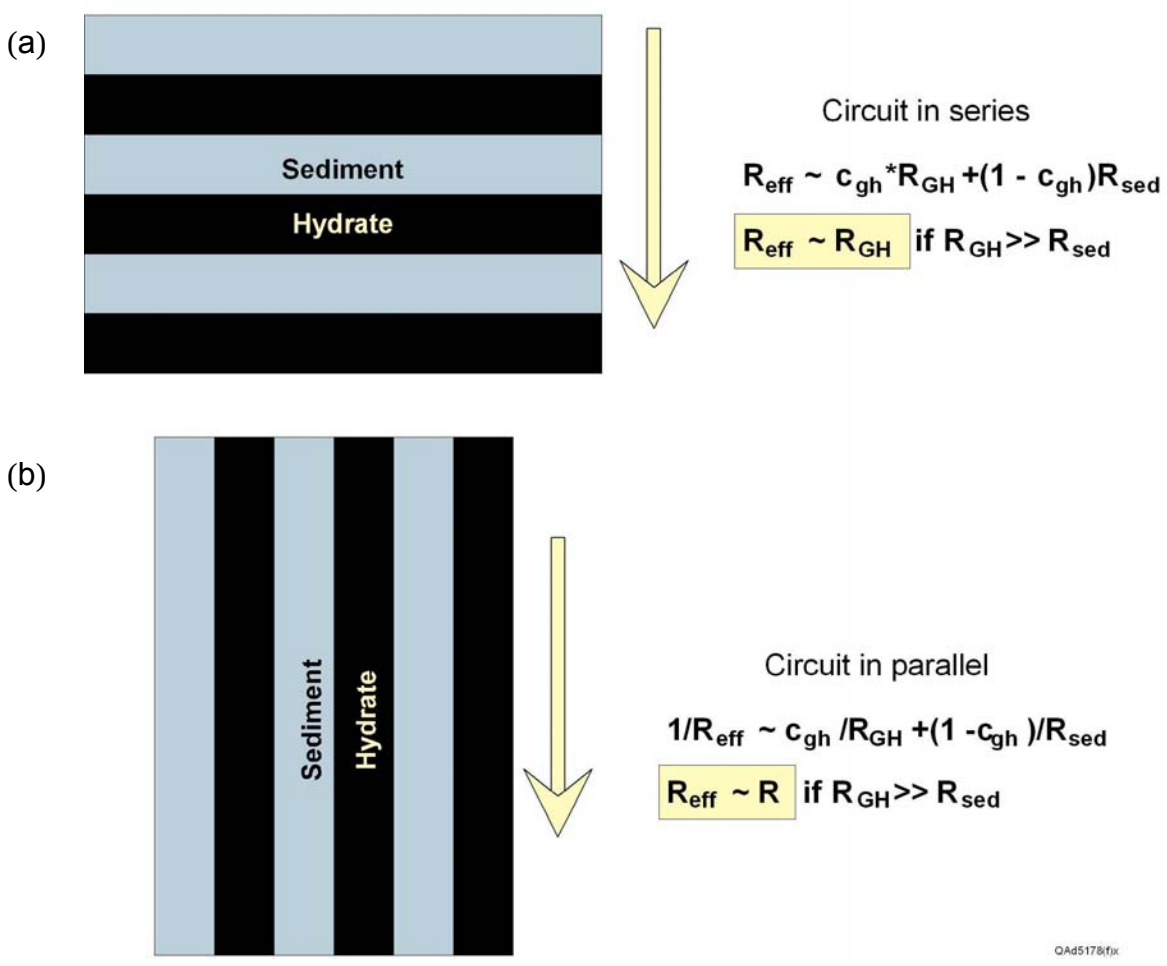

Figure 7. Resistivity model for a hydrate system in which hydrate is not disseminated throughout the host medium but occurs as pure-hydrate layers that are intercalated with layers of sediment. This model can be used for horizontal layering (a) or for vertical dikes and fractures (b). C_{gh} is the fraction of gas hydrate in the Earth volume for which effective resistivity R_{eff} is measured. Arrows show the direction in which resistivity is measured.

The possibility that hydrate may occur as vertical dikes in fine-grained sediments (Fig. 7b) is gaining favor with some deep-water hydrate researchers. This vertical-layer concept is based on the principle of **polygonal faults** and **polygonal fractures**, which are now recognized in many basins (Cartwright and others, 2003). A photograph of sand-filled polygonal fractures in a lithified dolomitic mud is shown as Figure 8. Larger-scale polygonal fault features can be seen in 3D seismic time slices displayed in Figure 9. These phenomena, whether at a fracture scale (cm) or at a fault scale (km), are assumed to be caused by (1) **syneresis**, the spontaneous volumetric contraction of a gel without evaporation, or (2) **density inversion**, a situation where denser (heavier) sediment is deposited atop a fine-grained layer, or (3) a gravity sliding of a weak, fine-grained interval (Cartwright and others, 2003). Deep-water, fine-grained sediments that form the host medium for many GOM hydrates are an ideal “gel” material in which any of these mechanisms, particularly syneresis, can occur.

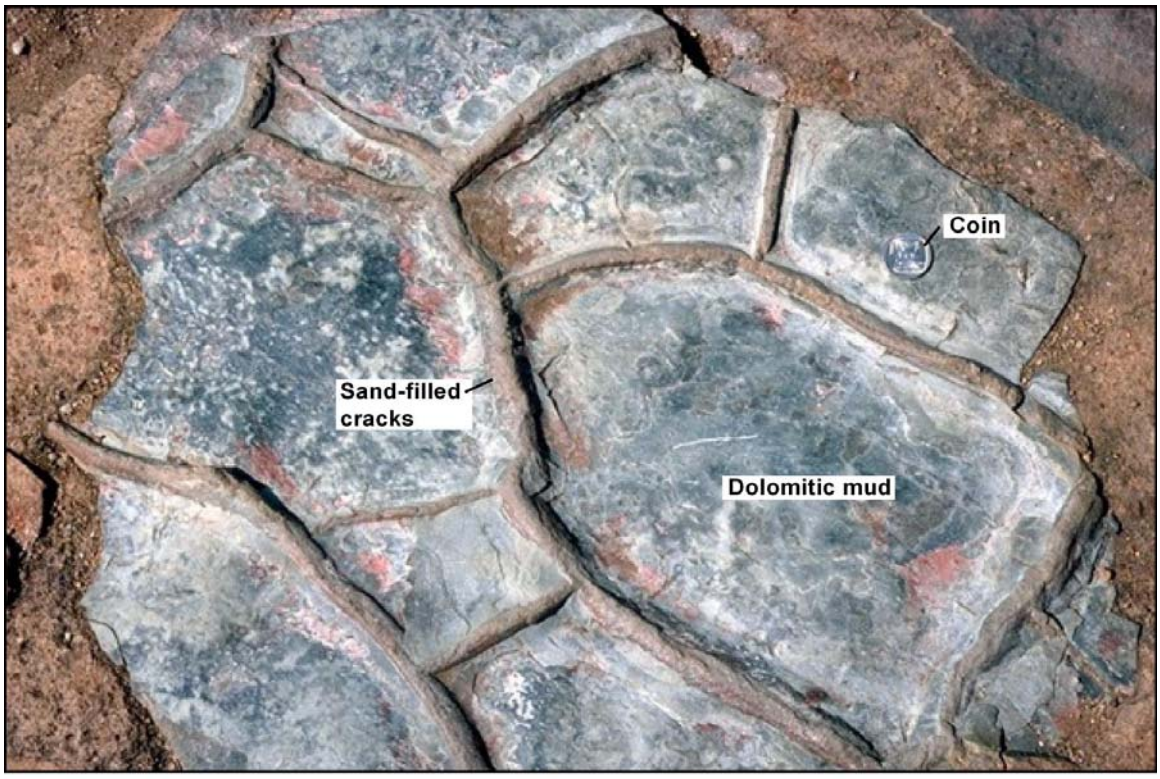

Figure 8. An outcrop of lithified dolomitic mud having a grid of sand-filled polygonal fractures. Photograph taken near Bourke’s Luck, South Africa, by Bruce M. Simonson, Department of Geology, Oberlin College.

To date, polygonal faults have not been observed in the GOM. However, polygonal faults were not noticed in other basins (for example the North Sea) until the 1980's, so the recognition of these features seems to require that a deliberate search has to be done to reveal their presence. Polygonal fractures, which are below the scale of seismic resolution, could be abundant across the GOM, yet difficult to recognize.

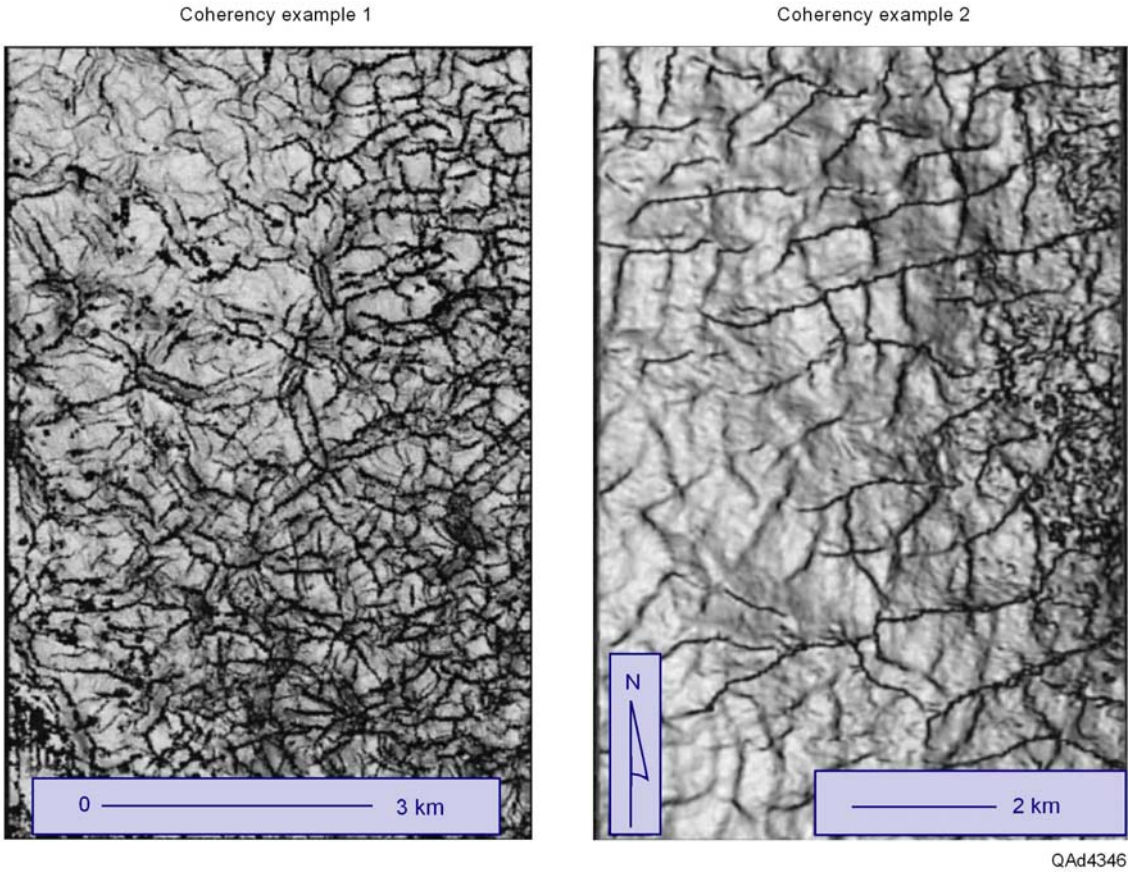

Figure 9. Time slices through 3D seismic coherency volumes showing polygonal faults extending through a fine-grained interval (Cartwright and others, 2003)

Archie Equation

The Archie Equation has been used to analyze resistivity responses of fluid-filled porous rocks for more than 6 decades (Archie, 1942). The clay-free form of this equation, with which we begin our analysis, can be written as

(1) $R = (aR_W\Phi^{-m})(S_W)^{-n}$,

where

- R = resistivity of the logged interval (ohm-m),
- a = dimensionless parameter related to the grain shape,
- R_W = resistivity of the pore fluid (ohm-m),
- Φ = porosity (dimensionless fraction),
- m = dimensionless parameter related to the cementation of the grains,
- S_W = water saturation (dimensionless fraction), and
- n = saturation exponent (a dimensionless parameter).

In a later section, we will utilize a corrected form of this equation that includes the effect of clay minerals on sediment resistivity. Because the Archie Equation is an empirical model, when it is applied to a specific rock matrix and a specific type of pore fluid, parameters a, m, and n must be derived and adjusted to create optimal agreement between resistivity readings and independent knowledge of R_W, Φ, and S_W for that rock-fluid system. In typical oil and gas reservoir applications, a is ~1.0, n = 2, and m usually ranges from 2.0 to 2.5.

There is limited experience in applying the Archie Equation to high-porosity mixtures of sediment, brine, and hydrate. In their analysis of the Blake Ridge resistivity data shown as Figure 1, Collett and Ladd (2000) used the following values for their formulation of the Archie Equation: a = 1.05, m = 2.56, n = 2, and R_W = 0.23 ohm-m. We cannot find the exact value of R_W that was used in their Blake Ridge study. We know only that the pore fluid salinity was assumed to be 32,000 ppm. If the hydrate formation temperature is assumed to be 65ºF, then R_W = 0.23 ohm-m. Given our application of the Hashin-Shtrikman bounds that will be discussed in the following sections, we conclude that the parameter values used for the Archie Equation at Blake Ridge are not optimal for high-porosity unconsolidated sediments found in deep water. In our formulation of the Archie Equation, we alter the values to a = 1.0, m = 1.2, n = 2, and R_W = 0.17 ohm-m. A value of m = 1.2 for unconsolidated sediments has been suggested by other researchers (Archie, 1942; Sen and others, 1981; Mendelson and Cohen, 1982). Our reasoning for these parameter choices will be further explained as we discuss our second analytical resistivity model, the Hashin-Shtrikman Lower Bound.

Hashin-Shtrikman Bounds

Calculation of Hashin-Shtrikman bounds is a valuable analysis technique for defining the maximum and minimum values that can be observed for magnetic, electrical, and thermal properties of rock systems that are mixtures of several distinct minerals and fluids (Hashin and Shtrikman, 1962). Previously, we have used Hashin-Shtrikman bounds to guide our logic as we developed rock-physics models that describe P-wave velocity (V_P) and S-wave velocity (V_S) behavior in deep-water hydrate systems that are mixtures of quartz, clay, hydrate, and brine and have found the functions to be invaluable for understanding the elastic properties of these complex mixtures (Hashin and

Shtrikman, 1963). We now expand our application of Hashin-Shtrikman bounds to analysis of the resistivity behavior of sediment-hydrate-brine mixtures.

We use the Earth model illustrated in Figure 6 to describe the sediment-hydrate-brine mixture that needs to be analyzed. For this medium, the Hashin-Shtrikman Upper Bound (**HS+**) for resistivity is given by

$$(2)\quad R_{HS+}^{-1} = \sigma_{HS-} = \sigma_{\min} + \frac{A\_}{1-\alpha\_A\_}$$

where subscript HS- indicates the Hashin-Shtrikman Lower Bound and

$$(3)\quad A\_ = \sum_{i=2}^{N} \frac{f_i}{(\sigma_i - \sigma_{\min})^{-1} + \alpha\_}$$

$$(4)\quad \alpha\_ = \frac{1}{3\sigma_{\min}}$$

In this notation, σ_i is the conductivity and f_i is the volume fraction of the ith constituent component of the mixture, with σ_1 being the minimum conductivity and σ_N the maximum conductivity of the individual components that form the mixture. The Hashin-Shtrikman Lower Bound (**HS-**) for resistivity is given by

$$(5)\quad R_{HS-}^{-1} = \sigma_{HS+} = \sigma_{\max} + \frac{A_+}{1-\alpha_+ A_+}$$

where

$$(6)\quad A_+ = \sum_{i=1}^{N-1} \frac{f_i}{(\sigma_i - \sigma_{\max})^{-1} + \alpha_+}$$

$$(7)\quad \alpha_+ = \frac{1}{3\sigma_{\max}}$$

Using subscripts Q for quartz, cl for clay, w for brine, and gh for gas hydrate, we defined the following values as conductivities of the constituent components of the deep-water medium:

(8) $\sigma_1 = \sigma_Q = 10^{-14}$ S/m,

(9) $\sigma_2 = \sigma_{gh} = 10^{-6}$ S/m,

(10) $\sigma_3 = \sigma_{cl} = 10^{-3}$ S/m, and

(11) $\sigma_4 = \sigma_W = 3$ S/m.

The order of this conductivity sequence is important because it is the "minimum-to-maximum" order of parameters that are required in the Hashin-Shtrikman theory, and the order conforms to the subscripting notation used in Equations 3 and 6.

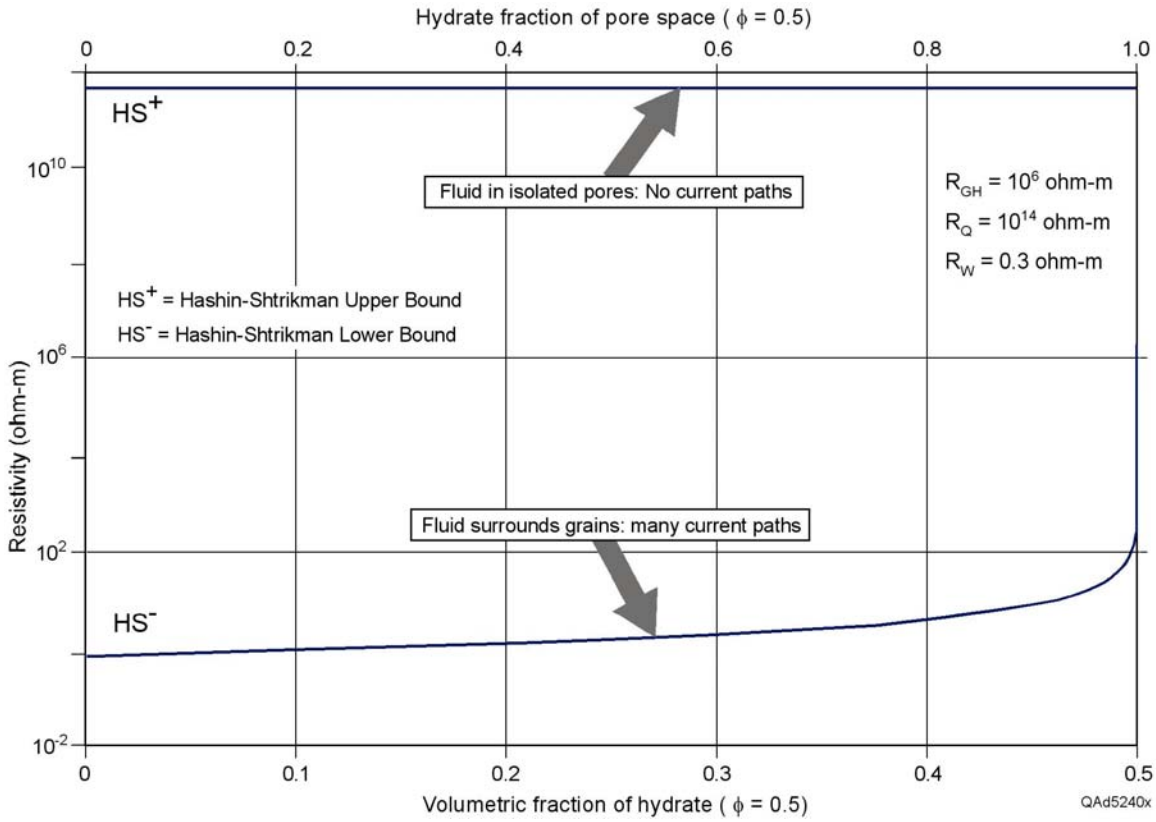

Figure 10. Hashin-Shtrikman Upper Bound (HS+) and Lower Bound (HS-) calculated for a mixture of quartz grains, hydrate, and brine. Porosity is assumed to be 0.5. The calculation is based on the dispersed-hydrate model illustrated in Figure 6.

We used these conductivity values and the dispersed-hydrate model illustrated in Figure 6 to calculate the Hashin-Shtrikman bounds. Graphical representations of the upper and lower resistivity bounds are illustrated in Figure 10, assuming that the porosity of the medium is 0.5. The range between upper and lower bounds is huge—approximately 10^{12} ohm-m. The upper bound is shown only for completeness of the analysis because this bound represents the hypothetical, physically unrealistic case in which conductive brine resides in isolated, unconnected pores and does not form any continuous conductive paths through the material. This assumption is invalid for most rocks and certainly is incorrect for deep-water, near-seafloor, high-porosity, hydrate-bearing sediments.

In contrast, the Hashin-Shtrikman Lower Bound represents resistivity behavior that results when brine surrounds each matrix grain and each hydrate clathrate cluster and creates a huge number of interconnected brine-filled paths for electrical current to pass through the sediment-brine-hydrate system. These current paths are shown by arrows in the dispersed-hydrate model depicted in Figure 6. Conditions associated with the Hashin-Shtrikman Lower Bound are a good description of the hydrate-sediment-brine mixture that exists in deep-water hydrate systems.

Hashin-Shtrikman Lower Bound

An analysis by Wempe (2000) is particularly germane to our study of the resistivity response of hydrate dispersed throughout unconsolidated, high-porosity, near-seafloor sediments. A key graphic of Wempe's study is reproduced as Figure 11a. Our modification of this graphic is shown as Figure 11b. In these figures, the horizontal axis is porosity and the vertical axis is normalized resistivity $\mathbf{R/R_W}$, where R is the resistivity measured across a medium of porosity $\mathbf{\Phi}$ and R_W is the resistivity of the fluid that fills the pores. The interval labeled $\mathbf{\Phi_C}$ defines the range of **critical porosity**, which is porosity where the grains of a high-porosity medium convert from a suspended state to a load-bearing condition in which each grain touches at least one other grain. Critical porosity varies from about 0.3 for poorly sorted sediments, to around 0.4 for well-sorted rounded grains, to about 0.6 for highly oblate (flat) grains.

The data plotted in Figure 11 are comprehensive and include laboratory measurements and field data gleaned from 11 studies referenced by Wempe (2000). A key concept demonstrated by these data (Fig. 11b) is that the resistivity behavior of all porous media converge to the Hashin-Shtrikman Lower Bound (HS-) when the porosity of the medium equals or exceeds critical porosity. Because the porosity of the deep-water, near-seafloor sediments that span the hydrate stability zone in the Green Canyon area equals or exceeds critical porosity, we are led to an important conclusion: *the Hashin-Shtrikman Lower Bound is an ideal function for describing the resistivity of deep-water hydrate systems.*

The Hashin-Shtrikman Lower Bound that we calculated in Figure 11 is replotted in Figure 12 to better illustrate how the resistivity of deep-water sediment varies as a function of hydrate concentration. As hydrate concentration increases from 0 to 60 percent of the pore space, resistivity increases from ~0.6 ohm-m to only 2 ohm-m. The implication is that with 60 percent of the pore space occupied by hydrate, a large number of connected paths of conductive brine continue to wend through the mixture (Fig. 6).

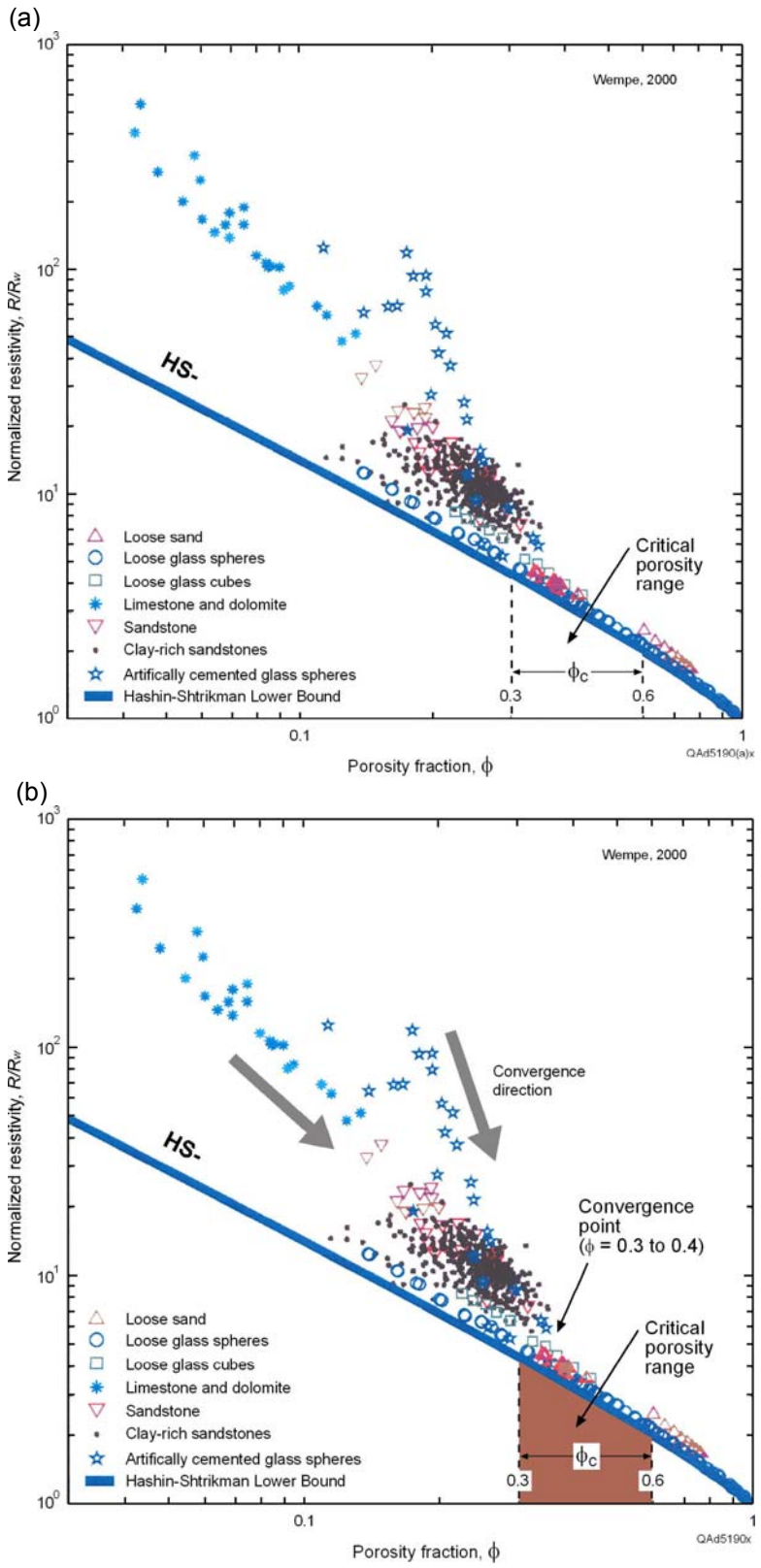

Figure 11.
(a) Crossplot of normalized resistivity (R/R_W) and porosity for a large number of laboratory tests and field-data observations that involve a wide range of conductive media (Wempe, 2000).
(b) Our modification of the crossplot to emphasize principles important for deep-water hydrate systems. R is measured resistivity; R_W is the resistivity of the pore-filling fluid. The shaded interval Φ_C is the range of critical porosity for grains of different geometrical shapes. Note that all data converge to the Hashin-Shtrikman Lower Bound as porosity increases and enters the critical-porosity range.

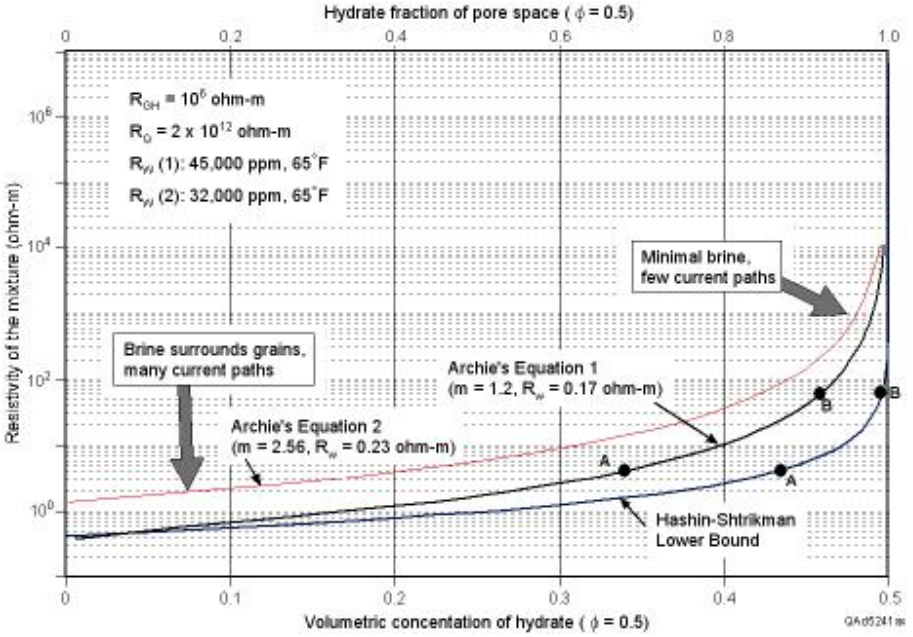

Figure 12. The Hashin-Shtrikman Lower Bound (HS-) and two formulations of the clay-free form of the Archie Equation (Eq. 1) displayed as functions of resistivity and hydrate fraction. Hydrate fraction is defined in terms of the pore volume (top axis) or the unit volume (bottom axis). Archie Equation 1 is our formulation for deep-water hydrate systems. Archie Equation 2 was proposed by Collett and Ladd (2000). We stress this fundamental principle: deep-water mixtures of sediment and dispersed hydrate must have resistivities that agree with, or approximate, the Hashin-Shtrikman Lower Bound. Points **A** and **B** show where zones A and B of the Alaminos Canyon well (Fig. 5) would be on the two preferred calibration curves.

Even when hydrate fills 80 percent of the pore space, there are enough current flow paths that the resistivity increases to only 4 ohm-m. One factor that keeps the resistivity of this sediment-brine-hydrate mixture at a low value, even though the hydrate concentration is high, is that as hydrate grows, it expels salt into the surrounding brine and makes the brine more conductive. In terms of electrical conductivity, a smaller number of electrical-current flow paths through this higher-salinity brine are equivalent to a larger number of flow paths through a reduced-salinity brine. In our analysis, however, we do not decrease pore-fluid resistivity as hydrate concentration increases. Using this constraint of a constant pore-fluid resistivity, the Hashin-Shtrikman Lower Bound implies that a significant increase in resistivity does not occur until hydrate concentration exceeds 90 percent of the pore space and the number of connected brine-filled paths is severely reduced.

Included in Figure 12 is a curve labeled **Archie Equation 1** that describes the resistivity behavior of the clay-free form of the Archie Equation (Eq. 1) that we think is appropriate for the hydrate systems that we are studying across Green Canyon. Also included is a curve (**Archie Equation 2**) that describes how the Archie Equation developed by Collett and Ladd (2000) at Blake Ridge would appear. The difference between the responses of these two Archie Equations is

created by different choices for **m** and $\mathbf{R_W}$. Specifically, the parameter values used in these two formulations of the Archie Equation are

Parameter	Collett and Ladd	Our Choice
a	1.05	1.0
m	2.56	1.2
n	2.0	2.0
Rw	0.23 ohm-m	0.17 ohm-m

We present the following arguments to support our parameter choices for the Archie Equation:

1. A major contributor to the difference between the two Archie Equations is the different values (2.56 versus 1.2) for the cementation exponent, m. Studies by Sen and others (1981) and by Mendelson and Cohen (1982) show that m should be reduced to approximately 1.2 for unconsolidated sediments. Cementation exponent values of approximately 2.5 are appropriate for consolidated rocks but appear to be inappropriate for unconsolidated sediments.
2. The valuable study by Wempe (2000) summarized in Figure 11 forces us to conclude that any resistivity equation that is used to analyze deep-water hydrate systems when porosities are equal to or greater than critical porosity must have a functional behavior that approximates the Hashin-Shtrikman Lower Bound. Our version of the Archie Equation is a reasonable approximation of the Hashin-Shtrikman Lower Bound (Fig. 12). We think that an Archie Equation that uses a large value of m deviates too far from the Hashin-Shtrikman Lower Bound and does not represent true resistivity conditions of a deep-water hydrate-sediment-brine mixture.
3. We use a value of 0.17 ohm-m for R_W because we assume that the pore fluid has a salinity of 45,000 ppm rather than 32,000 ppm, as was assumed by Collett and Ladd (2000) in their analysis of Blake Ridge resistivity logs. Pore fluid across a hydrate interval should have increased salinity because in converting local brine into clathrate cages, the hydrate-forming process expels NaCl and retains H_2O. The magnitude of salinity increase is unknown. We found one resistivity log in our study area to which the logging contractor added the comment that pore fluid salinity was 45,000 ppm. We decided to use that salinity value when we calculated Archie Equation 1 displayed in Figure 12.

Applying the Hashin-Shtrikman Lower Bound in Figure 12 to the resistivity log acquired in the Alaminos Canyon well (Fig. 5) suggests that the hydrate saturation in zones A and B differ by only 10 percent (0.88 vs. 0.98 of the pore space), even though the resistivity across the two zones differs by an order of magnitude (4 ohm-m vs. 40 ohm-m). The positions of zones A and B on the Hashin-Shtrikman Lower Bound and on the Archie Equation 1 curves are shown in Figure 12.

Laboratory Confirmation of Resistivity Behavior

The resistivity behaviors of the Hashin-Shtrikman Lower Bound and Archie Equation that we use for estimating hydrate concentrations are crucial and need to be confirmed by laboratory experiments, core analyses, and actual hydrate production tests whenever possible to determine the limitations and validity of these predictive models. We know of only one laboratory test that has measured the electrical conductivity of a simulated high-porosity hydrate-sediment mixture. The experimental data are shown as Figure 13. These tests were done by Professor Santamarina and his colleagues and students at Georgia Tech. Results were presented as a poster at the AAPG Hedberg Hydrate Conference in 2004.

In this experiment, measurements of electrical conductivity were made for clay and sand sediments that had a porosity of 0.37 and three different magnitudes of associated hydrate concentrations: 0, 50, and 100 percent of the available pore space. Test data (Fig. 13) show that electrical conductivity decreases by a factor of approximately 2 as hydrate concentration increases from 0 to 50 percent, which would cause resistivity to increase by a factor of approximately 2, just as indicated by the Hashin-Shtrikman Lower Bound (Fig. 12). Test data further indicate that conductivity decreases by 3 orders of magnitude (or resistivity increases by 3 orders of magnitude) as hydrate concentration increases from 50 to 100 percent of the pore space. However, the lab data do not define whether this large resistivity change is a linear or nonlinear function of hydrate concentration over this latter test range.

The Hashin-Shtrikman Lower Bound in Figure 12 indicates that the resistivity of a high-porosity mixture of mineral grains, hydrate clathrate clusters, and brine increases by about 3 orders of magnitude as the hydrate fraction grows from 50 to 100 percent of the pore space, in good agreement with the laboratory data. Our predictive equations further specify that the rate of change of resistivity in this mixture is highly nonlinear with respect to hydrate concentration, with most of the resistivity change occurring when the hydrate concentration exceeds 90 percent of the pore volume.

Well Log Database

The well logs illustrated in this report are replicas of hardcopy logs that we amassed across the Green Canyon area. We did not acquire digital log data for this study. The only log data that we could locate that measured properties of the hydrate stability zone were gamma-ray, resistivity, conductivity, temperature, and rate-of-penetration data. Strangely, no shallow log suites from the Green Canyon area included hole-caliper data. In some wells there were several resistivity curves, each one specifying resistivity at a different depth of investigation or presenting the resistivity data at a different display scale. We created a consistent petrophysical definition of the hydrate-bearing interval at each well by extracting only two log curves from each log suite: (1) the gamma-ray response and (2) a consistent depth-of-investigation resistivity curve, with this latter curve displayed by a scale ranging from 0 to 2 ohm-m.

(a)

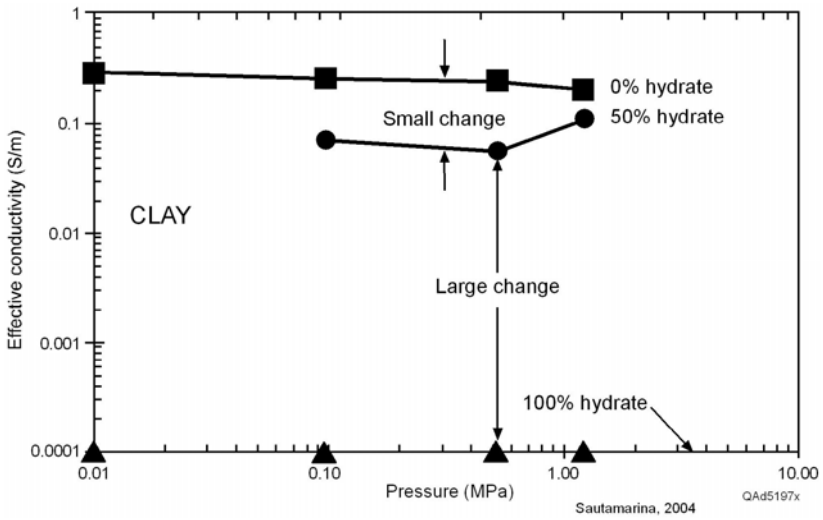

(b)

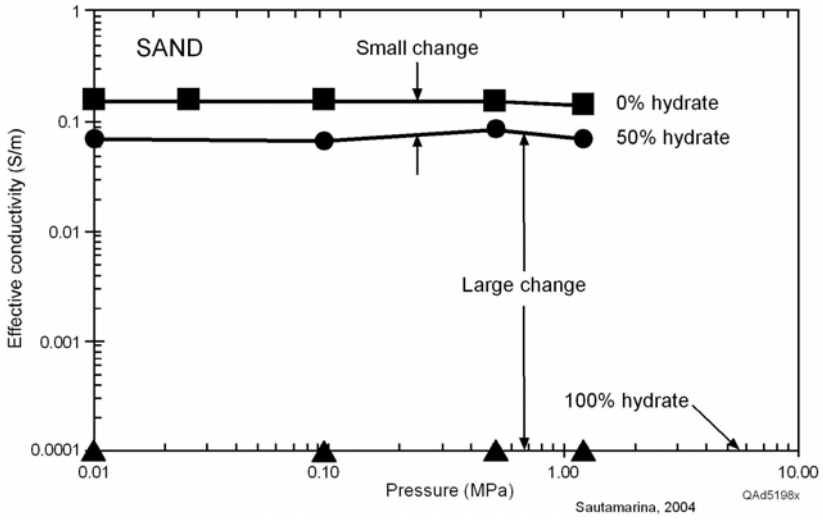

Figure 13. Laboratory measurements of the conductivity of homogeneous mixtures of quartz grains and simulated hydrate (Santamarina and others, 2004).

The most valuable data came from wells in which logging-while-drilling (**LWD**) technology was used to measure the resistivity of the hydrate stability zone. In some wells logged with LWD technology, there were short cyclic bursts of incorrect gamma-ray and resistivity responses at intervals of 90 ft (or at some multiple of 90 ft) when a new 90-ft section of drill pipe was added to the drill string. In these instances, the LWD system exhibited some type of temporary instability when a new 90-ft section of pipe was inserted into the data-communication link to the downhole sonde. These erroneous gamma-ray and

resistivity responses typically spanned only 10 to 20 ft (3 to 6 m) and were easily recognized. We identify some of these noise bursts in Figure 24 (Well H) and in Figure 32 (Well 6).

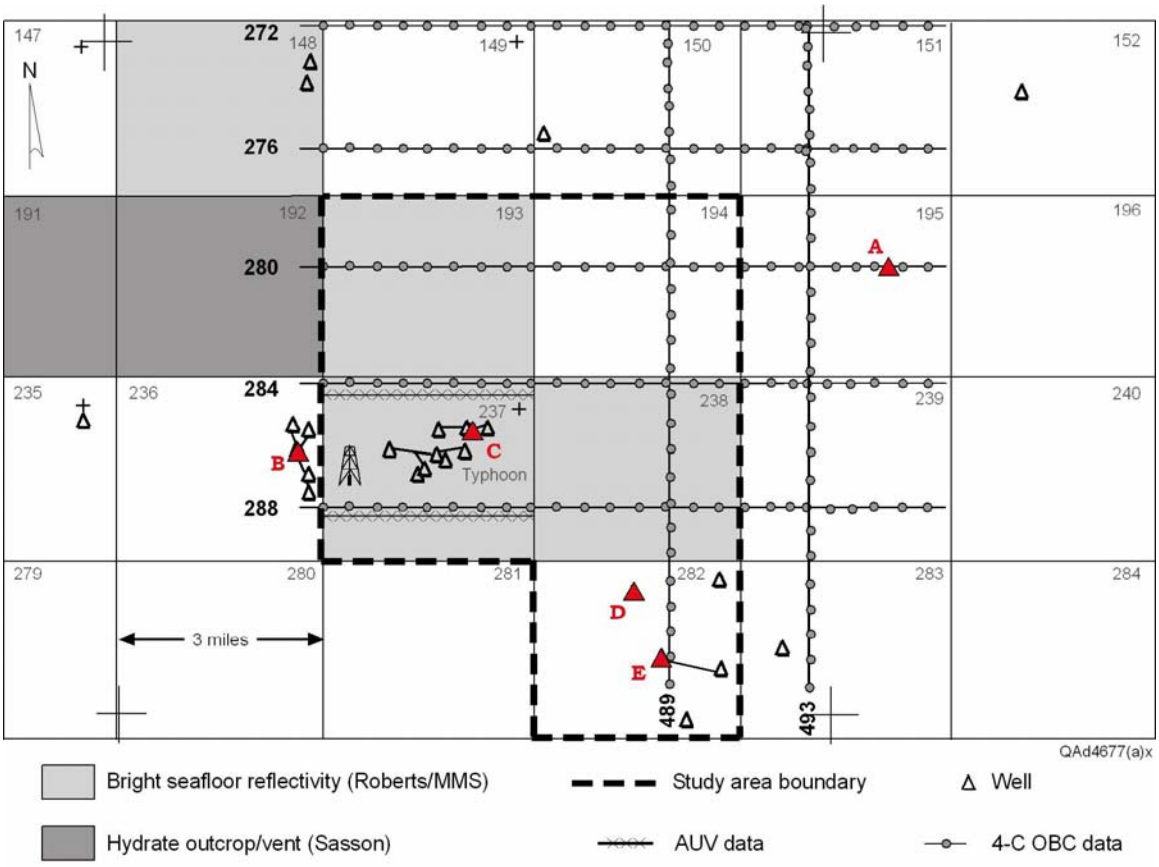

Figure 14. Map of Study Site 1, surrounding lease blocks, and local wells. Wells where log data existed that could be used for hydrate analysis are marked as lettered red triangles.

We interpreted the gamma-ray and resistivity curves on our hardcopy log plots, marked key intervals and important log features, and then passed our work to skilled draftspeople. Our drafting section used a digital scanner to make digital images of these marked hardcopies, traced the gamma-ray and resistivity curves, and replicated our interpretations of the data. Each drafted copy was then reviewed for accuracy. In each report figure that displays log data, we add labels that identify the lease block number and API number of the well from which the data were acquired. Readers can then locate the same log data and check the validity of our reproduced log curves if they wish to do so.

Well Log Data across Study Site 1

The Green Canyon lease blocks that we selected as our Study Site 1 are outlined in Figure 14. Superimposed on this map as lettered red triangles are the locations of five wells (A, B, C, D, E) where log data have been acquired that can be used to estimate hydrate concentration. Unfortunately, many of the wells in this local area were drilled in the 1980's before the widespread use of LWD technology. Logs from most of these wells could not be used for analyzing the hydrate system beneath Study Site 1 because, without LWD technology,

1. the acquisition of log data often started at depths below the base of the hydrate stability zone, or
2. the hydrate interval was not logged until several days after the interval was drilled and some hydrate had dissociated near the well, or
3. the resistivity sonde sometimes exhibited unacceptably poor sensitivity across intervals of near-seafloor sediment.

Wells local to Study Site 1 where log data were examined and found to not be useful for hydrate calibration are defined in Figure 15.

Well log cross sections along the profile of calibration wells B, C, and A and along the trend of wells B, D, and E are displayed as Figures 16 and 17, respectively. Only gamma-ray and resistivity data are used in these figures. Because these log data were acquired using LWD technology within a few minutes of the bit penetrating each logged depth, the data should define in situ resistivity before any significant hydrate dissociation occurred. The base of the hydrate stability zone (**BHSZ**) that is drawn on each profile was determined using the model that Milkov and Sassen (2001) developed. This Milkov/Sassen model is preferred for estimating the subseafloor depth of the BHSZ horizon rather than other estimation options because their model is based on the chemistry of gases venting from the seafloor in nearby Block GC185 and on geothermal gradients that are local to our study area.

The Milkov/Sassen estimation of the subseafloor thickness of the hydrate stability zone is shown by the three solid-line curves in Figure 18. These curves show that the BHSZ boundary moves deeper as the amount of methane decreases in the local natural gases and there is a greater percentage of heavier gases (ethane, butane, propane) trapped in the clathrate structures. We have added a fourth dash-line curve to this Milkov/Sassen model to represent (approximately) a natural gas that has 85-percent methane, which is a common gas chemistry across the GOM and a gas hydrate guideline suggested by scientists at the Minerals Management Service.

In Figures 16 and 17, the upper boundary of the hydrate-bearing interval labeled **BHDZ** represents the inferred base of the hydrate depletion zone. Above this horizon, hydrate is absent through chemical interactions with sulfates migrating down from the seawater, or by thermally induced dissociation caused by spin-off eddies from the warm Loop Current, or because of other biological, chemical, and physical processes.

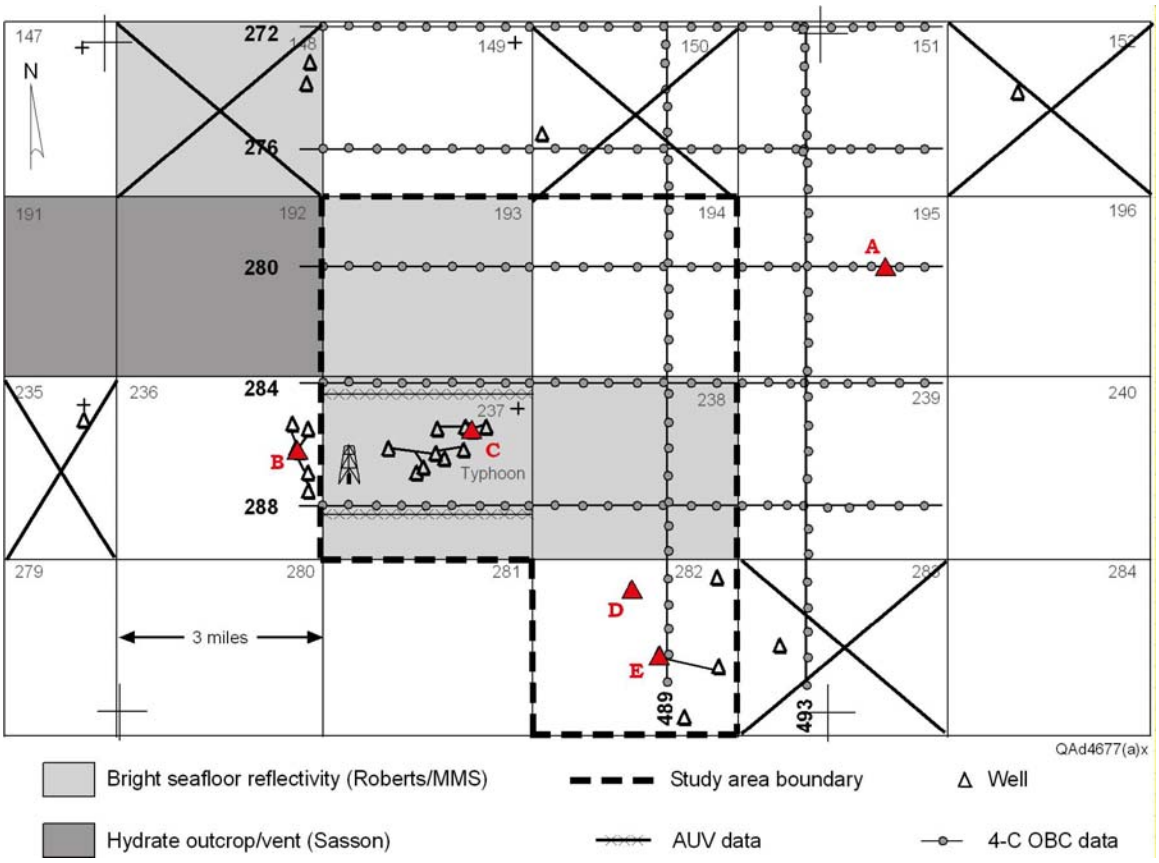

BLOCK	COMMENT
148	Logs start below hydrate zone
150	Logs start below hydrate zone
152	Poor-quality logs (1985 vintage)
235	Logs start below hydrate zone
283	No resistivity log

Figure 15. Wells local to Study Site 1 where log data could not be used for hydrate analysis. Blocks where unacceptable log data occur are marked with an X.

With resistivity behavior defined by the Hashin-Shtrikman Lower Bound and our Archie Equation 1 (Fig. 12) as guides, resistivity values less than 1 ohm-m represent low hydrate concentrations, typically less than 20 percent. Zones on the resistivity logs that have resistivities greater than 1 ohm-m are shaded gray on the cross-section profiles to define intervals that have increased hydrate concentration. Several intervals where grain size increases are shaded yellow on the gamma-ray curves indicate possible reservoir-quality lithofacies. Blue-shaded layers define units where increased resistivity (shaded red) indicates an increase in hydrate concentration internal to these larger-grain facies.

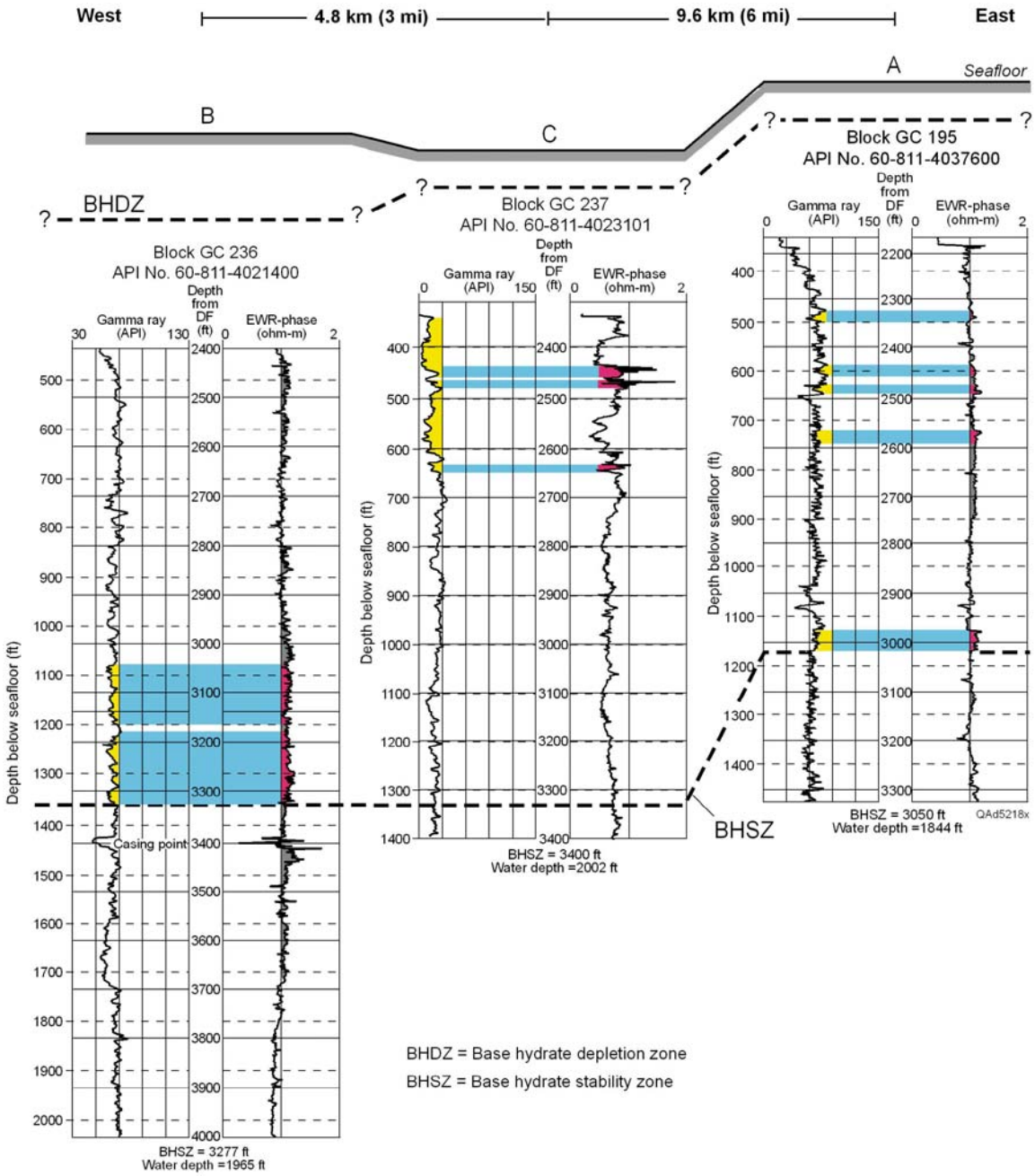

Figure 16. Well log cross section across calibration wells **B**, **C**, **A**, Study Site 1. There is a low concentration of hydrate along this profile. Well locations defined in Figure 14. The BHSZ depth labeled below each log suite is the depth of the base of the hydrate stability zone associated with the 90.4 percent methane curve in Figure 18. At each well, the BHSZ horizon is drawn at a resistivity anomaly that is “close to” the depth coordinate interpolated from this 90.4 percent methane curve. Gray zones emphasize intervals where resistivity exceeds 1 ohm-m. Yellow zones indicate larger-grain facies. Red identifies units that have both increased grain size and increased resistivity.

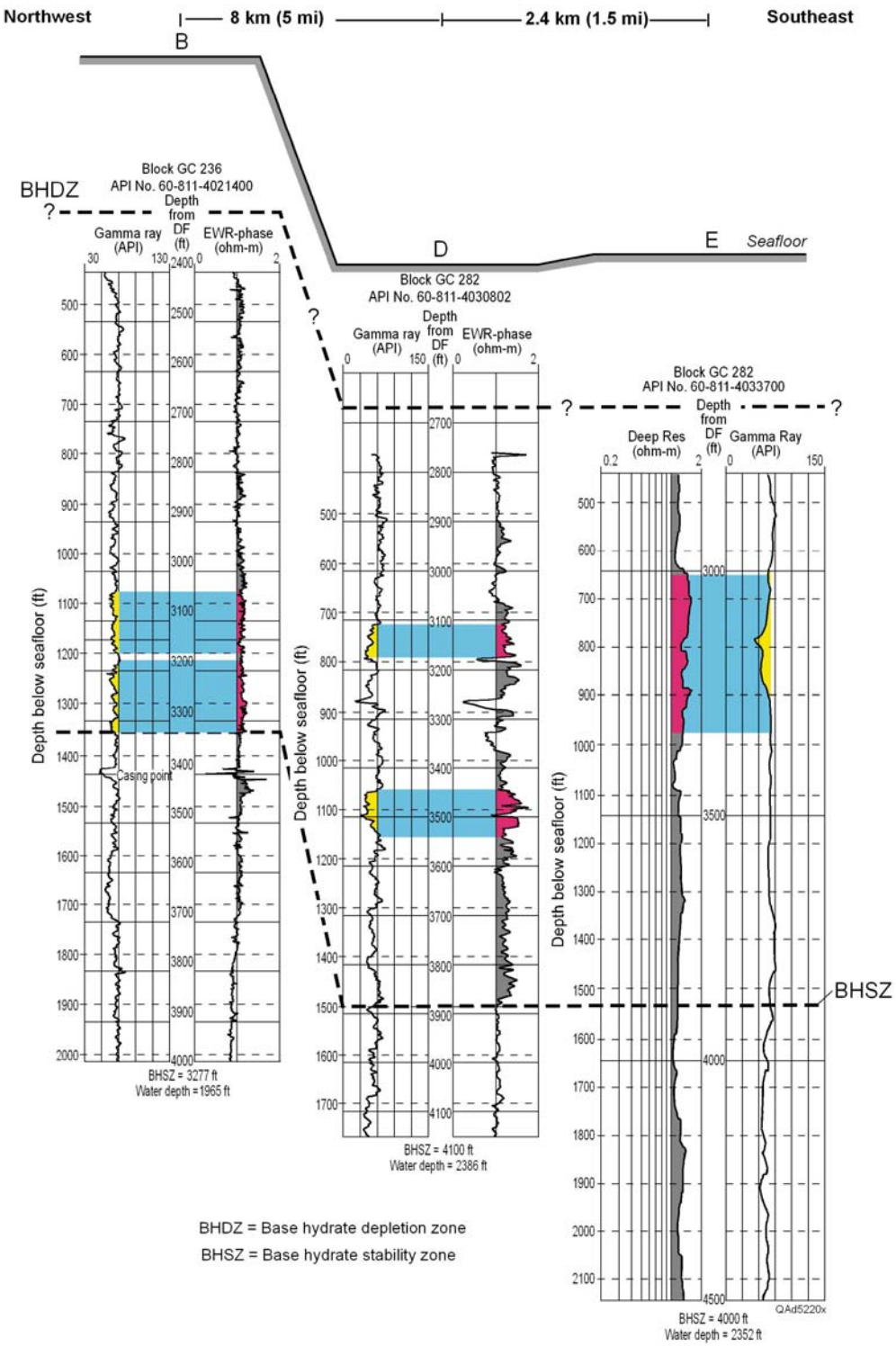

Figure 17. Well log cross section along the profile of calibration wells **B**, **D**, **E**, Study Site 1. Well locations defined in Figure 14. Concentration of hydrate increases along the southeast part of this profile. Horizon BHSZ, colors, and shadings are explained in the caption of Figure 16.

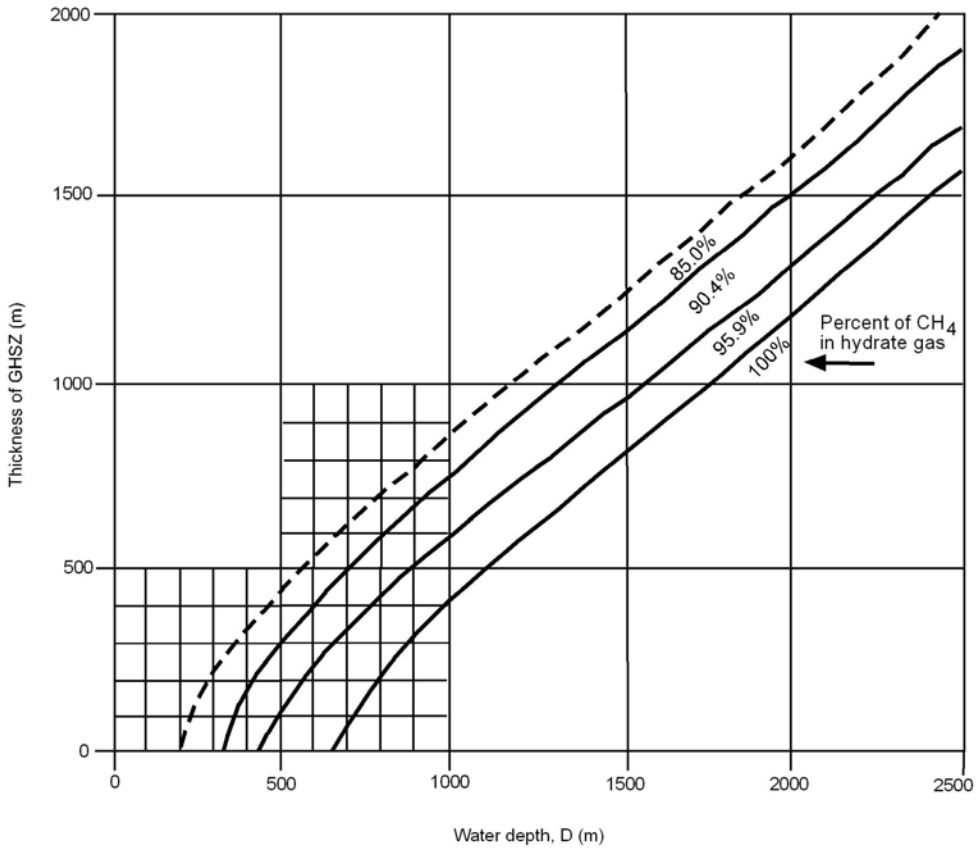

Figure 18. Thicknesses of hydrate stability zones for various water depths and gas chemistries. The three solid-line curves were developed by Milkov and Sassen (2001) and are based on gas chemistry from Block GC185 near our study sites and on local geothermal gradients. The dash-line curve is our approximation of the behavior of the thickness of the stability zone for a natural gas that has 85-percent methane, a gas chemistry favored by some scientists at the Minerals Management Service. We added a detailed coordinate grid that covers the range of water depths encountered across our research area.

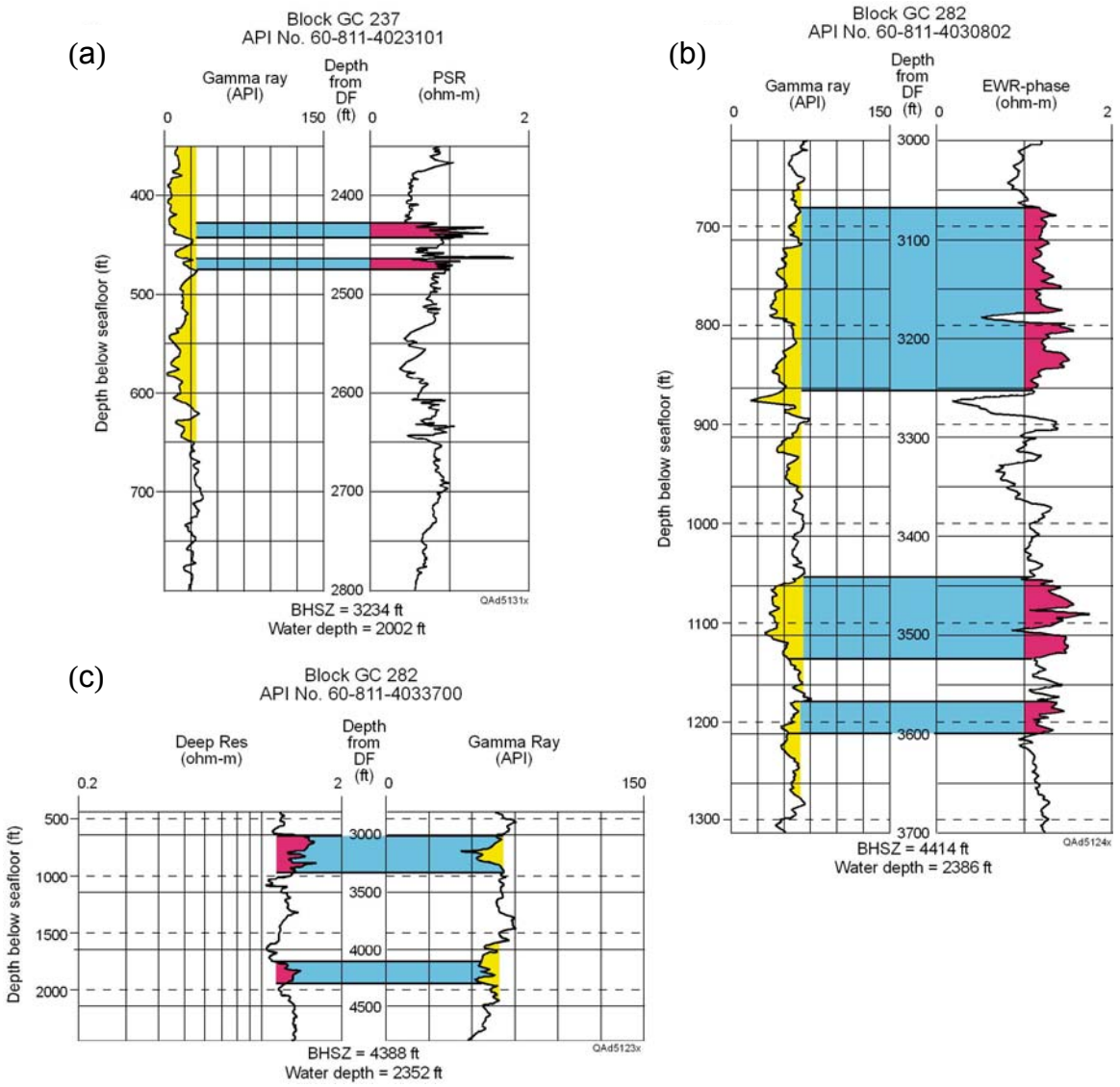

Figure 19. Examples of specific hydrate zones, Study Site 1. Larger-grain lithofacies are shaded yellow on the gamma-ray curve. Zones of increased resistivity within these larger-grain intervals are shaded red. The logs in panel (c) differ from all other logs in our database in that the logging contractor interchanged the positions of the gamma-ray and resistivity curves and used a depth scale of 1 inch = 1,000 ft to display the data. The shaded hydrate zone at the top of panel (c) is huge, with a thickness of about 350 ft (~106 m). The log curves in (c) were stretched to match the depth scales of other logs in cross section BDE (Fig. 17, Well E).

These blue/red zones are candidates for hydrate production tests because they are not only a better reservoir facies but also represent a local increase in the concentration of hydrate. Expanded views of some of these hydrate-concentration zones are displayed in Figure 19.

Some observations that can be made upon examining the resistivity data in Figures 16 through 19 are:

1. The hydrate-bearing interval beneath Study Site 1 spans approximately 460 m (~1,500 ft).

2. The resistivity relationships defined in Figure 12 imply the hydrate concentration within the zone of hydrate stability ranges from about 20 to 40 percent of the available pore space.

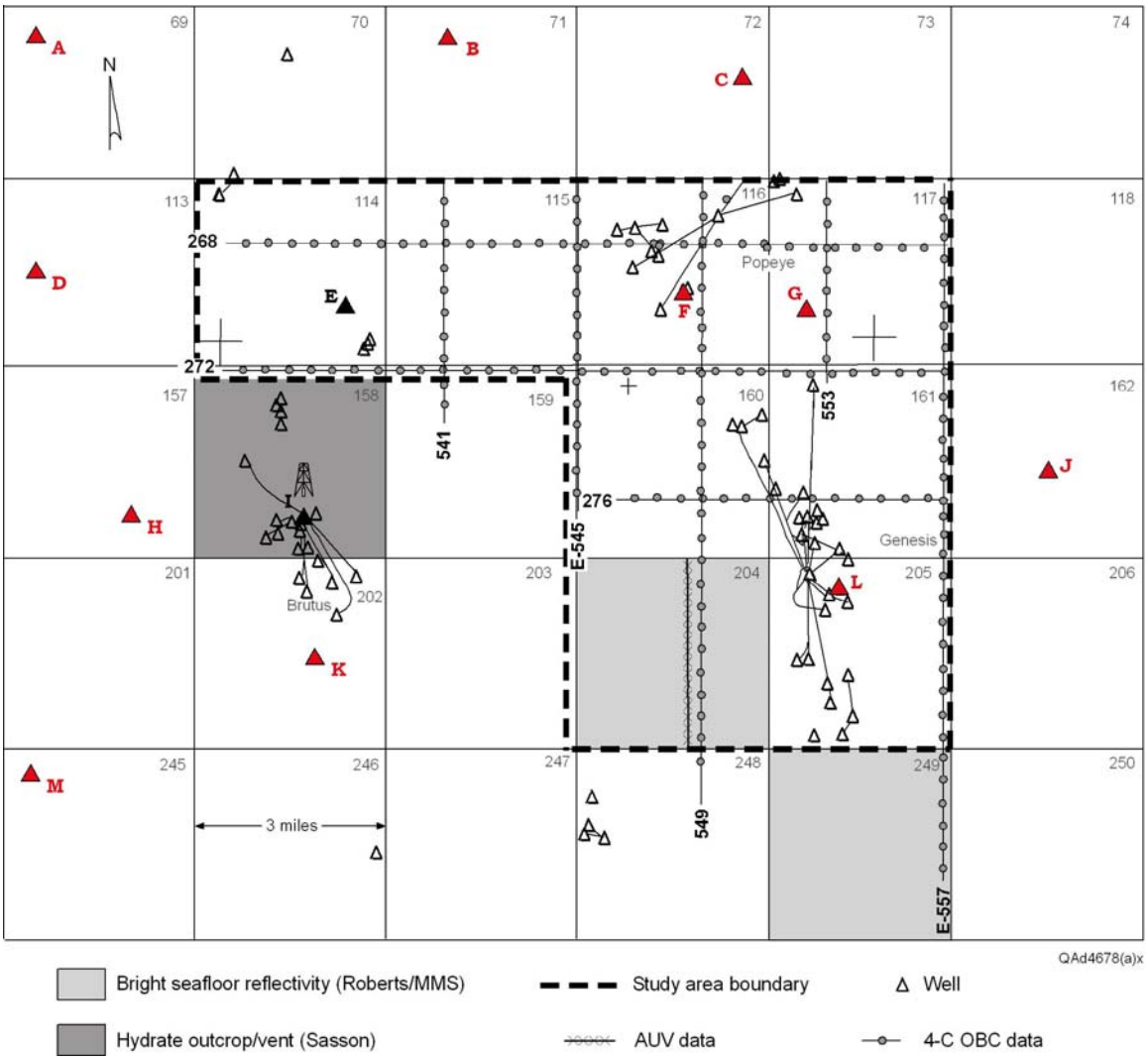

Figure 20. Map of Study Site 2, surrounding lease blocks, and local wells. Wells where log data exist that can be used for hydrate analysis are marked as lettered red triangles.

Well Log Data across Study Site 2

The lease blocks chosen for Study Site 2 are outlined in Figure 20. The red triangles define wells where log data exist that are appropriate for

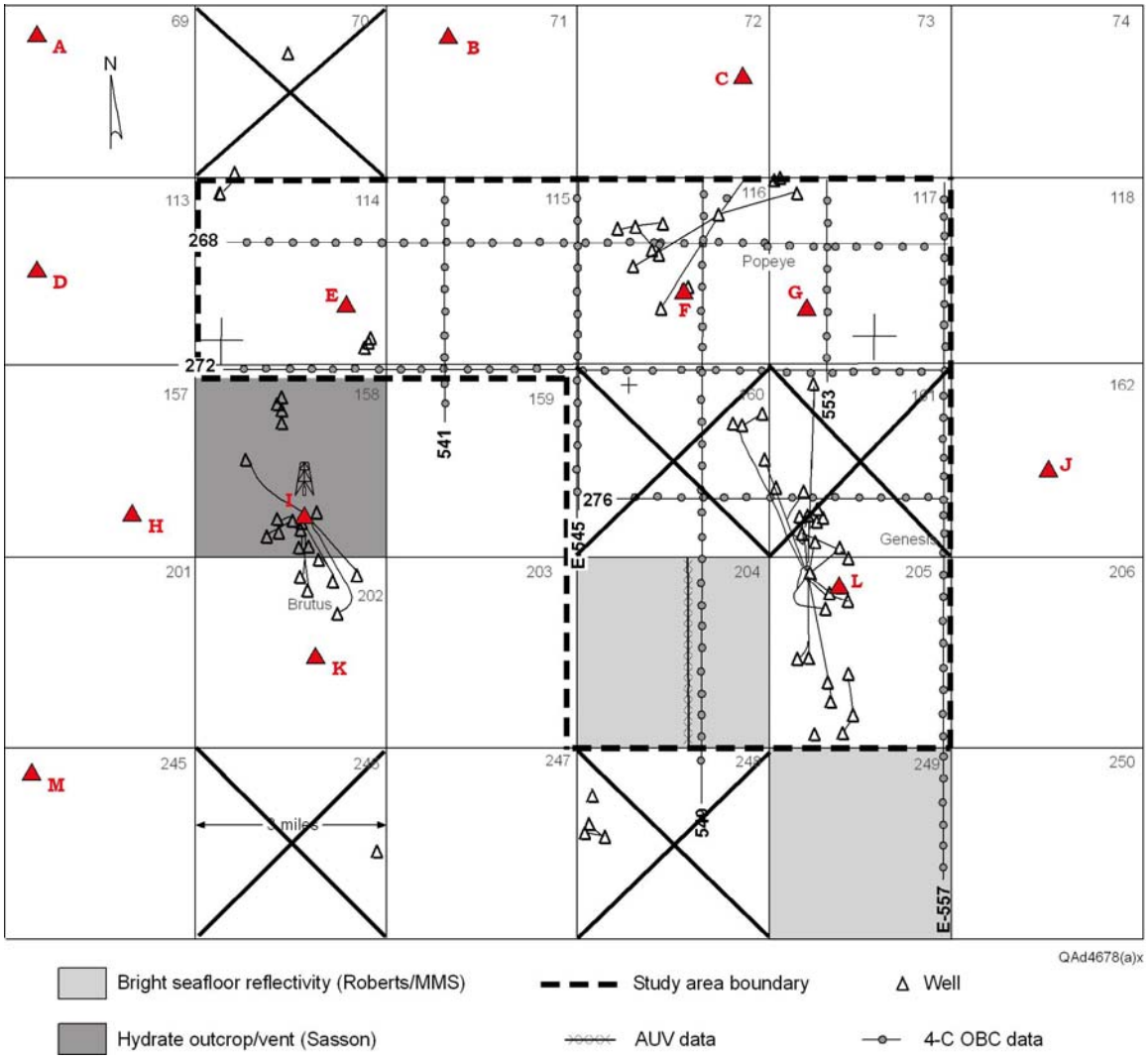

BLOCK	COMMENT
70	Poor-quality logs (1984 vintage)
160	Drilled from Block 205
161	Drilled from Block 205
246	Cannot find logs
248	Cannot find logs

Figure 21. Wells local to Study Site 2 where log data could not be used for hydrate analysis. Blocks where unacceptable log data occur are marked with an X.

determining hydrate concentration. There are more hydrate-calibration wells (13) across Study Site 2 than across Study Site 1 (5) because more wells were drilled in the area of Study Site 2 after the early 1990's, when LWD logging technology was widely used by GOM operators. We document in Figure 21 those lease

blocks local to Study Site 2, where log data were examined but not found to be useful for hydrate calibration.

These numerous calibration wells allow a variety of cross-section profiles to be made across Study Site 2. We show west-to-east profiles along wells A, B, C in Figure 22, along wells D, E, F, G in Figure 23, and along wells H, I, L, J in Figure 24. The BHSZ horizons drawn on these profiles were defined in the same manner as that done at Study Site 1 using the Milkov and Sassen (2001) model defined in Figure 18. In interpreting these resistivity profiles, we used the following guidelines dictated by our Archie Equation 1 and the Hashin-Shtrikman Lower Bound (Fig. 12):

1. A resistivity value ≤1 ohm-m indicates a hydrate concentration of <20 percent.
2. Resistivities >1 ohm-m indicate hydrate concentration in excess of 20 percent, with a resistivity of 2 ohm-m representing a hydrate concentration of about 60 percent.
3. Reduced gamma-ray readings indicate larger-grain sediment (shaded yellow), and within some of these larger-grain intervals are units (shaded blue/red) with relatively high hydrate concentration.

These log data imply that a particularly robust hydrate system extends across Study Site 2. Specifically the data indicate that

- The hydrate interval varies from about 365 m (~1,200 ft) at wells A and B (Fig. 22) to about 760 m (~2,500 ft) at well I (Fig. 24). Well D (Fig. 23) is unusual in that the resistivity response indicates that no hydrate is present.
- Hydrate occupies 20 to 40 percent of the pore volume over most of the interval between the boundaries marked BSRZ and BHSZ.

Numerous units, some as thick as approximately 50 ft (~15 m) have hydrate concentrations that exceed 60 percent, for example the intervals labeled **A** in Figures 25b, 26a, and 27b.

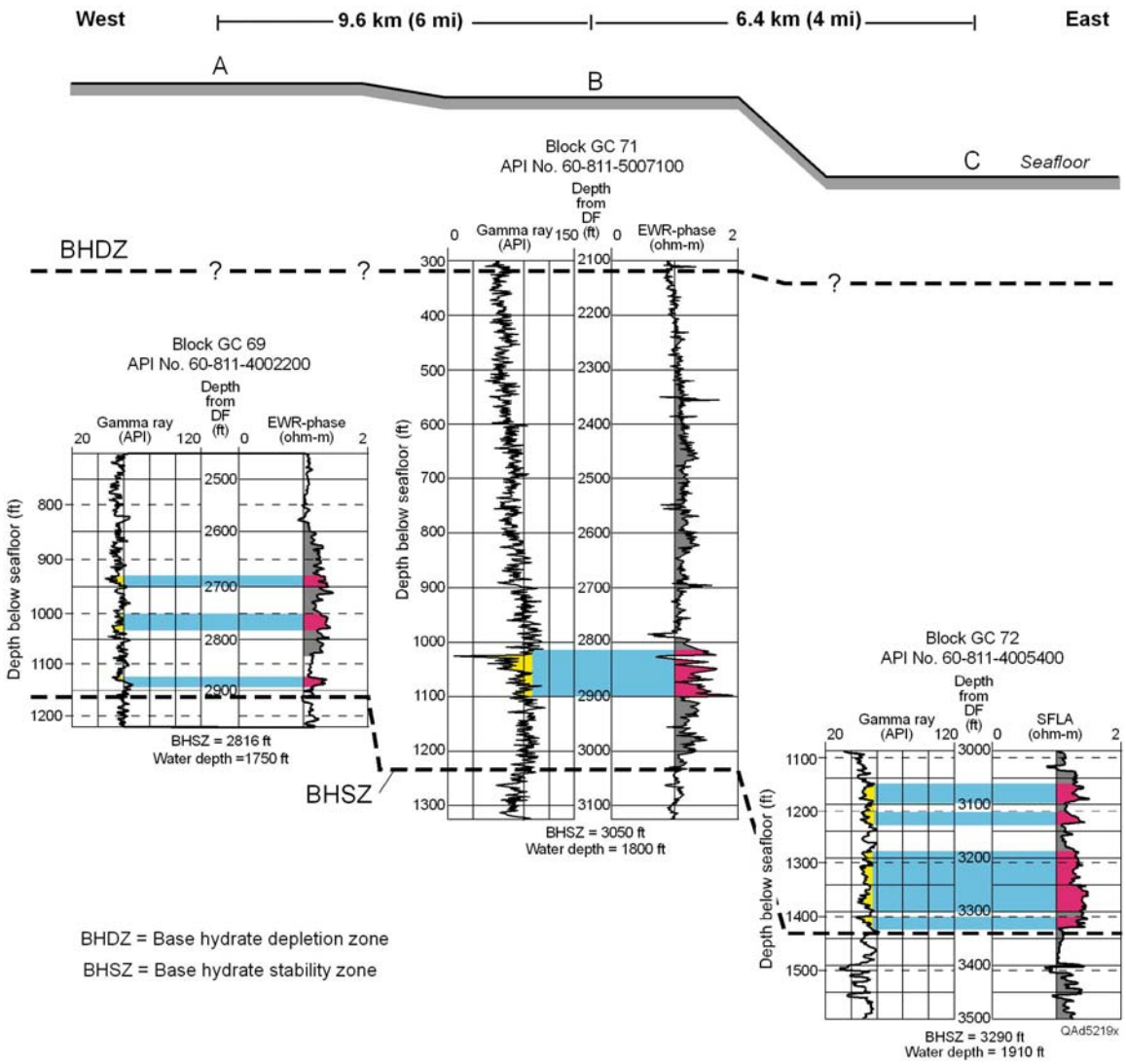

Figure 22. Well log cross section along the profile of calibration wells **A**, **B**, **C**, Study Site 2. There is a robust hydrate system along this profile. Well locations defined in Figure 20. The BHSZ depth labeled below each log suite is the depth of the base of the hydrate stability zone associated with the 90.4 percent methane curve in Figure 18. At each well, the BHSZ horizon is drawn at a resistivity change that is “close to” the depth coordinate interpolated from this 90.4 percent methane curve. Gray zones emphasize intervals where resistivity exceeds 1 ohm-m. Yellow zones indicate larger-grain facies. Red identifies units that have both increased grain size and increased resistivity.

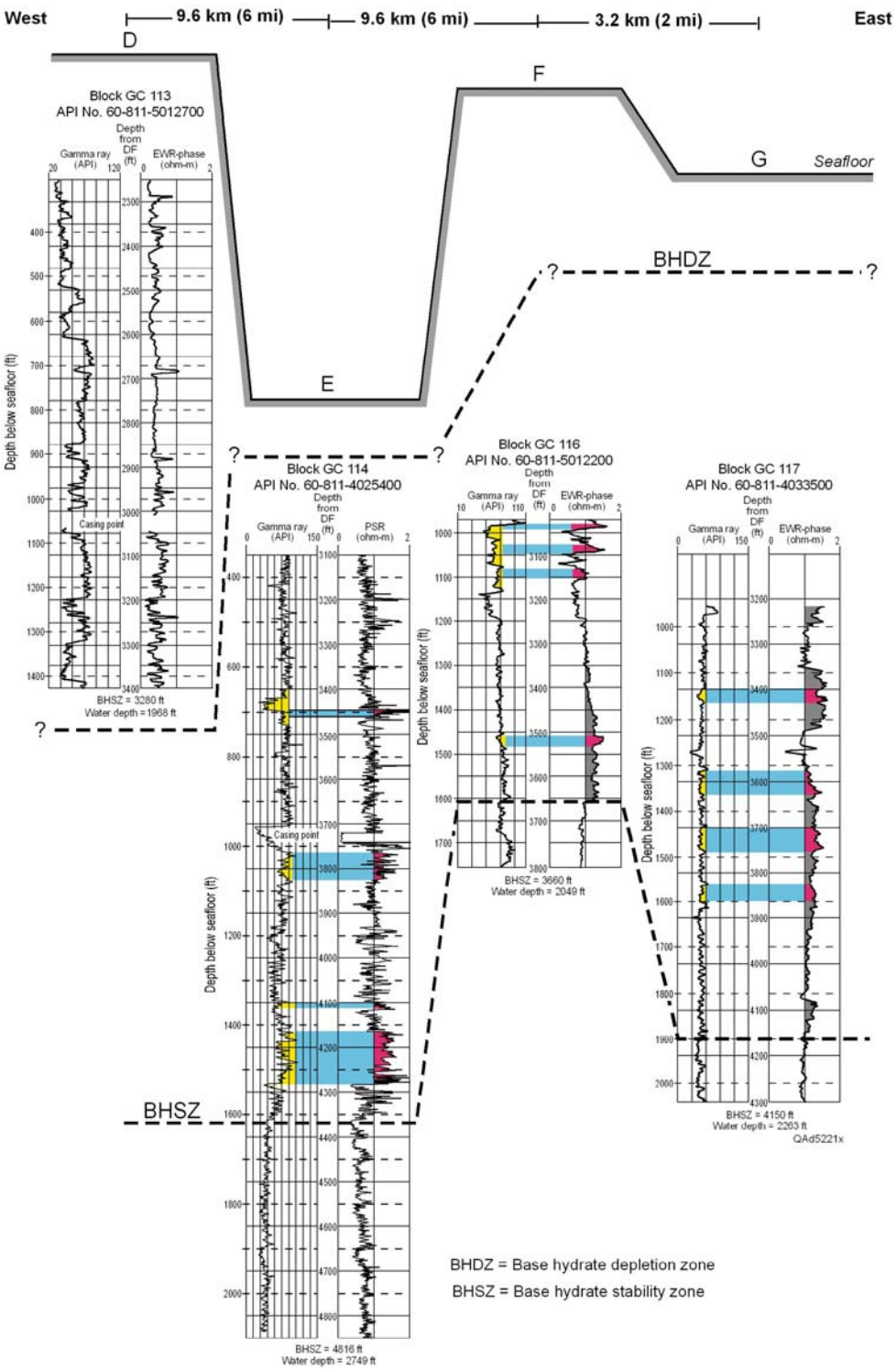

Figure 23. Well log cross section along the profile of calibration wells **D**, **E**, **F**, **G**, Study Site 2. This profile shows that there is no hydrate at well D but identifies several hydrate intervals that enlarge to the east. Well locations are defined in Figure 20. Horizon BHSZ, colors, and shadings are explained in the caption of Figure 22.

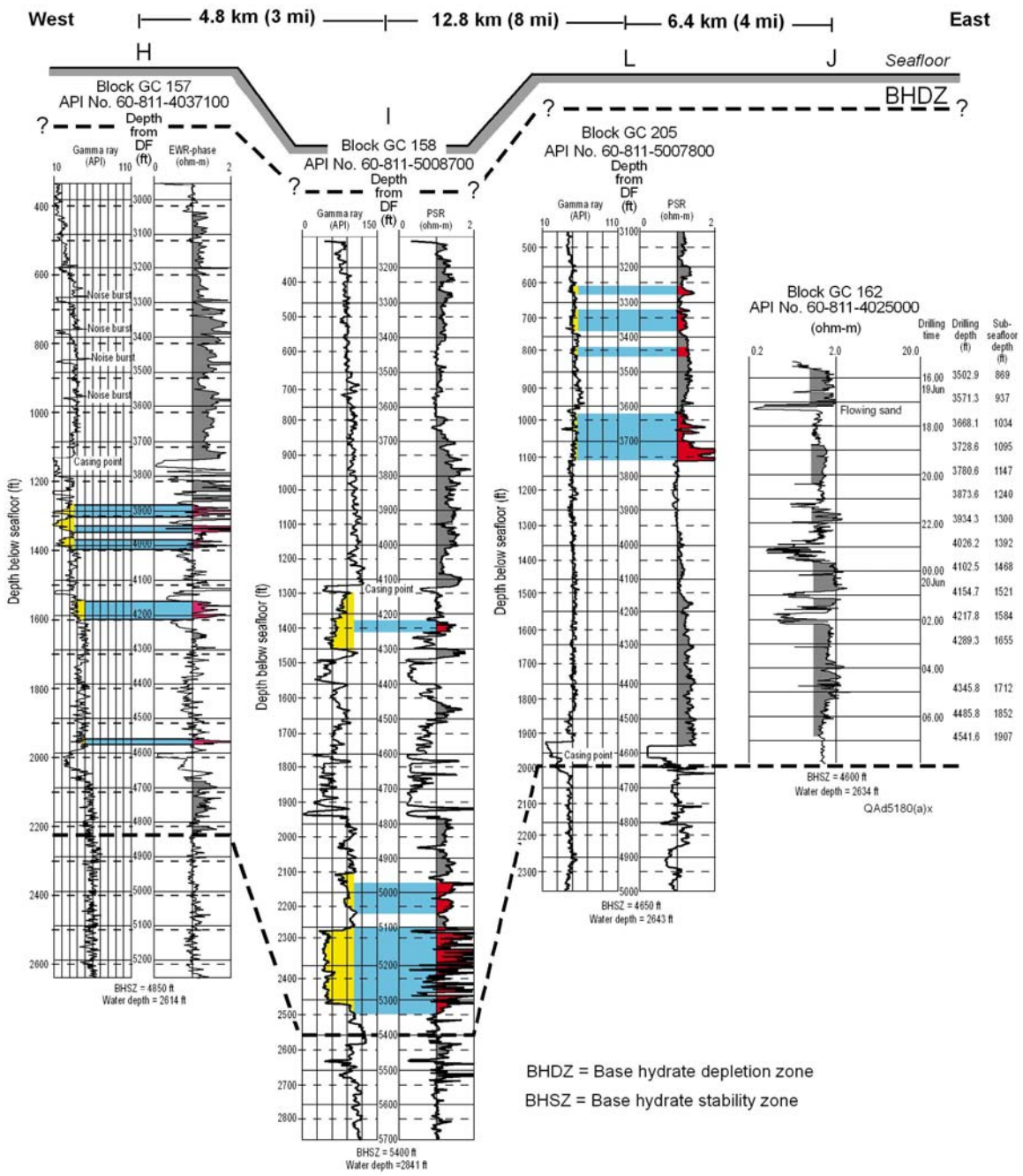

Figure 24. Well log cross section along the profile of calibration wells **H**, **I**, **L**, **J**, Study Site 2.This profile traverses thick hydrate sections. Well locations defined in Figure 20. Horizon BHSZ, colors, and shadings are explained in the caption of Figure 22.

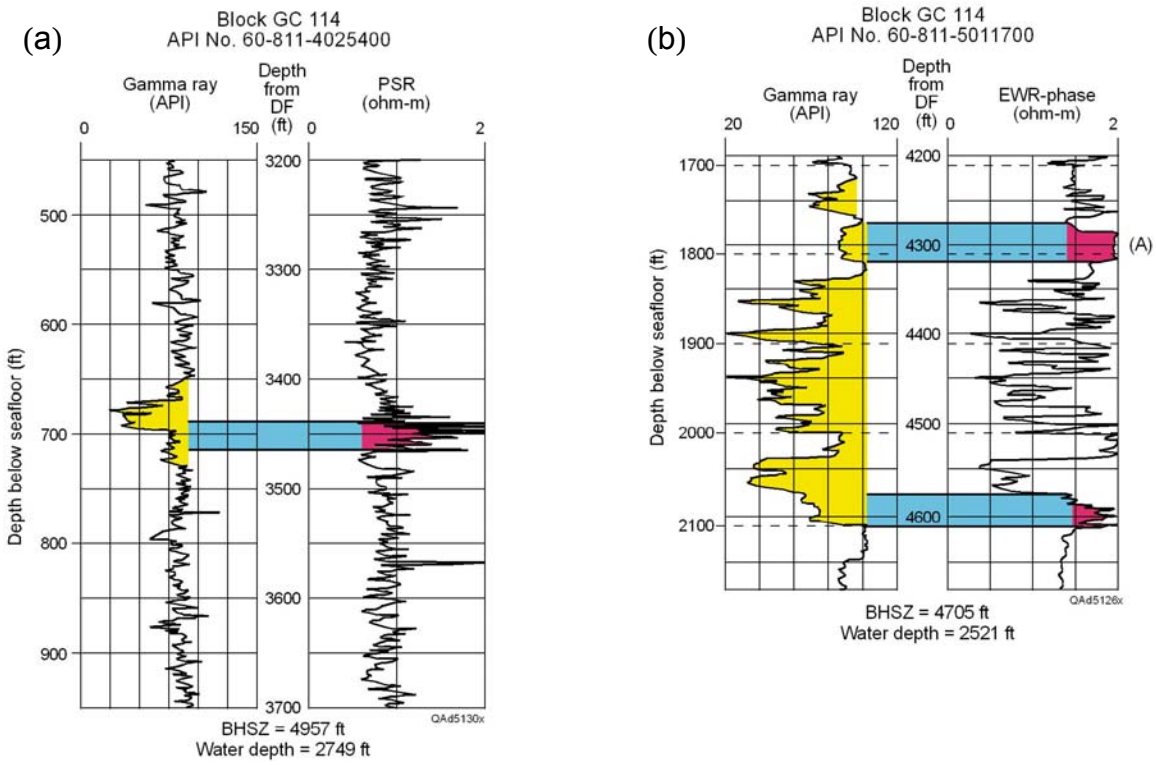

Figure 25. Examples of specific hydrate zones, Study Site 2. Larger-grain lithofacies are shaded yellow on the gamma-ray curve. Zones of increased resistivity within these larger-grain intervals are shaded red. With the HS- and Archie Equation 1 curves in Figure 12 as guides, note that zones such as **A** in panel (b), where resistivity increases to 2 ohm-m, should have a hydrate concentration of 60 percent or more.

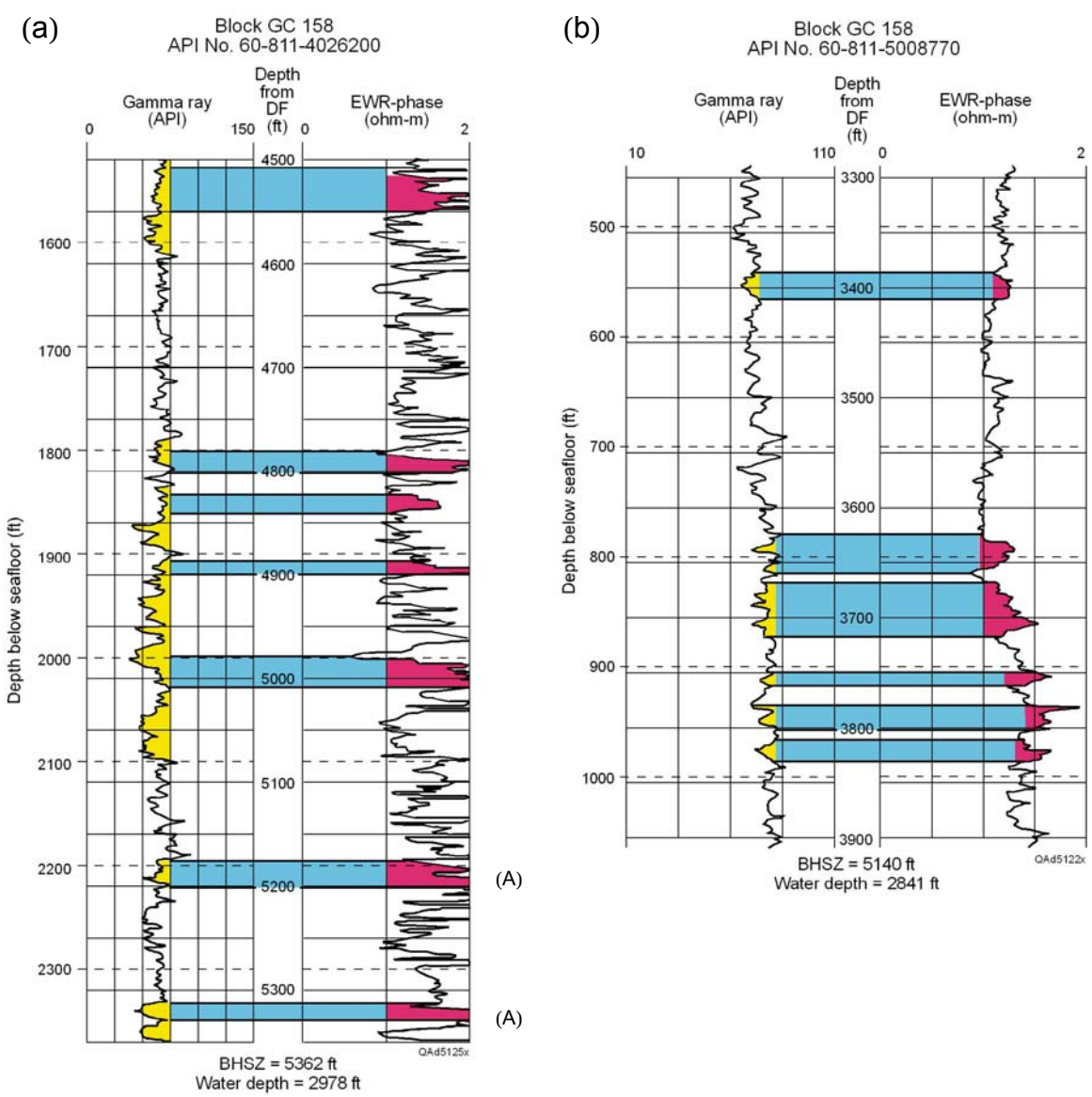

Figure 26. Examples of specific hydrate zones, Study Site 2. Larger-grained lithofacies are shaded yellow on the gamma-ray curve. Zones of increased resistivity within these larger-grain intervals are shaded red. With the HS- and Archie Equation 1 curves from Figure 12 as guides, note that zones such as **A** in panel (a), where resistivity exceeds 2 ohm-m, should have a hydrate concentration that exceeds 60 percent. The log format clipped the resistivity curve at zones **A** and did not show any data wrap-around.

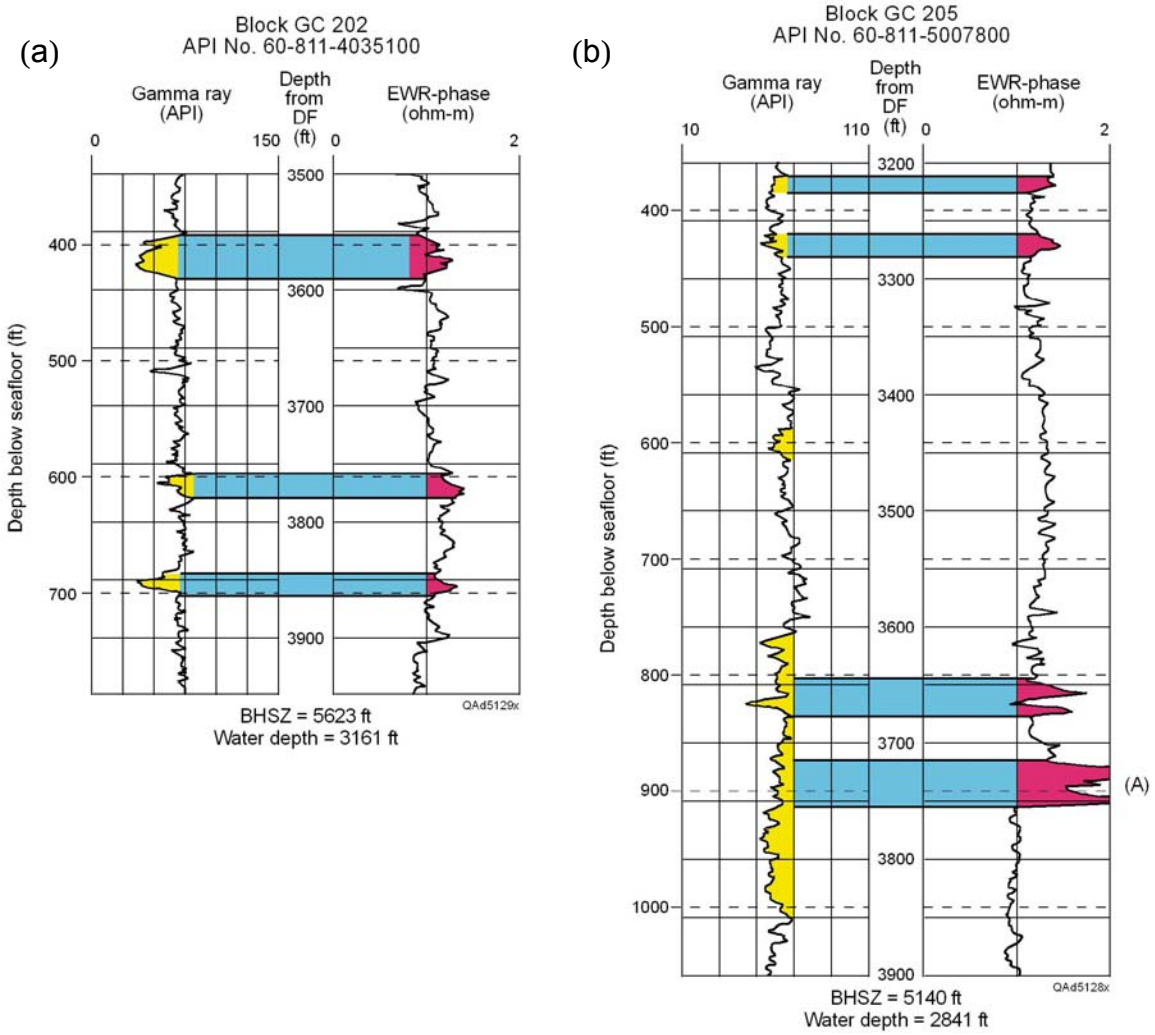

Figure 27. Examples of specific hydrate zones, Study Site 2. See comments for Figures 25 and 26.

Maps of Generalized Properties of Hydrate Systems

The log-based cross sections shown from Figures 16 up to 24 indicate that the hydrate systems at Study Sites 1 and 2 are complex. The distances between adjacent control wells on these cross sections are too great to construct a detailed stratigraphic model of the hydrate-bearing interval beneath either study site. However, upon examining the general appearance of each cross section, we can conclude that stratigraphy, sediment type, and hydrate concentration vary rapidly in the vertical and lateral directions across sites 1 and 2.

We have found it helpful to make the following qualitative inferences about the hydrate system defined at each control well displayed on the well log cross sections:

1. The accumulated thickness over which resistivity exceeds 1 ohm-m is either “thin” or “thick,” where “thin” and “thick” are arbitrary judgments, not quantitative measurements. At Site 1, an example of a “thin” hydrate system at occurs at well C (Fig. 16); an example of a “thick” system is the geology described by well D (Fig. 17).
2. The hydrate concentration is either “high” or “low” in a “significant number” of individual hydrate-system units, where “high,” “low,” and “significant number” are again arbitrary judgments that differ from person to person. At Site 2, examples of what we consider to be “low” hydrate concentrations are shown by wells D and E (Fig. 23); an example of a “high” concentration is the resistivity behavior at well I (Fig. 24).

These generalized descriptors of the hydrate systems at Study Sites 1 and 2 are best assessed in map views. Maps of Study Sites 1 and 2, which display the areal extents of these system properties, are shown as Figures 28 and 29, respectively. The hydrate system at each site is divided into two domains identified as **A** and **B**. Domain **B** is a hydrate system more robust than domain **A**.

The fundamental objective of our study is to determine what facies-sensitive attributes extracted from multicomponent seismic data can be used to define critical properties of deep-water hydrate systems. To achieve this objective, we conclude that the ideal study site is one where 4C OBC seismic lines traverse an area that has little or no hydrate and also an adjacent area that has abundant hydrate. Spatial variations in candidate hydrate-sensitive seismic attributes can then be directly associated with hydrate thickness and concentration. Maps in Figures 28 and 29 show that this hydrate-system behavior is exactly the situation that exists at both Study Sites 1 and 2. At each site, 4C OBC lines traverse both a weak hydrate system (Domain **A**) and a robust hydrate system (Domain **B**). On the basis of the resistivity log evidence presented in this report, we are convinced that we have selected ideal sites for the seismic-attribute research that we have proposed to do.

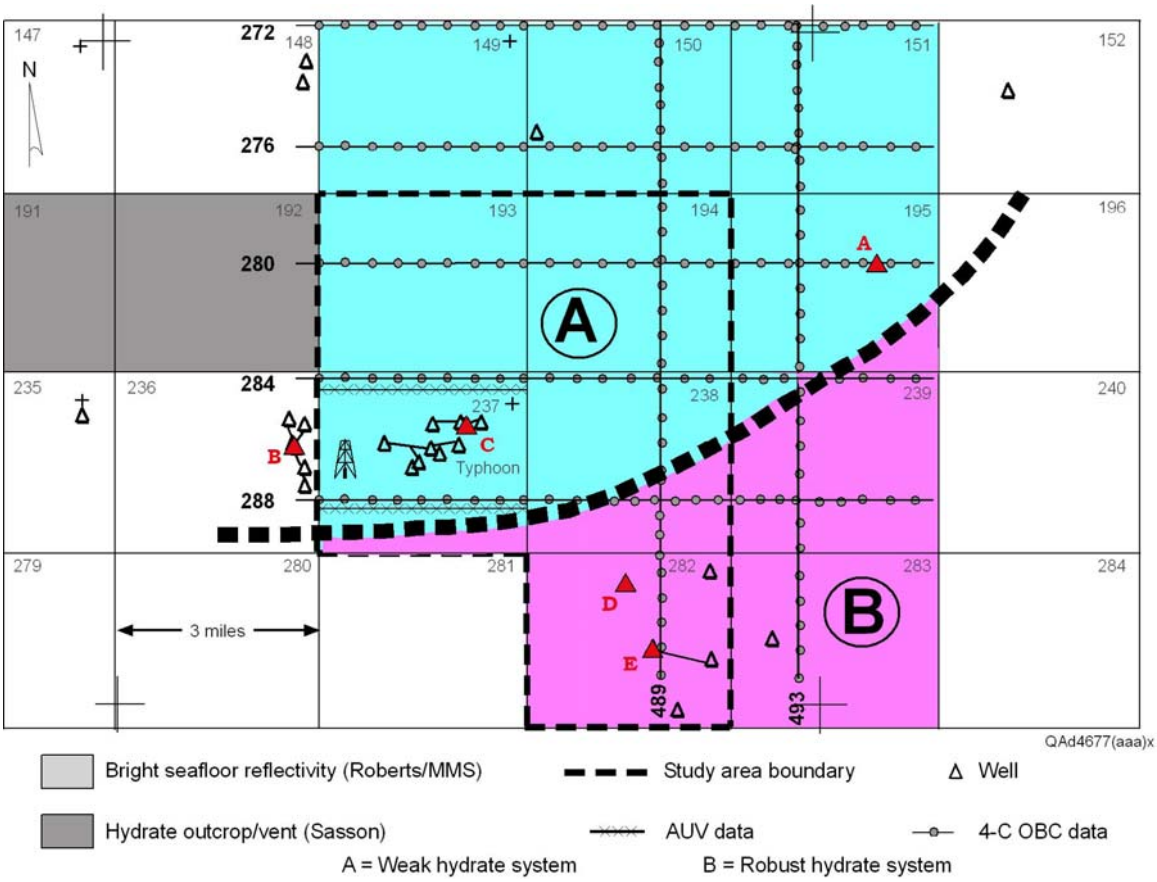

Figure 28. Generalized properties of the hydrate system across Study Site 1. The system can be segregated into two domains, **A** and **B**. Domain **A** has thin hydrate intervals and/or low hydrate concentration, as illustrated along well profile BCA (Fig. 16). Domain **B** has thick hydrate intervals and numerous units with high hydrate concentrations, as shown by well profile BDE (Fig. 17).

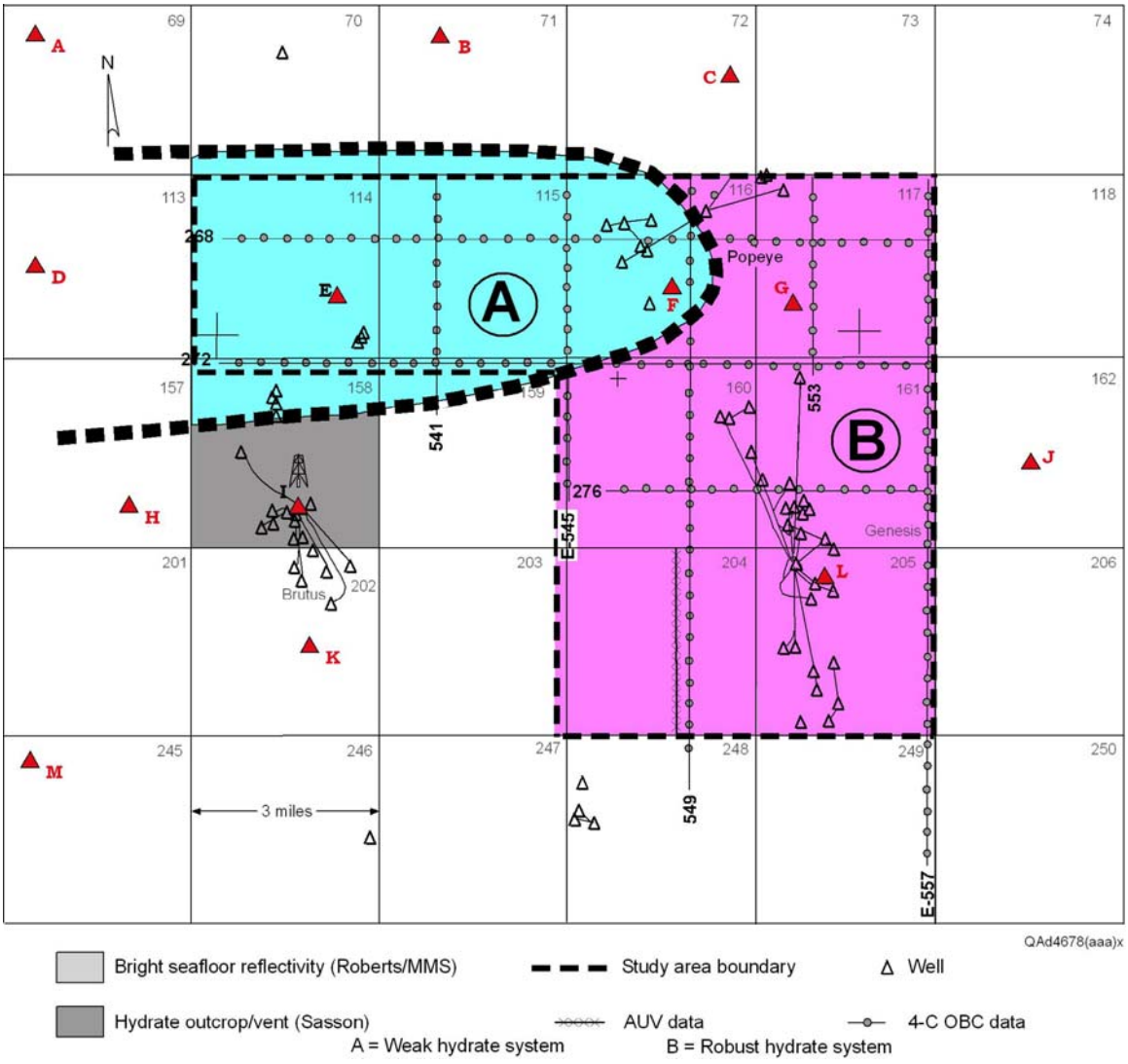

Figure 29. Generalized properties of the hydrate system across Study Site 2. The system can be segregated into two domains, **A** and **B**. Domain **A** has thin hydrate intervals and/or low hydrate concentration, with examples being wells D and E in Figure 23. Domain **B** has thick hydrate intervals and numerous units with high hydrate concentrations, as illustrated by well profiles in Figures 22 and 24.

Well Log Data from Remote Lease Blocks

One objective of our petrophysical analysis was to determine whether we could find any site inside our Green Canyon 4C OBC seismic grid where log data indicated that there is a more robust hydrate system than the systems that exist at Study Sites 1 and 2. The map in Figure 30 shows lease blocks outside of Study Sites 1 and 2, but inside the hydrate-stability corridor spanned by 4C seismic profiles, where we were able to acquire log data that could be used for identifying hydrate intervals. Included as Figures 31 through 33 are the only logs

from blocks outside of our study areas where we could find any usable log data across any part of the hydrate stability zone. Logs in Figures 31 and 32 are from lease blocks between Study Sites 1 and 2. Logs in Figure 33 are from wells in lease blocks east of Study Site 2. Only logs from Area 3 (between Sites 1 and 2, Fig. 30) indicate a hydrate interval and a hydrate concentration that are similar to conditions in the hydrate systems beneath Study Sites 1 and 2 (see Figs. 31 and 32). All other logs indicate thinner hydrate intervals or lower hydrate concentrations than what exist at Study Sites 1 and 2. We conclude that the hydrate systems across Area 3 may be equivalent to those at Study Sites 1 and 2, but that Area 3 is not a better hydrate prospect than the sites we have selected. All other hydrate evidence shown by these remote logs is inferior to the hydrate evidence found at Study Sites 1 and 2. We conclude that our original two choices for our research study sites are optimal for this area of Green Canyon.

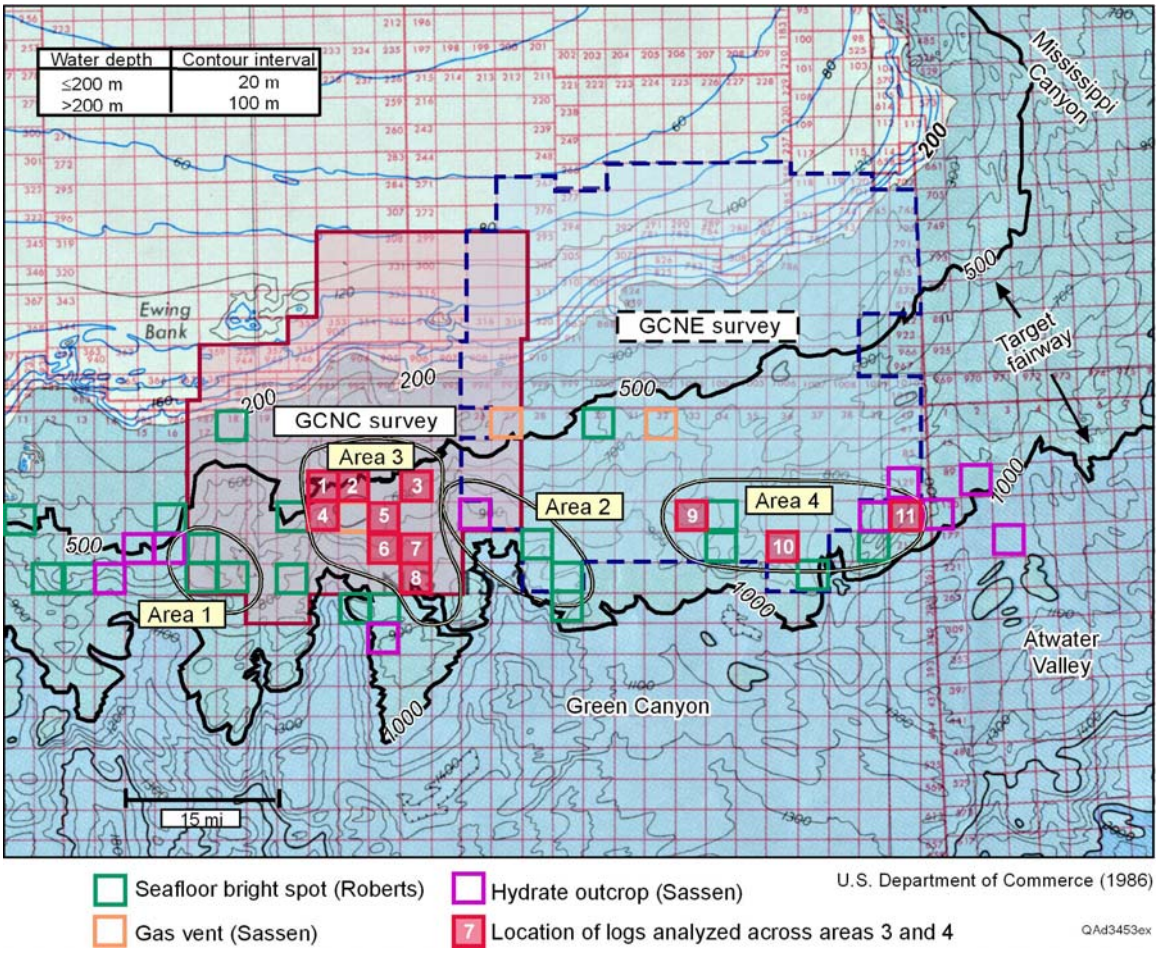

Figure 30. Map of the 4C OBC seismic survey area and its associated "*Target Fairway*" where hydrate study sites have to be positioned. Ellipses labeled **Area 1** and **Area 2** correspond to our Study Sites 1 and 2, respectively. Lease blocks where log data were found outside of Sites 1 and 2 that could be used for hydrate analysis are identified by shaded squares **1** through **11**.

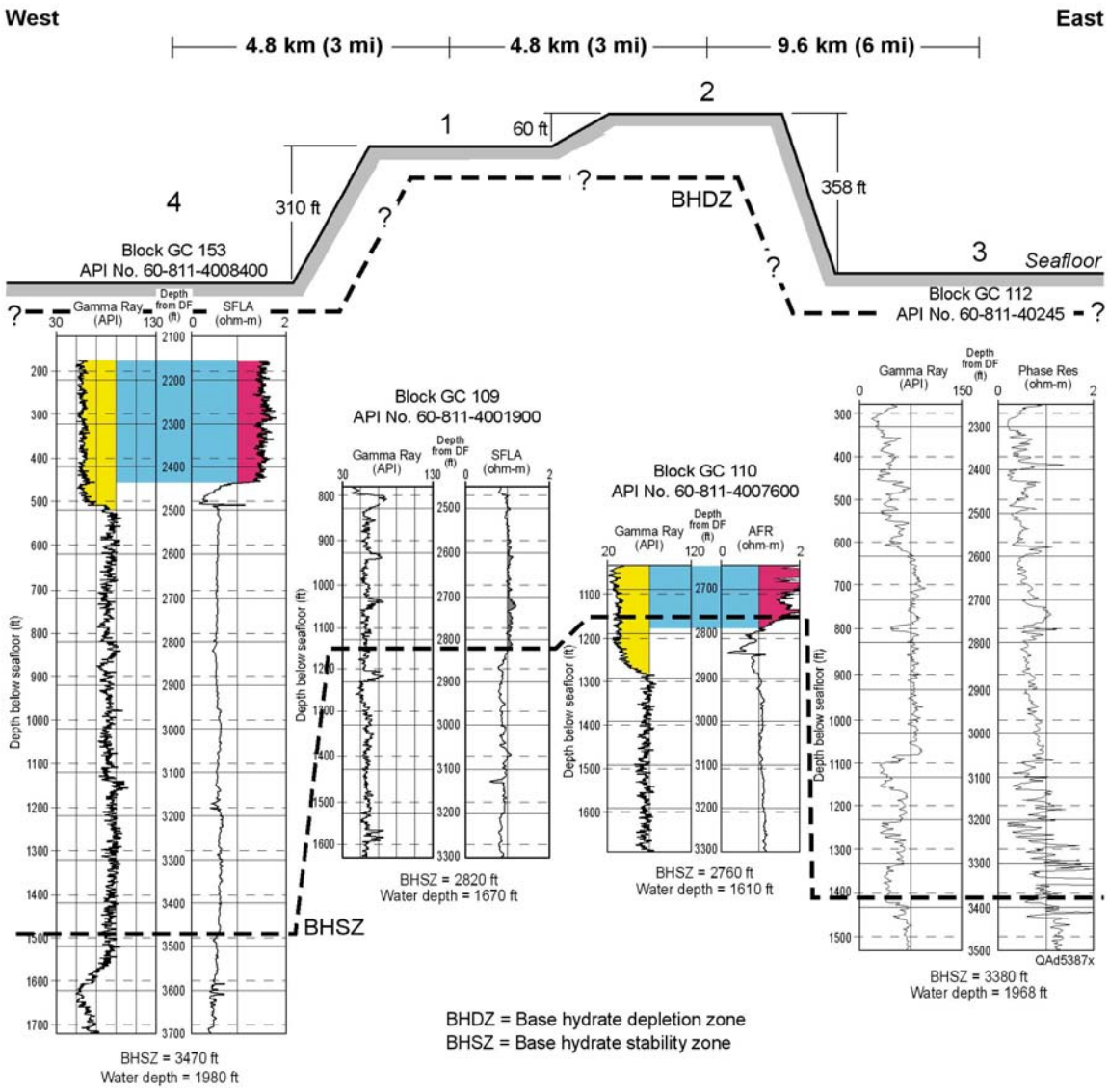

Figure 31. Log data across the hydrate stability zone at wells drilled in **Area 3** between Study Sites 1 and 2. Locations of wells **4**, **1**, **2**, and **3** used in this profile are labeled on the map in Figure 30.

Profile 4-1-2-3 in Figure 31 is particularly interesting. This profile shows two thick sand units at different subseafloor depths in wells 4 and 2, approximately 6 mi (9.6 km) apart, that have high resistivities indicative of high hydrate concentrations. On the east and west sides of these impressive hydrate-bearing sands, wells (1 and 3) show that hydrate concentration is quite low. This profile, combined with all other profiles exhibited in this report, lead us to conclude that all of the technology that has been developed during the past 2 decades to characterize complex oil and gas reservoirs will have to be employed for us to understand the internal architecture of deep-water hydrate systems.

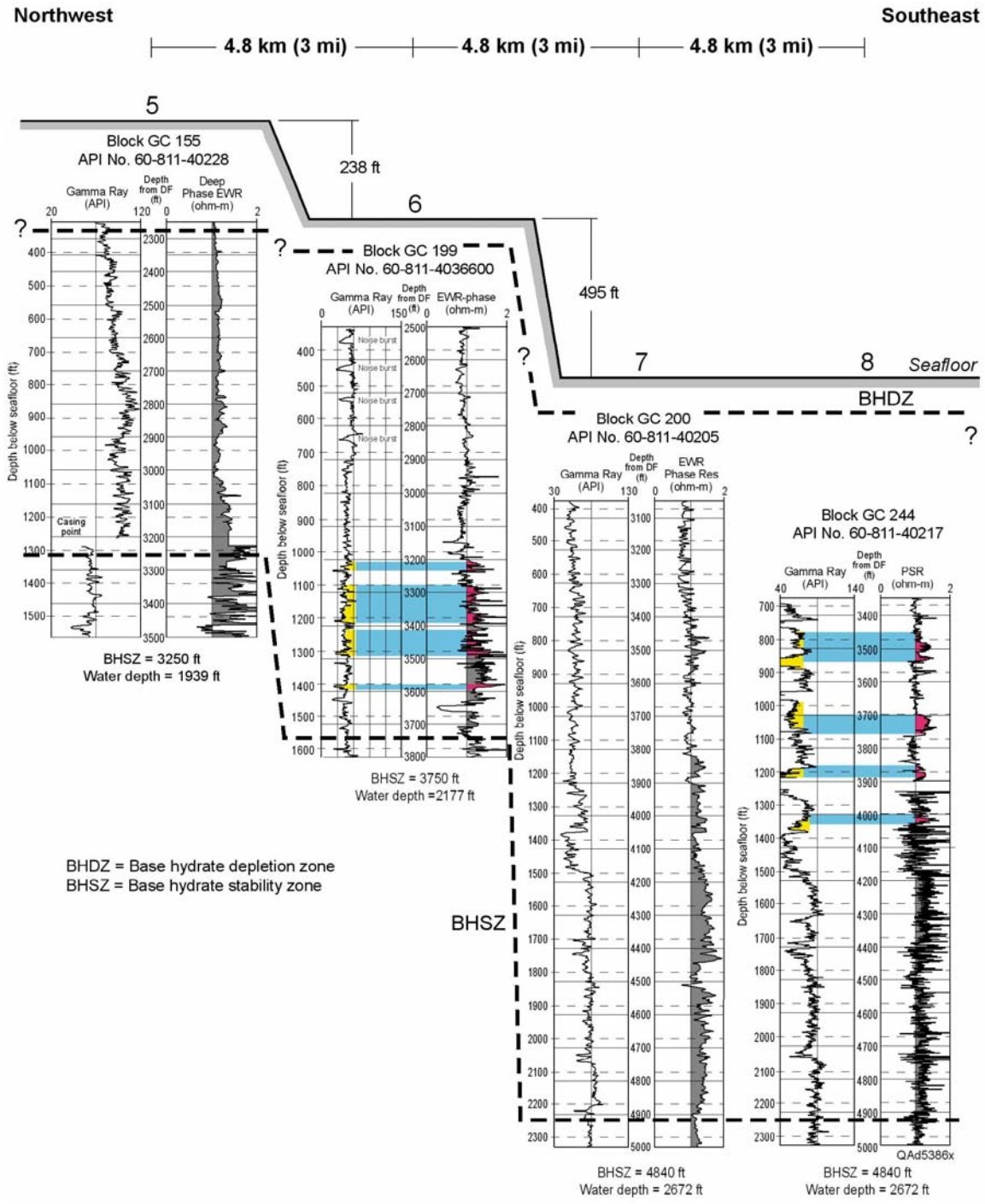

Figure 32. Log data across the hydrate stability zone at wells drilled in **Area 3** between Study Sites 1 and 2. Locations of wells **5**, **6**, **7**, and **8** are identified on the map in Figure 30.

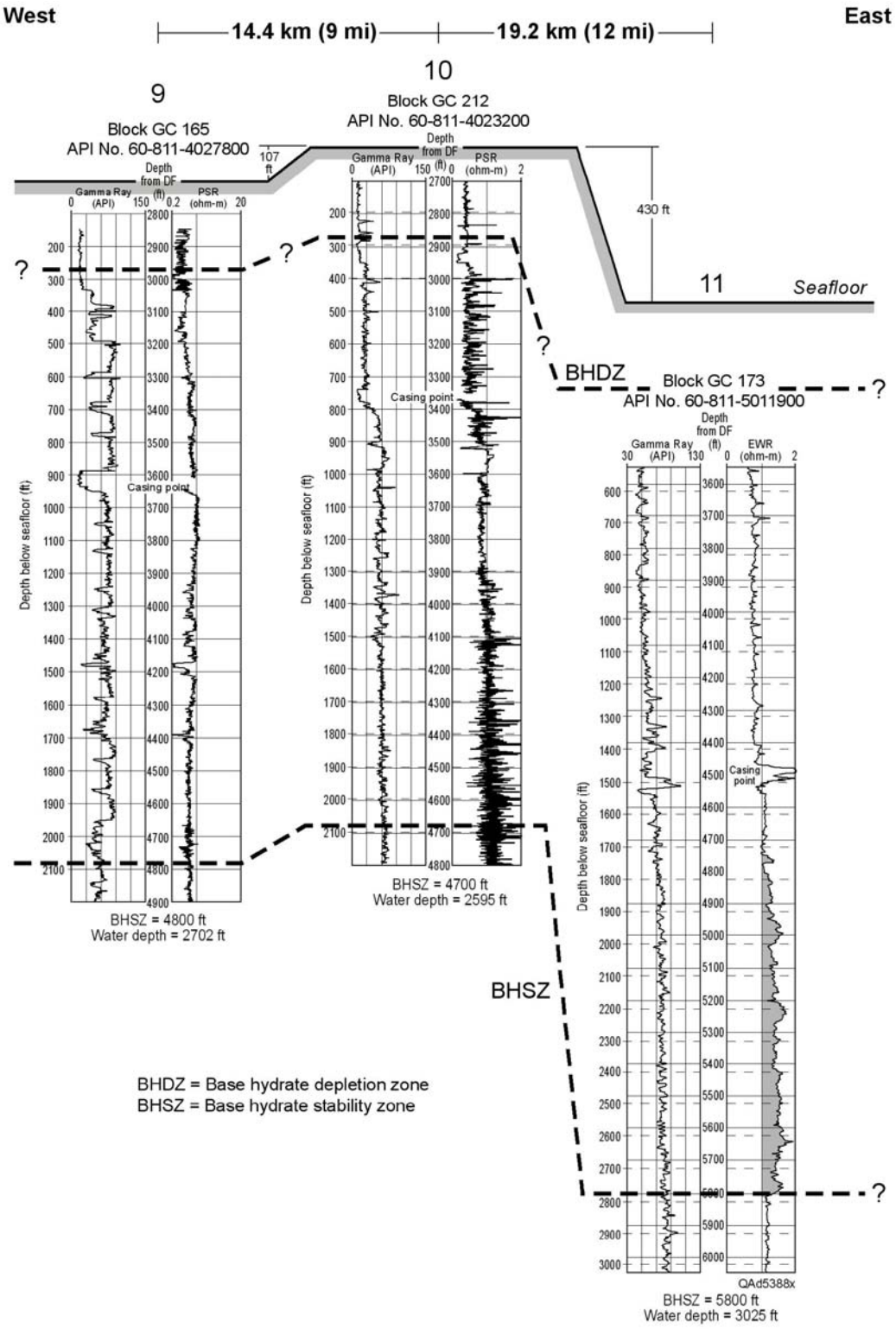

Figure 33. Log data spanning the hydrate stability zone in wells drilled in **Area 4** east of Study Site 2. Locations of wells **9**, **10**, and **11** used in this profile are identified on the map in Figure 30.

Archie Equation Corrected for Clay

The Archie Equation is an empirical law that was developed to determine water saturation in clean sands from measurements of resistivity and porosity across a sand-fluid mixture. The principal assumption of this empirical law is that electrical current travels only through the brine phase of fluid-saturated sediments because quartz minerals and hydrocarbon fluids are great insulators. However, when clay minerals are present in these sediments, the original form of the Archie Equation (Eq. 1) is no longer accurate. Clay minerals have significantly lower resistivity than clean sands and can have a large impact on the resistivity of a rock formation. If the presence of clay minerals is ignored and the simple form of the Archie Equation is applied to clay-rich sands, water saturation is overestimated at all porosity values. As a result, the saturation of any nonconductive phase that may be in the pores, for example, gas hydrates, will be underestimated.

Schlumberger Wireline Services (1998) proposed a modification to the Archie Equation that takes into account the presence of clay. This modified Archie Equation is valid for several types of clay distribution (clay can be disseminated, structural, or layered). Key parameters required for implementing this modified equation are the volume of clay (V_{cl}) present in the sediments and the resistivity (R_{cl}) of the clay minerals. Volume of clay can be determined from gamma-ray log data, and the resistivity of clay minerals can be measured in the laboratory. If no core samples are available for lab testing, we must use resistivity data measured across pure-clay intervals from nearby geology or rely on published resistivity measurements of clays. These information sources confirm that R_{cl} spans a large range of 1 to 1,000 ohm-m (Rider, 1991).

The modified Archie Equation proposed by Schlumberger (1998) is

$$\frac{1}{R} = \frac{\phi^m}{aR_w(1-V_{cl})} S_w^n + \frac{V_{cl}}{R_{cl}} S_w^{n-1}, \quad n = 2 \tag{12}$$

where, in our deep-water applications,

- R is the measured resistivity of sediments containing gas hydrates,
- R_w is the resistivity of the brine in these hydrate-bearing sediments,
- ϕ is the porosity of the sediments,
- a is the geometric factor (a ~1.08),
- m is the cementation factor (m ~ 1.2 to 1.7 for unconsolidated sediments),
- V_{cl} is the volume of clay estimated from gamma-ray log data,
- R_{cl} is the resistivity of clay mineral (R_{cl} ~ 1 to 1,000 ohm-m),
- S_w is the water saturation, and
- n is the saturation exponent (n ~ 2).

This form of the Archie Equation should be compared with Equation 1, the form of the equation for clean sands. If V_{cl} = 0, Equation 12 reduces to Equation 1, the classical form of Archie's Equation.

If we consider the saturation exponent **n** to be 2, as most published papers suggest, then Equation 12 is quadratic in S_w, and its positive root is

$$(13) \qquad S_w = \frac{1}{2} a \phi^{-m} R_w (1 - V_{cl}) \left[\sqrt{\left(\frac{V_{cl}}{R_{cl}} \right)^2 + 4 \frac{\phi^m}{a R R_w (1 - V_{cl})}} - \frac{V_{cl}}{R_{cl}} \right].$$

This expression for S_w estimates water saturation when the Archie Equation is modified for clay content. By definition, the concentration (c_{gh}) of gas hydrate in the sediments is 1-S_w, or

$$(14) \qquad c_{gh} = 1 - \frac{1}{2} a \phi^{-m} R_w (1 - V_{cl}) \left[\sqrt{\left(\frac{V_{cl}}{R_{cl}} \right)^2 + 4 \frac{\phi^m}{a R R_w (1 - V_{cl})}} - \frac{V_{cl}}{R_{cl}} \right].$$

Figure 34 illustrates the difference between the gas-hydrate concentration calculated using this modified clay-volume Archie Equation and the gas-hydrate concentration derived using the Archie Equation for clean sands. The difference between the two estimates represents the magnitude of the underestimation of gas-hydrate concentration that will occur in porous seafloor sediment when we ignore the presence of clay. The same input parameters were used in the calculations for both forms of Archie Equations. The porosity of the sediment was assumed to be 50 percent—a porosity value provided by lab measurements of water content of local core samples that we found documented in engineering reports across our study area. Resistivity of the brine was set at R_W = 0.17 ohm-m. This resistivity corresponds to a pore-water salinity of 45,000 ppm and a temperature of 65ºF. The cementation exponent **m** was allowed to vary from 1.2 (for highly unconsolidated sediments) to 2.1 (better consolidated sediments). The geometric parameter **a** was fixed at 1.0. The resistivity of clay was also fixed at 100 ohm-m. We assumed that the targeted hydrate interval had an observed logged value of formation resistivity equal to 2 ohm-m, a resistivity value exhibited by numerous logs illustrated in this report.

Using these values, we computed the gas-hydrate concentration on the basis of the two Archie Equations, using Equation 1 for clean sands and Equation 12 for shaly sands. The difference between the two estimates shown in Figure 34 is due only to the presence of clay. Each curve on the figure represents a different value for the cementation exponent. Results show that the error in estimating gas-hydrate concentration increases as the cementation

exponent increases. This behavior occurs because small values of cementation exponent imply a highly unconsolidated medium for which the electrical current travels freely through the conductive brine phase. In such a medium, the conductivity of the clay-quartz matrix plays a minor role. When the cementation exponent **m** increases, the pathways for current through the brine are more obstructed, and the clay in the matrix plays a larger role in conducting electrical current.

For larger values of m, ignoring clay in the sediments induces large errors in the estimation of gas-hydrate concentration in the pores. Even for small values of cementation exponent, which is the parameter range for the high-porosity unconsolidated sediments across our areas of study, errors in hydrate concentration that result from ignoring clay content are significant. For example, if the volume of clay is 70 percent and the cementation exponent is 1.2, then the difference between the gas-hydrate concentration derived by ignoring the clay content is 20 percent less than the value derived by accounting for clay volume.

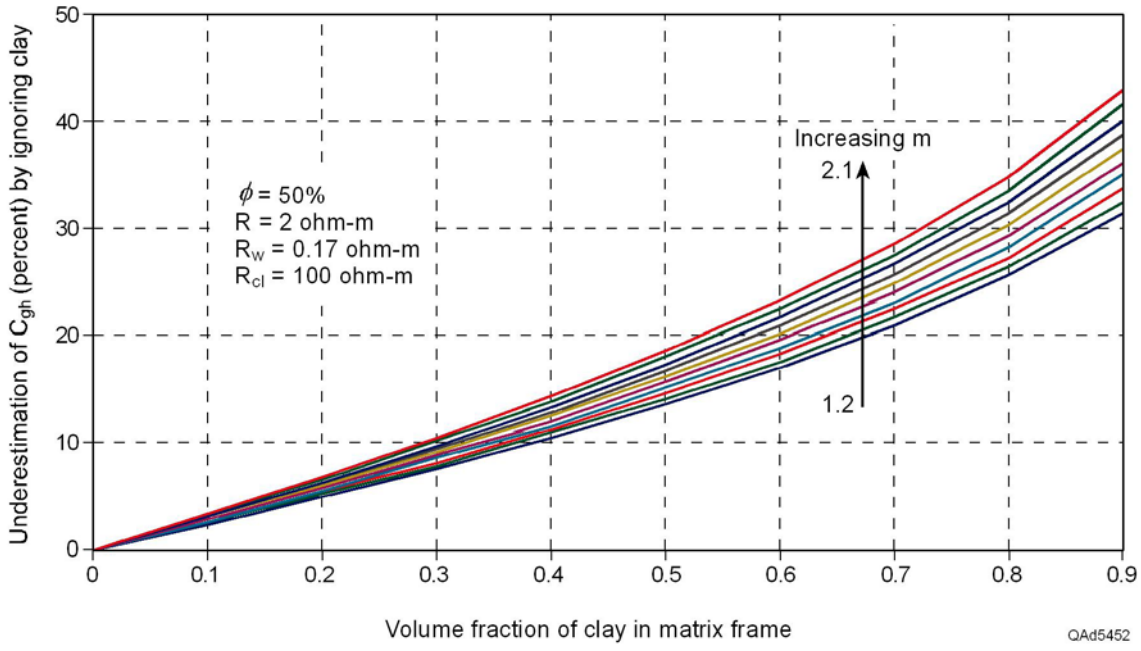

Figure 34. The difference between gas-hydrate concentration determined from the Archie Equation modified for clay content and gas-hydrate concentration derived using the Archie Equation for clean sands. Curves correspond to different values of cementation exponent **m**. Arrow indicates direction in which **m** increases from 1.2 to 2.1 in increments of 0.1. The figure shows the underestimation of gas-hydrate concentration that occurs when clay content is ignored. The sediment has a porosity of 50 percent and a log-measured resistivity of 2 ohm-m.

Figure 35 illustrates the same calculations when cementation exponent **m** is kept constant at 1.2 (for unconsolidated sediments), but different clay resistivities are assumed. The arrow indicates the direction of increasing clay

resistivity in a log-scale format that varies from 1 to 100 ohm-m. As expected, the error in hydrate concentration that results when the presence of clay is ignored decreases as the resistivity of clay increases. This finding implies that the lower the resistivity of the clay, (1) the larger the impact of the clay on the overall resistivity of the sediments and (2) the greater the error in hydrate concentration caused by ignoring the presence of clay.

However, if resistivity of the clay is significantly higher (two orders of magnitude) than the brine resistivity, then the error produced by ignoring clay content is only weakly dependent on resistivity of the clay. This principle is illustrated in Figure 36. Also, hydrate concentration, when estimated by the Archie Equation modified for volume of clay, is not sensitive to resistivity of the clay if R_{cl} is more than two orders of magnitude larger than the brine resistivity (Figure 37). This is an important observation because the resistivity values of clay minerals will not be available in many hydrate study areas.

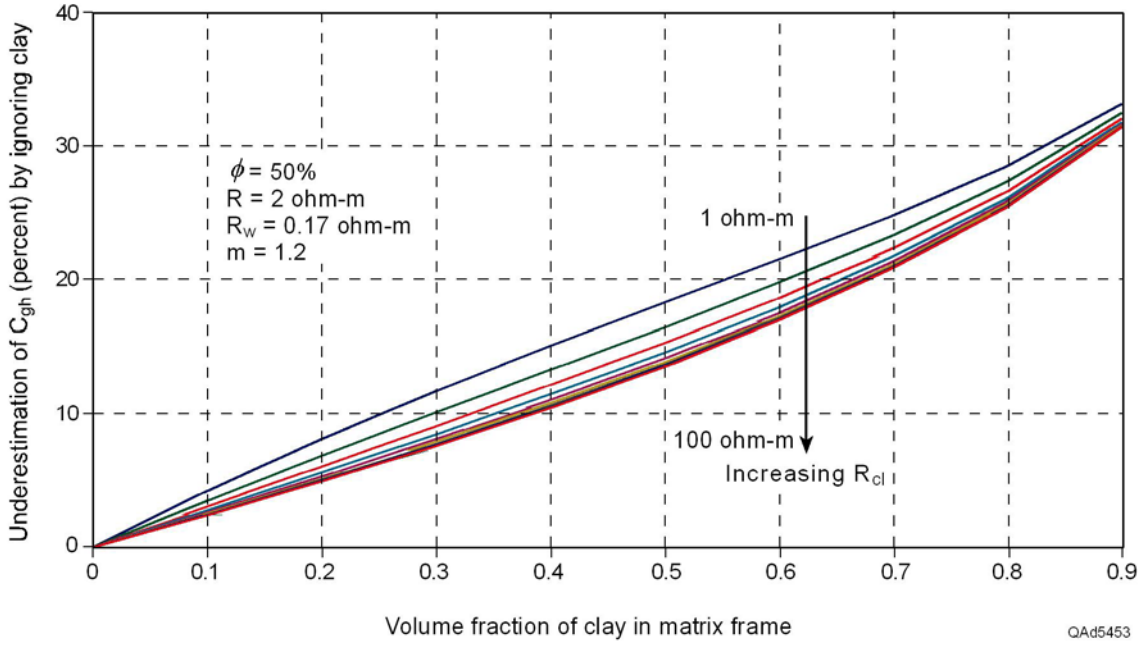

Figure 35. The difference between gas-hydrate concentration calculated from the Archie Equation modified for clay content and gas-hydrate concentration derived using the Archie Equation for clean sands. Curves correspond to different values for assumed resistivity of clays when clay resistivity is low. Arrow indicates direction in which clay resistivity increases (R_{cl} is in log-scale units ranging from 1 to 100 ohm-m). The figure shows the underestimation of gas-hydrate concentration that occurs when clay content is ignored. The sediment has a porosity of 50 percent and a log-measured resistivity of 2 ohm-m.

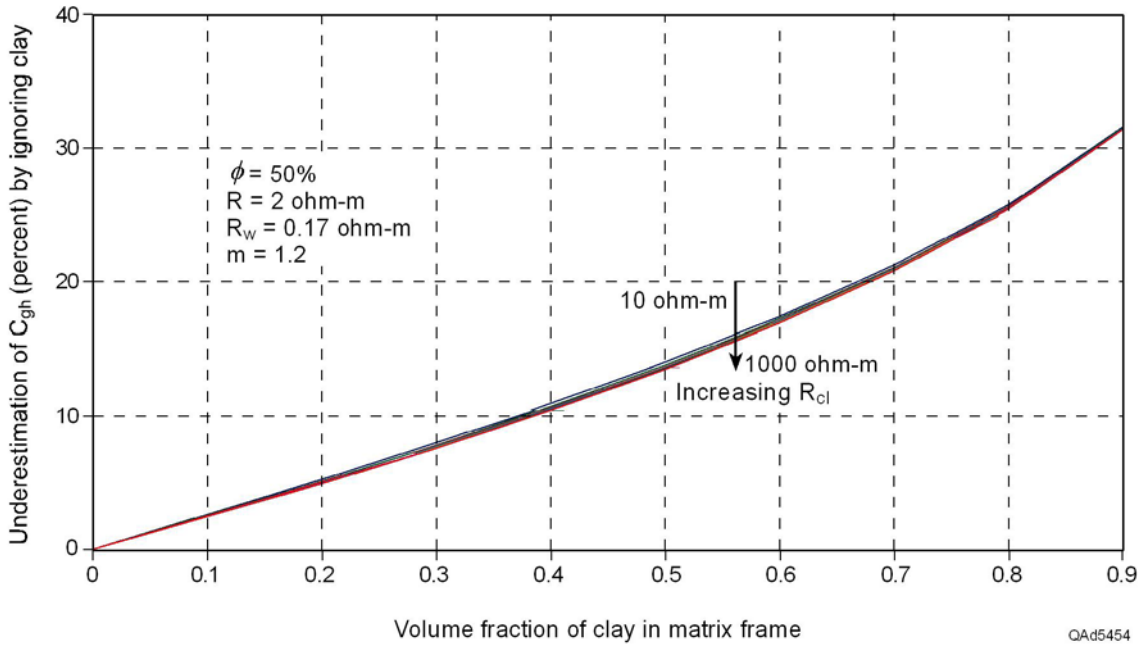

Figure 36. The difference between gas-hydrate concentration using the Archie Equation modified for clay content and gas-hydrate concentration derived using the Archie Equation for clean sands. Curves correspond to different values for resistivity of clays when clay resistivity is high. Arrow indicates direction of increasing clay resistivity in a log-scale format that ranges from 10 to 1,000 ohm-m. The figure shows the underestimation of gas-hydrate concentration when clay content is ignored. The sediment has a porosity of 50 percent and a log-measured resistivity of 2 ohm-m.

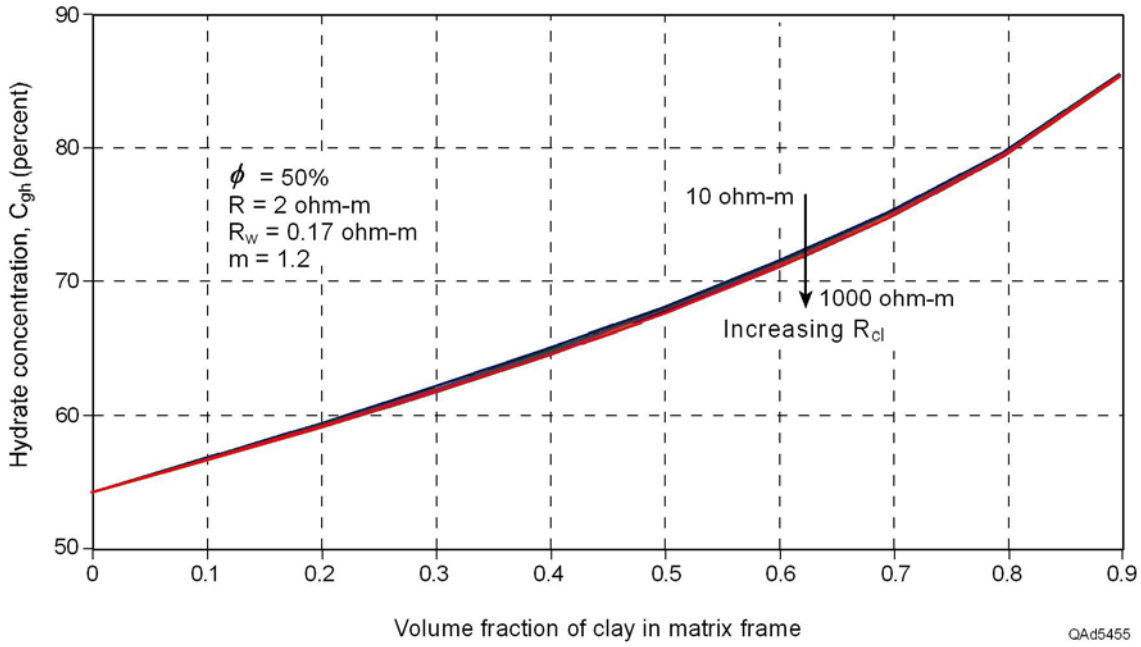

Figure 37. The estimated gas-hydrate concentration in clay/quartz sediments when the Archie Equation is modified to accommodate clay volume. Curves represent different values for resistivity of clay minerals (R_{cl} is shown in a log-scale format ranging from 10 to 1,000 ohm-m). Log-measured resistivity of the sediments is 2 ohm-m, and porosity is 50 percent. Hydrate concentration C_{gh} is expressed as fractions of the available pore space (Φ = 50 percent).

Monte Carlo Approach

Motivation for Quantifying Uncertainty

Archie's original resistivity equation (Eq. 1) and its modified version for clay content (Eq. 12) are empirical, deterministic laws that are commonly used to compute water saturation of porous media. In this study, we adjusted the ranges of the parameters used in these Archie Equations so that the equations could be used to estimate the concentration of gas hydrate in deep-water sediments. As stated in the preceding section, the parameters required to evaluate the Archie Equation are

- resistivity of the formation (R) ,
- resistivity of the brine saturating the pores (R_w),
- porosity of the sediments (Φ),
- geometrical parameter (a),
- cementation exponent (m),
- saturation exponent (n),
- volume of the clay minerals present in the sediments (V_{cl}), and
- resistivity of the clay minerals present in the sediments (R_{cl}).

Most of these input parameters vary over a wide range and can be challenging to estimate. Resistivity of the formation can be obtained from electrical wireline logging. However, like any physical measurement, an uncertainty is associated with the observed values of wireline resistivity because of instrument, calibration, and operational errors. Sediment porosity is usually obtained from well log data as well. For the shallow part of the marine sediments within the gas-hydrate stability zone (GHSZ) across our study areas, however, the only available logs were resistivity and gamma-ray data obtained using logging-while-drilling technology. Neutron-porosity or density-porosity logs were not recorded across these zones. Sometimes engineering data, such as water content, were available from which porosities for near-seafloor strata could be derived (Hardage and others, 2006). In this study, we extrapolated porosity information from these lab-measured water-content data to well locations where resistivity and gamma-ray logs were acquired. Detailed porosity information therefore has a degree of uncertainty across our targeted stratigraphic intervals.

Other empirical factors utilized in the Archie Equation, such as the geometrical parameter and the cementation exponent, also vary over large ranges, and uncertainty is associated with these parameters as well. The volume of clay over intervals of interest was determined from gamma-ray log data, using the following transformation:

$$V_{cl} = \frac{GR - \min(GR)}{\max(GR) - \min(GR)} \quad (15)$$

where V_{cl} is the estimated volume of clay, GR is the value on the gamma-ray log, and min(GR) and max(GR) represent, respectively, minimum and maximum

readings on the gamma-ray log. Because this calculation is not a direct measurement of the volume of clay, uncertainty is also associated with the V_{cl} estimates that we use.

Resistivity of clays is a difficult parameter to obtain as well. Although clay resistivity can be measured on cores in a laboratory, these measurements are not cost effective and are not performed on a regular basis. Therefore, we, like many researchers, rely on published lab measurements of resistivity of clay minerals from environments similar to those of our study area.

Most gas-hydrate concentrations that are predicted from resistivity logs using the Archie Equation are represented in the literature by a single number, without any measure of the uncertainty associated with the calculation. Also, some of these single-number estimates of gas-hydrate concentration are not accurate because values of the input parameters used in the analyses are not optimal choices (such as large cementation-exponent values being used for unconsolidated sediments).

For all of these reasons, log-based estimates of gas-hydrate concentration should be based on a careful analysis of the possible range of variability of each input parameter, and these estimates should always be accompanied by a measure of the uncertainty associated with parameters and the final calculation.

Uncertainty in Estimating Gas-Hydrate Concentration

Our approach to estimating the uncertainty in gas-hydrate concentration calculated from resistivity logs is based on stochastic simulations. We represent input parameters used in the deterministic Archie's Law and in its modified version for clay content by various probability distribution functions (**pdf**) that express mathematically the variation and uncertainty of these values. These probability distribution functions are either (1) uniform distributions over the possible range of variability for each input parameters or (2) Gaussian distributions. A uniform distribution assumes that any value for an input parameter is equally likely over the range of variability that is allowed. A Gaussian distribution suggests that the most likely value for the parameter is the mean of its associated Gaussian distribution and that the variance of its distribution function is a measure of the uncertainty about that mean value.

Therefore, we represent each input parameter in the Archie Equation not by a single number, but by a probability distribution function that allows us to incorporate the inherent uncertainty about that input into the calculation of hydrate concentration. These distribution functions permit us to use constraints on each parameter that are based on measurements or on knowledge acquired over similar environments. After we assign a probability distribution function to each input parameter, we then run Monte Carlo simulations over these distributions. We randomly draw a set of values of R, R_w, Φ, a, m, V_{cl}, and R_{cl} from their respective pdf's and compute the gas-hydrate concentration using the modified Archie Equation (Eq. 12). Then we draw again, randomly and independently, another set of values for these input parameters and obtain another possible realization of the gas-hydrate concentration using the same

Archie Law Equation. We repeat this procedure many times (N = 5,000 or more), and we end up with many possible realizations for gas-hydrate concentration at a certain subseafloor coordinate. From these many realizations of the possible gas-hydrate concentration at a certain location, we derive a probability distribution function of the estimated hydrate concentration, which mathematically represents the uncertainty of our prediction of hydrate concentration at that target point. From this distribution of gas-hydrate concentration we derive our best estimate of the hydrate concentration, which we express as the expected concentration value (defined as the mean value of the pdf) and the uncertainty (the standard deviation of the pdf).

This procedure allows us to incorporate the inherent uncertainty of all of the input parameters into our final calculation result and to estimate the impact of all these uncertainties on our final estimate of hydrate concentration. Another advantage of our approach is that it allows us to understand the sensitivity of gas-hydrate concentration to each of the individual input parameters. In this way we can decide which parameters are the most critical for reducing the inherent uncertainty associated with our predictions of gas-hydrate concentration.

Our definitions of the probability distribution function (**pdf**) associated with each parameter used in the modified Archie Equation (Eq. 12) are illustrated in Figure 38. These distribution functions form the basis of the Monte-Carlo-based random and independent “draws” of parameter values that we used to calculate hydrate concentration. In addition, we assigned an uncertainty to the resistivity log readings that were used in the Archie Equation calculations. For example, the pdf used for a log reading of 2 ohm-m is shown in Figure 39.

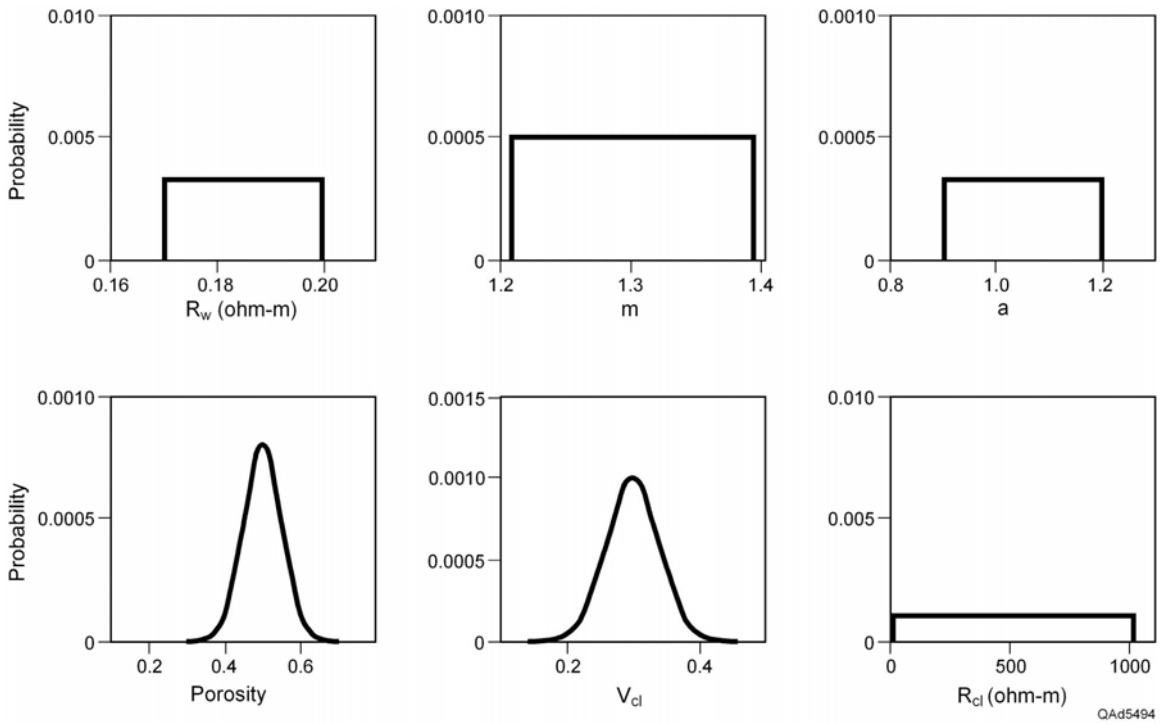

Figure 38. Distribution functions used to define the uncertainty of each parameter involved in the modified Archie Equation.

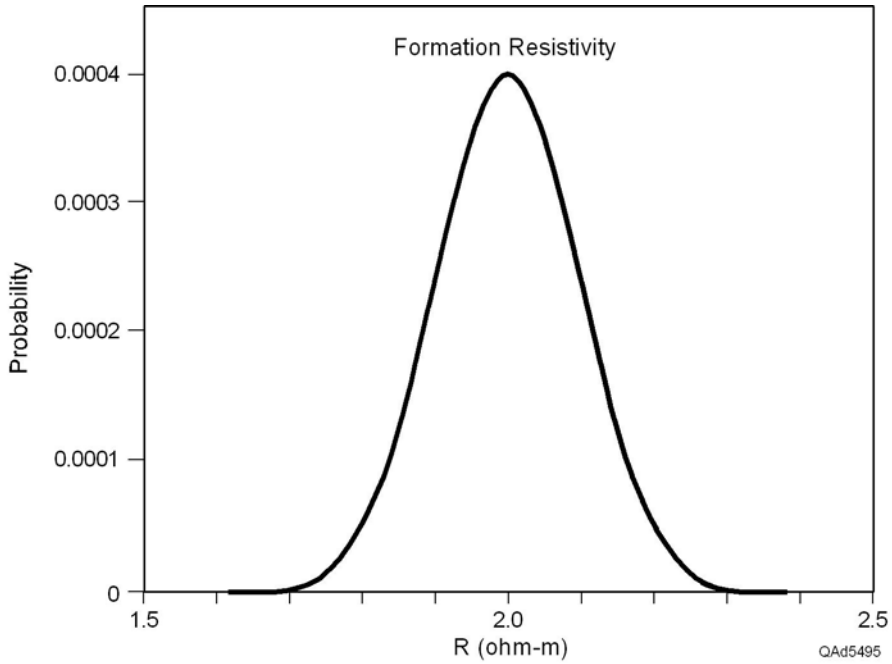

Figure 39. Example of a Gaussian distribution function used to describe the uncertainty of a resistivity log measurement. In this example, the log reading is 2 ohm-m.

We now illustrate our statistical approach to estimating hydrate concentration across selected intervals of the hydrate systems that span our study area. We chose one target interval from each of five logged wells across the area, in which the mean values of the resistivity log response were, respectively, 2.0, 1.75, 1.5, 1.3, and 0.35 ohm-m. These choices of resistivity readings span the range of resistivity values observed vertically and laterally across our study sites and allow us to demonstrate the magnitudes of hydrate concentrations that occur throughout the area without resorting to excessive graphical displays.

Gamma-ray and resistivity logs across these targeted intervals are displayed on Figures 40 through 44. In each figure, the specific interval over which hydrate concentration was estimated is indicated by the bracket drawn along the right edge of the resistivity curve. Two estimates of hydrate concentration were calculated for each interval. One estimate used the clay-free form of the Archie Equation (Eq. 1), and the other used the clay-dependent form (Eq. 12). The pdf of hydrate concentration produced by each form of the Archie Equation is identified on each figure.

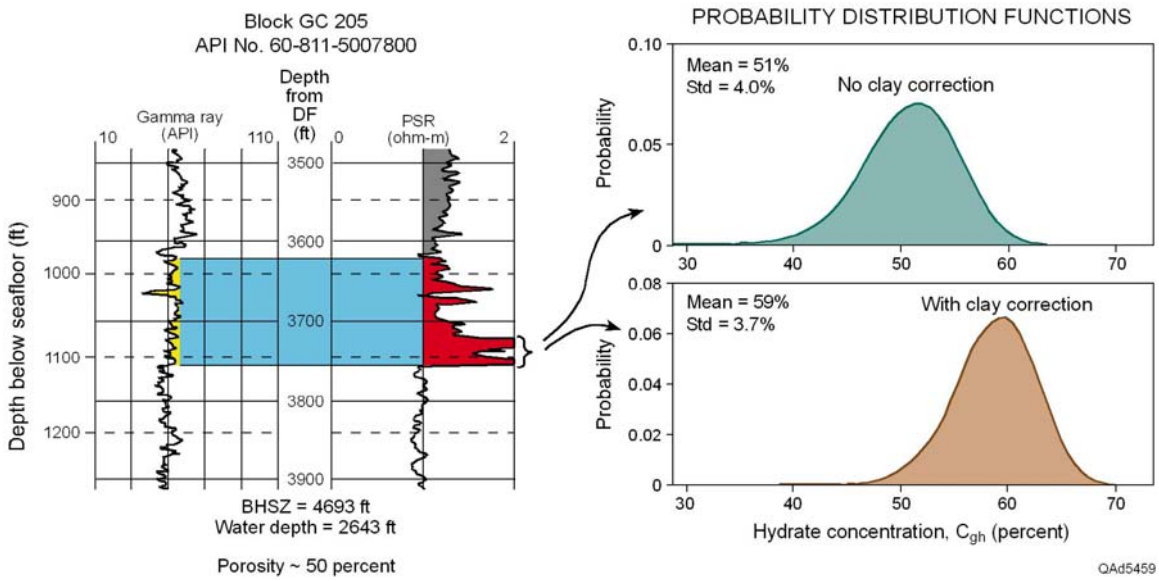

Figure 40. Hydrate concentration calculated in example well W1 across depth interval 3,720 to 3,760 ft. The upper pdf results when the clay-free form of the Archie Equation (Eq. 1) is used. The lower pdf results when the clay-dependent form (Eq. 12) is used. The mean reading of the resistivity log across this interval is 2 ohm-m. The average porosity is ~ 50 percent.

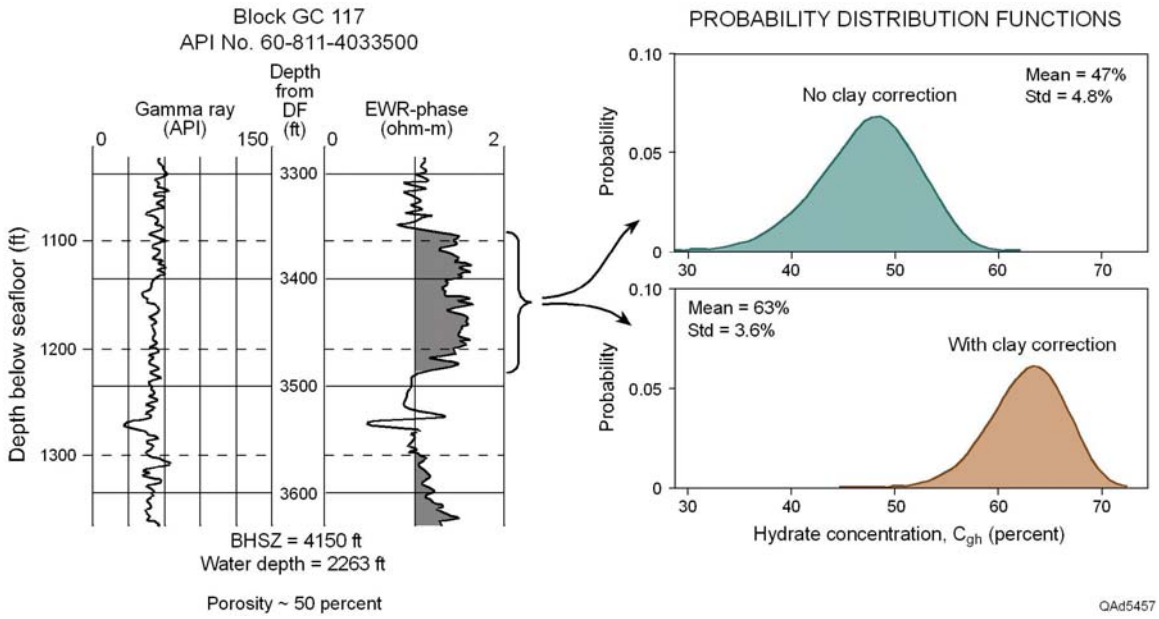

Figure 41. Hydrate concentration calculated in example well W2 across depth interval 3,370 to 3,500 ft. The upper pdf results when the clay-free form of the Archie Equation (Eq. 1) is used. The lower pdf results when the clay-dependent form (Eq. 12) is used. The mean reading of the resistivity log across the interval is 1.75 ohm-m. The average porosity is ~50 percent.

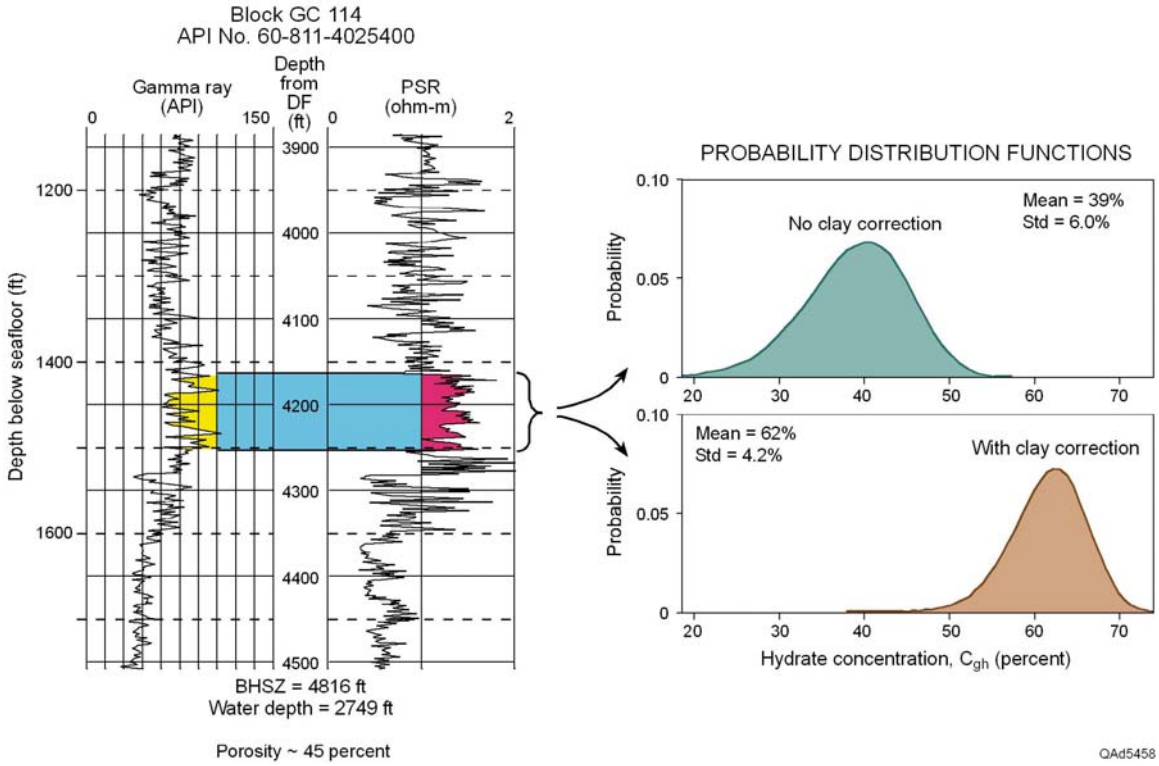

Figure 42. Hydrate concentration calculated in example well W3 across depth interval 4,170 to 4,270 ft. The upper pdf results when the clay-free form of the Archie Equation (Eq. 1) is used. The lower pdf results when the clay-dependent form (Eq. 12) is used. The mean resistivity log reading across the interval is 1.5 ohm-m. The average porosity is ~45 percent.

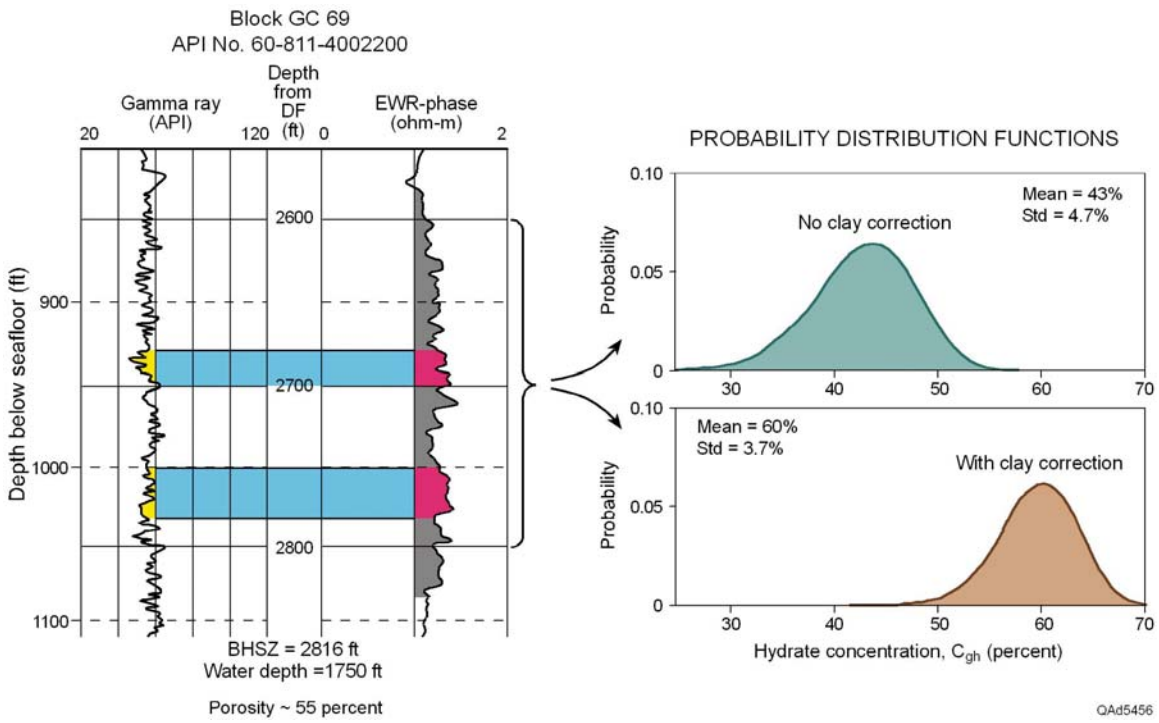

Figure 43. Hydrate concentration calculated in example well W4 across depth interval 2,600 to 2,800 ft. The upper pdf results when the clay-free form of the Archie Equation (Eq. 1) is used. The lower pdf results when the clay-dependent form (Eq. 12) is used. The mean of the resistivity log readings across the interval is 1.3 ohm-m. The average porosity is ~55 percent.

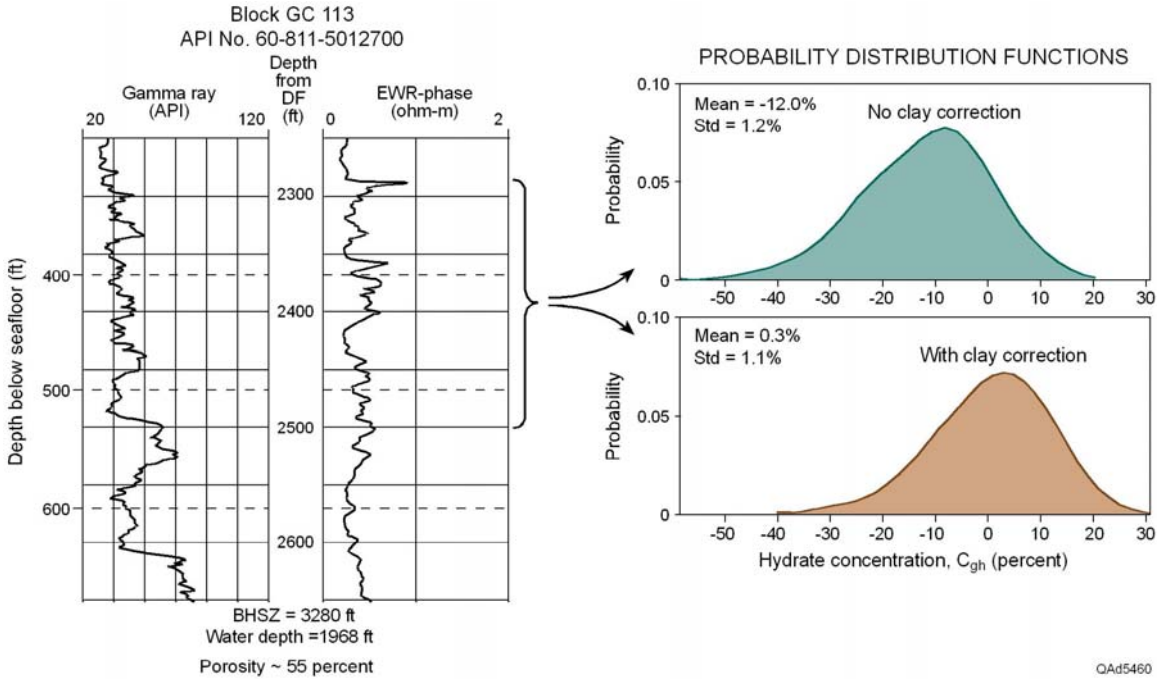

Figure 44. Hydrate concentration calculated in example well W5 across depth interval 2,270 to 2,500 ft. The upper pdf results when the clay-free form of the Archie Equation (Eq. 1) is used. The lower pdf results when the clay-dependent form (Eq. 12) is used. The mean of the resistivity log readings across the interval is 0.35 ohm-m. The average porosity is ~55 percent.

The clay-dependent form of the Archie Equation always yields a higher estimation of hydrate concentration (greater mean value of the pdf) than does the clay-free form of the equation, and it always has less uncertainty associated with its estimation (smaller standard deviation of the pdf). When clay content is high within an interval, the difference between the two estimations of hydrate concentration is large (Fig. 42). Note that in the sequence of Figures 40 through 43 that even though formation resistivity drops from about 2 ohm-m (Fig. 40) to approximately 1.3 ohm-m (Fig. 43), the clay-dependent form of the Archie Equation predicts a consistent hydrate concentration of about 60 percent, meaning hydrate occupies about 0.6 of the space available between sediment grains. In contrast, the clay-free form of the Archie Equation produces a wide range of hydrate estimations varying from a concentration of around 39 percent (Fig. 42) to a concentration of about 51 percent (Fig. 40). In Figure 44, where the formation resistivity is much less than 1 ohm-m, the clay-free form of the Archie Equation yields a ridiculous estimate of -12 percent for the hydrate concentration. In contrast, the clay-dependent form of the equation predicts a realistic value of less than 1 percent concentration.

Our calculation procedure allows us to present our estimations of hydrate concentration in a depth-based log-curve format, in which the calculated hydrate fraction is displayed at each depth point across a targeted interval. Examples of such displays are shown as Figures 45 through 49. The intervals portrayed in these figures are the same intervals that are illustrated in Figures 40 through 44. The clay-fraction curves shown in this latter set of figures were calculated using Equation 15. Either data display option (Figures 40–44 or Figures 45–49) is valuable, depending on the application needed for the data.

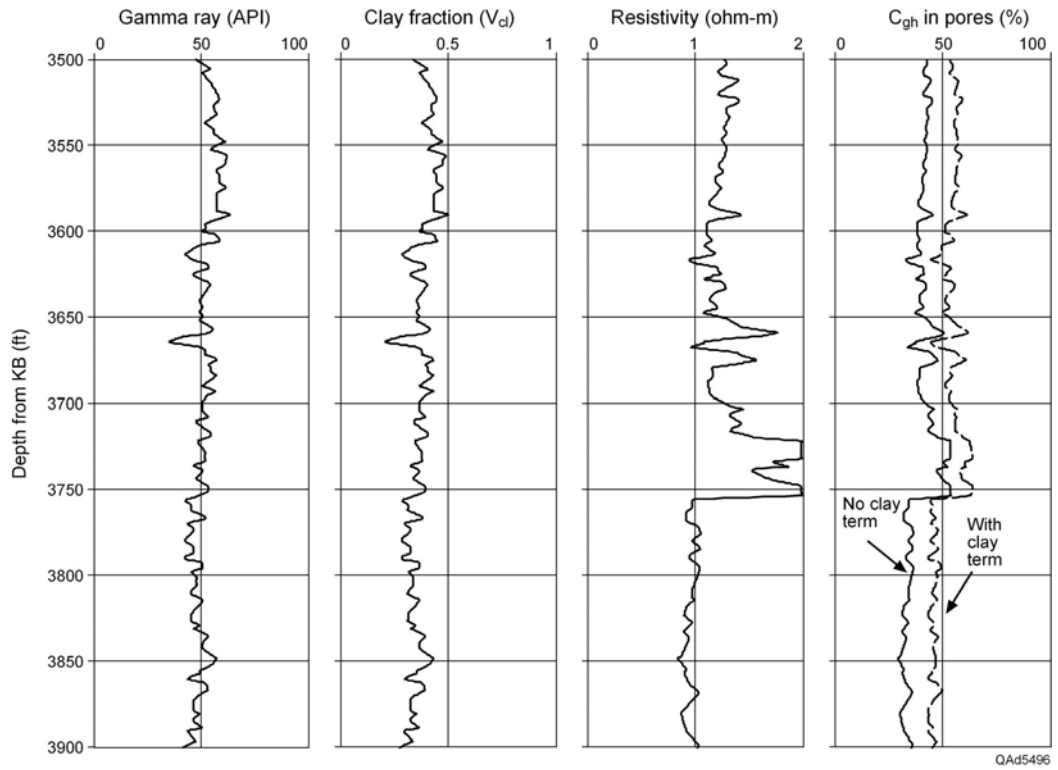

Figure 45. Clay fraction (V_{cl}) and hydrate concentration (C_{gh}) expressed as depth-based log curves across a target interval of example well W1. Compare with Figure 40.

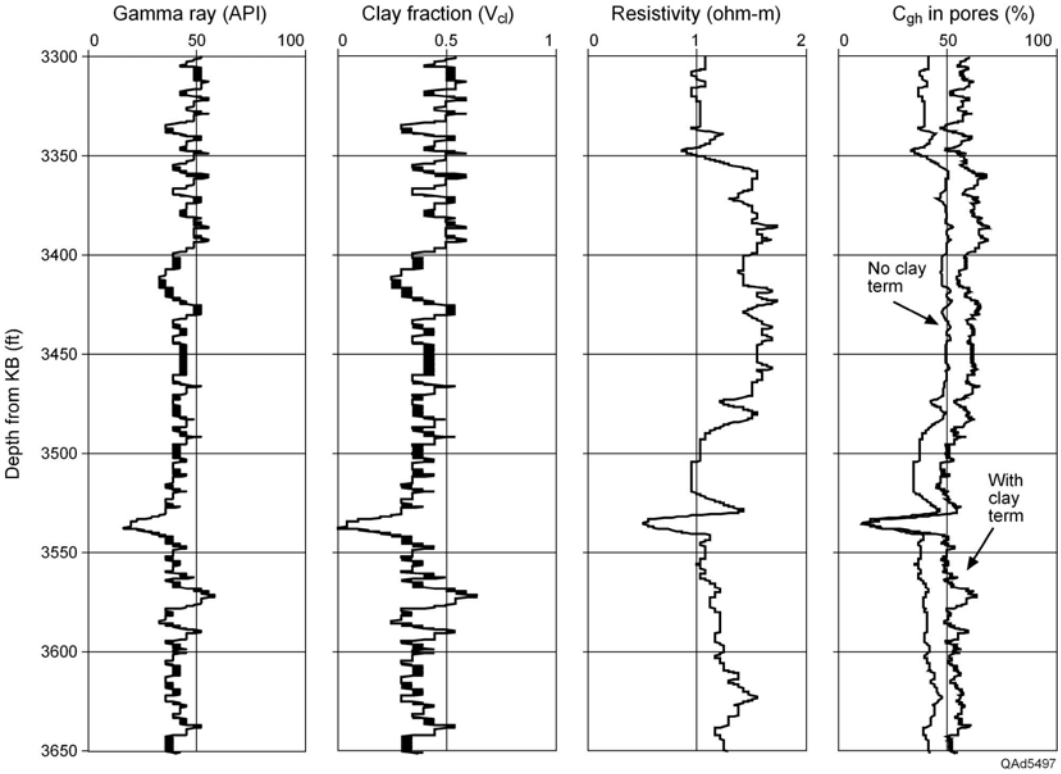

Figure 46. Clay fraction (V_{cl}) and hydrate concentration (C_{gh}) expressed as depth-based log curves across a target interval of example well W2. Compare with Figure 41.

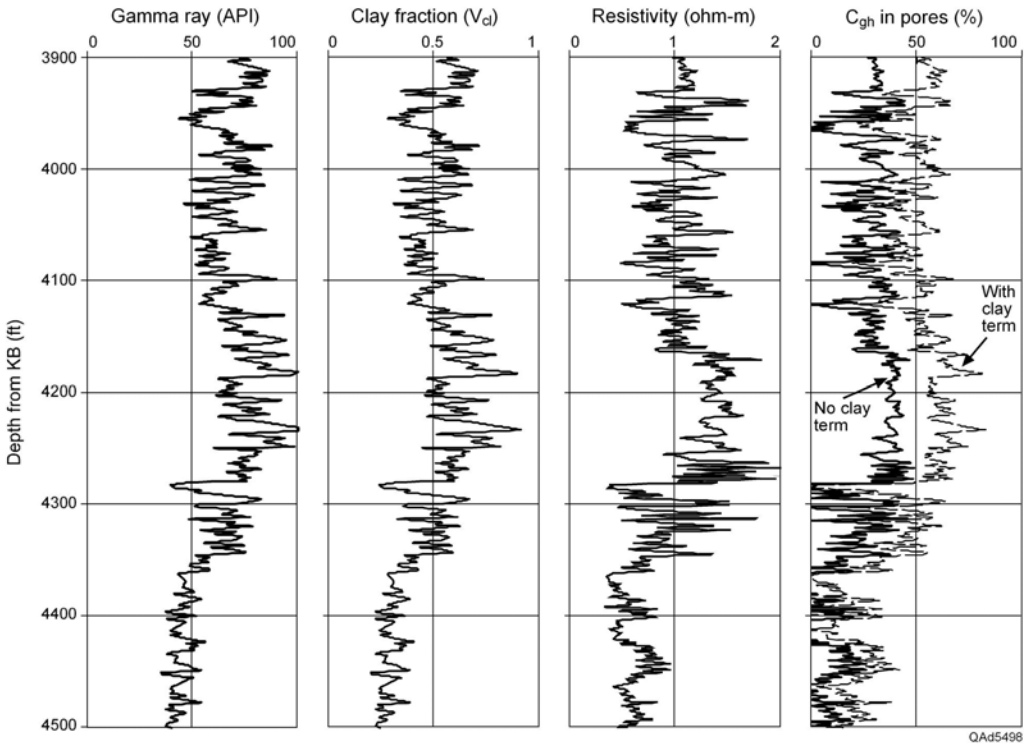

Figure 47. Clay fraction (V_{cl}) and hydrate concentration (C_{gh}) expressed as depth-based log curves across a target interval of example well W3. Compare with Figure 42.

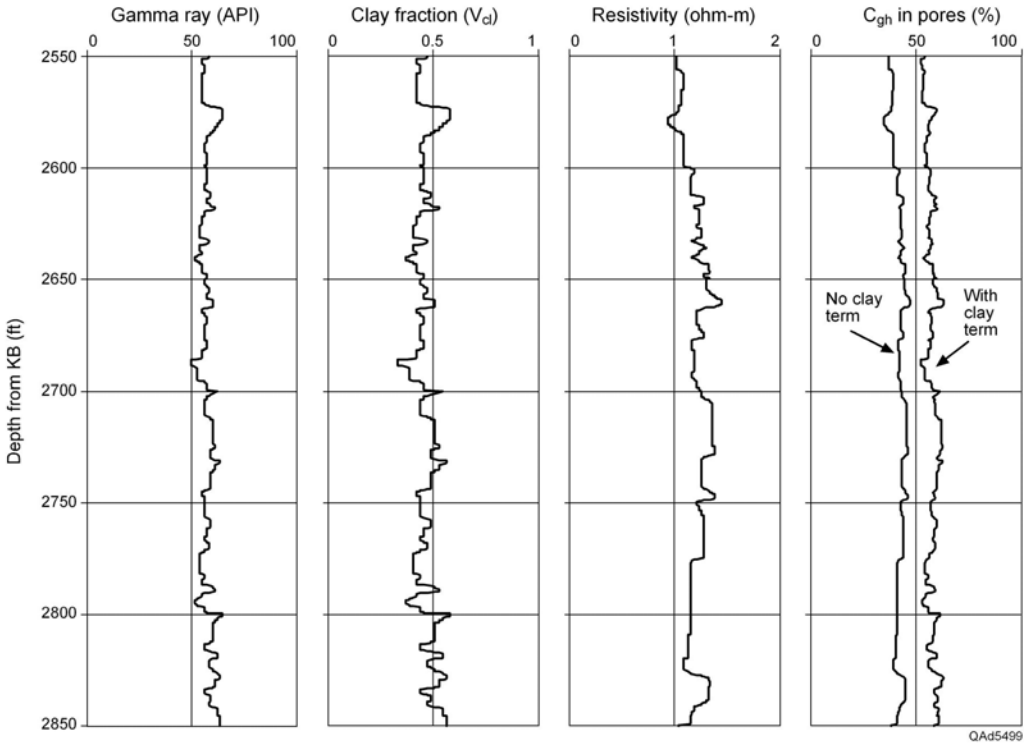

Figure 48. Clay fraction (V_{cl}) and hydrate concentration (C_{gh}) expressed as depth-based log curves across a target interval of example well W4. Compare with Figure 43.

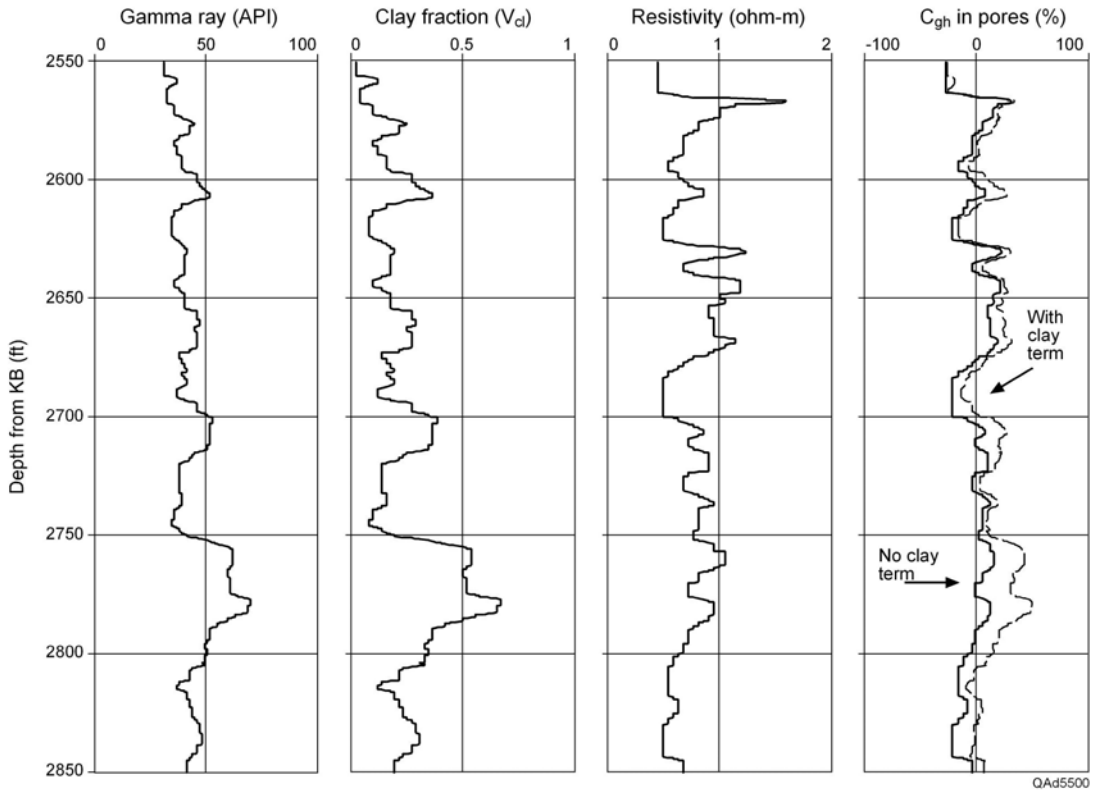

Figure 49. Clay fraction (V_{cl}) and hydrate concentration (C_{gh}) expressed as depth-based log curves across a target interval of example well W5. Compare with Figure 44.

Conclusions

The hydrate systems at our Study Sites 1 and 2 are extensive and robust, particularly the system spanning Study Site 2. At these two research sites, thicknesses and areal extents of hydrate distributions and concentrations of hydrate within these distributions equal or exceed those at any of the remaining lease blocks spanned by the 4C OBC seismic grid that is available for this study. An impressive amount of hydrate-bearing sediment was found across part of the area between our Study Sites 1 and 2. However, there is no compelling evidence that the hydrate systems found at these sites midway between our two selected study areas are superior to the proven systems at our Study Sites 1 and 2.

Principal criteria used to select our Study Sites 1 and 2 at the onset of this project were: (1) hydrate outcrops and gas vents were observed at the sites by Sassen and others (1999), (2) bright seafloor reflectivity and prolific communities of methane-dependent biota were found at the sites by Roberts (2001), and (3) seismic evidence of upwelling methane expulsion chimneys was found inside each site boundary. Our original maps of the study sites that indicated the lease blocks where Roberts and Sassen made their observations are used again in Figures 14 and 20 of this report to emphasize that our original premise for site selection was correct: *if you wish to study robust hydrate systems across the northern shelf of the GOM, you should select a site with bright seafloor reflectivity, hydrate outcrops, and gas vents, along with accompanying evidence*

of a deep-rooted expulsion pathway that allows thermogenic gases to access the hydrate stability zone. Now that this extensive log analysis across the region is completed, we are more convinced than ever that the seafloor criteria promoted by Roberts (bright reflectivity caused by methane-dependent organisms) and by Sassen (gas vents and outcropping hydrates), when coupled with evidence of local expulsion chimneys that reach to significant depths, are reliable indicators of subseafloor hydrate systems across the northern GOM shelf.

An important aspect of the research reported here relates to the resistivity response that we assign to a high-porosity mixture of sediment and hydrate. We present evidence and logic that the Hashin-Shtrikman Lower Bound should dictate the functional behavior for resistivity of a high-porosity mixture of sediment, hydrate, and conductive brine. In our terminology, “high porosity” means that the porosity of the mixture equals or exceeds critical porosity, which is the porosity condition across almost the entire hydrate stability interval at our study sites. We are not aware of any other hydrate research that concludes that the resistivity behavior of high-porosity, deep-water hydrate systems should converge to, or equal, the functional trend of the Hashin-Shtrikman Lower Bound. We demonstrate that the popular Archie Equation can be used to infer hydrate concentrations in deep-water hydrate systems if the equation is modified to account for the clay fraction that is present and if the empirical constants embedded in the equation are chosen to make the function closely track the Hashin-Shtrikman Lower Bound. We show such a formulation for the Archie Equation.

When calculating hydrate concentration, we emphasize that each parameter that is used in the Archie Equation should be described in terms of a realistic probability distribution function, not as a single numerical value. This approach allows uncertainty associated with each parameter to be incorporated into our estimates of hydrate concentration. Using this philosophy, we express our estimates of hydrate concentrations as probability distribution functions. The mean value of each pdf represents the “best estimate” of the hydrate concentration across the interval being analyzed, and the standard deviation of the pdf represents the “uncertainty” that should be assigned to the estimation.

Our implementation of the Archie Equation shows that measured formation resistivities of 1 ohm-m and 2 ohm-m in the clay-quartz sediment mixtures found across our study sites often indicate hydrate saturations that are 0.6 of the pore space. Numerous thick stratigraphic intervals across Study Sites 1 and 2 have resistivities greater than 1 ohm-m, and many zones within these intervals have resistivities of 2 ohm-m or more. This resistivity behavior is the fundamental evidence that leads us to conclude that the hydrate systems across Study Sites 1 and 2 are robust and are ideal targets for our research.

We emphasize that our calculations are based on the assumption that hydrate is distributed throughout the sediment as clusters of the fundamental clathrate unit volumes by which hydrate deposits grow. These unit volumes vary in size from 6 linked clathrates (Structure H) to 24 linked clathrates (Structure II) and were illustrated and described by Hardage and Roberts (2006). In our resistivity model (Fig. 6), these basic volumetric building blocks of hydrate can be

either load-bearing components of the sediment matrix, or they can be free-floating objects in the spaces between sediment grains. This model leads to low estimations of hydrate concentrations across intervals where there are low resistivity log readings, as illustrated, for example, by well W5 in Figures 44 and 49. If the hydrate morphology within the interval analyzed in example well W5 could be described as vertical layers of pure hydrate, the resistivity model shown in Figure 7b, then our results underestimate hydrate concentration for this interval of well W5 by a significant amount. Until information becomes available indicating that a different specific hydrate morphology exists across our study area, we will continue to base our work on the hydrate distribution model defined in Figure 6.

References

Archie, G. E., 1942, The electric resistivity log as an aid in determining some reservoir characteristics: AIME Transactions, v. 46, p. 54.

Cartwright, J., James, D., and Bolton, A., 2003, The genesis of polygonal fault systems—a review, *in* Van Rensbergen, P., Hillis, R. R., Maltman, A. J., and Morley, C. K., eds., Subsurface Sediment Mobilization: The Geological Society, London, p. 223-243.

Collett, T. S., 1993, Natural gas hydrates of the Prudhoe Bay and Kuparak River area, North Slope, Alaska: American Association of Petroleum Geologists Bulletin, v. 77, no. 5, p. 793-812.

Collett, T. S., and Ladd, J., 2000, Detection of gas hydrate with downhole logs and assessment of gas hydrate concentrations (saturations) gas volumes on the Blake Ridge with electrical resistivity log data, *in* Paull, C. K., Matsumoto, R., Wallace, P. J., and Dillon, W. P., eds., Proceedings of the Ocean Drilling Program, scientific results, v. 164, p. 179-191.

Dallimore, S. R., Uchida, T., and Collett, T. S., 1999, Summary, *in* Dallimore, S. R., Uchida. T., and Collett, T. S., eds., Scientific Results from JAPEX/JNOC/GSC Mallik 2L-38 Gas Hydrate Research Well, Mackenzie Delta, Northwest Territories, Canada: Geological Survey of Canada Bulletin 544 (4403 pages), p. 1-10.

Hardage, B. A., and Roberts, H. H., 2006, Gas hydrate in the Gulf of Mexico: what and where is the seismic target?: The Leading Edge, v. 25, p. 566-571.

Hardage, B. A., Murray, P. E., and Sava, D. C., 2006, Research database: Combining multicomponent seismic attributes, new rock physics models, and in situ data to estimate gas-hydrate concentrations in deep-water, near-seafloor strata of the Gulf of Mexico: Phase 1 report of DOE award DE-PS26-05NT42405.

Hashin, Z., and Shtrikman, S., 1962, A variational approach to the theory of the effective magnetic permeability of multiphase materials: Journal of Applied Physics, v. 33, no. 10, p. 3125-3131.

Hashin, Z., and Shtrikman, S., 1963, A variational approach to the elastic behavior of multiphase materials: Journal of Mechanics and Physics of Solids, v. 11, p. 127-140.

Hyndman, R. D., Yuan, T., and Moran, K., 1999, The concentration of deep sea gas hydrates from downhole electrical resistivity logs and laboratory data: Earth and Planetary Science Letters, v. 172, p. 167-177.

Lee, M. W., 2000, Gas hydrates amount estimated from acoustic logs at the Blake Ridge, sites 994, 995, and 997, *in* Paull, C. K., Matsumoto, R., Wallace, P. J., and Dillon, W. P., eds., Proceedings of the Ocean Drilling Program, scientific results, v. 164, p. 193-198.

Mendelson, K. S., and Cohen, M. H., 1982, The effect of grain anisotropy on the electrical properties of sedimentary rocks: Geophysics, v. 47, p. 257-263.

Milkov, A. V., and Sassen, R., 2001, Estimate of gas hydrate resource, northwestern Gulf of Mexico continental slope: Marine Geology, v. 179, p. 71-83.

Paull, C. K., Matsumoto, R., and Wallace, P., 1996, Proceedings of the Ocean Drilling Program, Initial Reports 164: Ocean Drilling Program, College Station, TX, 623 p.

Rider, M. H., 1991, The Geologic Interpretation of Well Logs, revised edition: Cathness, Scotland, Whittles Publishing.

Roberts, H. H., 2001, Fluid and gas expulsion on the northern Gulf of Mexico continental shelf—mud-prone to mineral-prone responses: Geophysical Monograph, 124, p. 145-161.

Santamarina, J. C., Francisca, F., Yun, T. S., Lee, J. Y., Martin, A. I., and Ruppel, C., 2004, Mechanical, thermal, and electrical properties of hydrate-bearing sediments: AAPG Hedberg Conference on Hydrates, Victoria, B.C., Canada, poster presentation.

Sassen, R., Joye, S., Sweet, S., DeFreitas D., Milkov, A., and McDonald, I., 1999, Thermogenic gas hydrates and hydrocarbon gases in complex chemosynthetic communities—Gulf of Mexico continental slope: Organic Geochemistry, v. 30, p. 485-497.

Schlumberger Wireline Services, 1998, Log interpretation principles/applications: Schlumberger Educational Services, Houston, TX.

Sen, P. N., Scala, C., and Cohen, M. H., 1981, A self similar model of sedimentary rocks with application to the dielectric constant of fused glass beads: Geophysics, v. 46, p. 781-796.

Wempe, W., 2000, Predicting flow properties using geophysical data—improving aquifer characterization: Stanford University, Ph.D. dissertation.